



European Organisation for the Exploitation of Meteorological Satellites

Technical Department

Technical Memorandum No. 3

Review on Scatterometer Winds

by

Jochen Kerkmann

August, 1998

This paper is an Internal Publication; permission to quote from it should be obtained from EUMETSAT.

Review on scatterometer winds

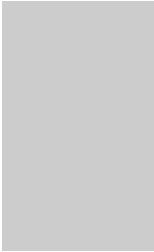
Jochen K. Kerkmann

Meteorological Division

European Organisation for the Exploitation of Meteorological Satellites

(EUMETSAT)

Am Kavalleriesand 31, D-64295 Darmstadt, Germany



Contents

1. Introduction	1
2. The scatterometer instruments	4
3. From raw data to sigma naughts	9
4. The physical problem (the wind connection)	12
5. The transfer function and the inversion problem	20
6. Ambiguity removal	27
7. Quality control of retrieved wind data	34
8. Geophysical calibration and validation of scatterometer winds	36
9. Assimilation of scatterometer winds in NWP models	41
10. Impact of scatterometer winds on NWP and Ocean Forecasting	47
11. Perspectives for ASCAT	58
Bibliography	63
Acronyms and abbreviations	71

ABSTRACT

In 1991 ESA launched the European Remote Sensing satellite, ERS-1, which includes as part of its payload a C-band scatterometer to measure wind vectors over the sea surface under all weather conditions. ERS-2, launched in 1995, also carried a scatterometer resulting in a contiguous dataset of sea surface winds from 1991 to the present. With a resolution of 50 km and a sampling distance of 25 km, the ERS scatterometer produced about 160000 valid three-beam measurements per day. This has led to a radical increase of surface wind observations over the world's oceans. Furthermore, it has been shown that scatterometer winds have a higher accuracy than conventional surface wind observations.

Scatterometer measurements were and will be continued through the NSCAT mission on the Advanced Earth Observing Satellite, ADEOS-I, launched in 1996, and the SeaWinds mission aboard QuikSCAT and ADEOS-II, to be launched in late 1998 and 2000 respectively. Current plans are for the European operational polar satellite Metop to also include an advanced scatterometer, ASCAT, to ensure long-term availability of operational data with high area coverage and spatial resolution.

The strength, direction and circulation patterns of the surface wind are of great importance for Numerical Weather Prediction (NWP), nowcasting and climate studies. Since January 1996 ambiguous scatterometer winds have been operationally assimilated in the ECMWF model with a strong impact on the analysis and the short-range forecast in the Southern Hemisphere where conventional observations are sparse. As regards the medium-range forecast, a positive impact of scatterometer winds was found whenever strong cyclones were present in the area of investigation. The high area coverage offered by scatterometer winds over the oceans is also essential for the monitoring and forecasting of tropical cyclones. A remaining problem is the underestimation of the wind speed for winds above 20 m/s, which may lead to a wrong estimation of the intensity of tropical cyclones. Recently, scatterometer winds have been successfully used in studies of interseasonal climate variations such as the El Niño/Southern Oscillation (ENSO), which affect the weather over large parts of the planet.

This Memorandum gives a brief introduction on the applications of scatterometer measurements (chapter 1). The scatterometer instruments and the transformation from raw measurements to triplets of sigma naughts are briefly described in chapters 2 and 3, respectively. The main topics are a summary of the physical relationship between the scatterometer measurements and the wind vector (chapter 4), a description of the geophysical transfer or model function (chapter 5) and of the various ambiguity removal techniques (chapter 6). Chapters 7 and 8 summarise the quality control and the validation of scatterometer winds. Information on the assimilation of scatterometer winds in NWP models and on the impact of scatterometer winds on numerical weather and ocean forecasting can be found in chapter 9 and 10, respectively.

Beyond the original mission of scatterometers, a large number of previously unforeseen applications have emerged, such as the retrieval of soil moisture, sea ice concentration, sea ice age and snow conditions. These emerging applications, which will probably further develop in future, are not described in this review but will be dealt with in relevant workshop proceedings.

1

Introduction

As early as the 1940s it was found that ocean waves caused large unwanted echoes on the radar screen when scanning at low elevation angles. The backscattered echoes from the sea became larger with wind speed. The same is true when scanning the ocean surface from space. Microwave radars on polar orbiting satellites measure the amount of backscattered radiance from the rough (ocean) surface. For a given satellite height, a given target size, a given viewing angle and a given polarisation of the radar beam, it is the roughness of the (ocean) surface that determines how much of the incoming microwave radiation will be backscattered into the direction of the satellite. The roughness of the ocean surface, on the other hand, is mainly determined by the wind speed, which explains the correlation found between the wind speed and the intensity of the backscattered echo.

All this assumes that essentially no absorption is taking place on the way through the atmosphere and that the backscatter from the ocean surface does not depend on sea temperature, plankton content and other parameters. The first assumption is a very good one if C-band radars are used (see tab. 1.1 and fig. 1.1). In the C-band of the microwave region measurements of the ocean surface are neither hindered by clouds nor by rain, whereas in the Ku-band strong rain attenuates the radar signal (see fig. 1.2) leading to an underestimation of the wind speed in the vicinity of tropical (and extra-tropical) cyclones. The validity of the second assumption is not that easy to assess. An effect on the intensity of the returned signal has so far been demonstrated for the sea state (sea spray, breaking waves) and for naturally and man-made surface slicks.

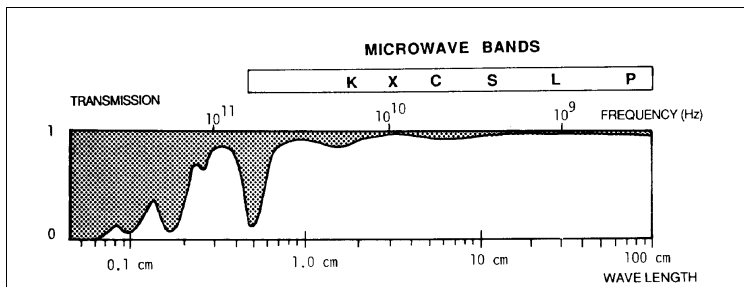


Fig. 1.1: Atmospheric transmission in the microwave part of the electromagnetic spectrum (from Askne, 1990).

Band	Frequency [GHz]	Wavelength [cm]
P-band	0.225-0.39	133-77
L-band	0.39-1.55	77-19
S-band	1.55-3.90	19-7.7
C-band	3.90-6.20	7.7-4.8
X-band	5.75-10.9	5.2-2.8
Ku-band	10.9-18.0	2.8-1.7
Ka-band	18.0-36.0	1.7-0.8

Tab. 1.1: Microwave frequency bands.

With the availability of scatterometer-derived wind data the amount of wind observations over the world oceans has radically increased, especially over the Southern Oceans. Whereas before there were only scattered measurements from ships (and a few buoys, see fig. 1.3), the

scatterometer instrument provides data with a 25 or 50 km horizontal resolution covering most of the ocean surface in two to three days (fig. 1.4). Not only the quantity, but also the quality of the wind observations over the oceans has improved. It has been demonstrated that scatterometer winds have a slightly higher quality than ship measurements. The latter suffer from the inaccurately known movement of the ship, the rolling of the ship and the measurement taken at the wrong height (not at 10 m, which is the WMO standard height). Also buoy measurements are not always the most accurate ones, because the sea state influences the measurement. In addition, in-situ measurements from ships and buoys are not representative for a large area like the box of a model grid and therefore a-priori less useful for NWP models than scatterometer observations, and any comparison of these two data types should consider this difference.

The disadvantages of scatterometer winds are their low accuracy at low wind speeds and at the inside part of the swath, the increasing rms error at high wind speeds due to representativeness errors (other geophysical parameters not represented in the “sigma-naught-to-wind transfer function” become important at high wind speeds) and the measurements not being taken simultaneously at synoptic times. With the introduction of the 4-D Variational Analysis the latter shortcoming can be eliminated, at least for NWP applications. Other difficulties have been mentioned in the literature, like the dependence of the transfer function on local static stability of the atmosphere (e.g. Brown, 1988) and the difficulties in areas of rapidly changing winds (i.e. close to frontal disturbances, e.g. see Stoffelen and Anderson, 1997)), but are of less importance.

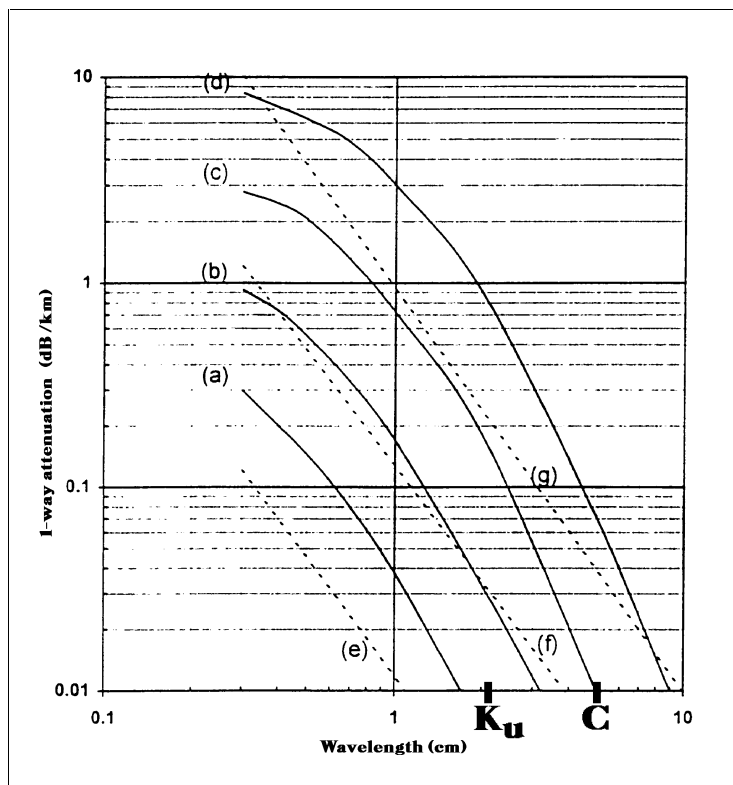


Fig. 1.2: Theoretical attenuation of radar waves caused by rain (curves a-d) or by fog (curves e-g) for different wavelengths (from Farrow, 1975):

- a) 0.25 mm/h (drizzle);
- b) 1 mm/h (slight rain);
- c) 4 mm/h (moderate rain);
- d) 16 mm/h (strong rain);
- e) 0.032 g/m³ (about 600 m visibility);
- f) 0.32 g/m³ (about 130 m visibility);
- g) 2.3 g/m³ (about 30 m visibility).

Primary users of scatterometer data are NWP Centres and Oceanographic Institutes (the operators of ocean general circulation models). The surface wind, by transferring momentum and energy to the upper ocean layers, is a substantial source of energy for a variety of oceanic processes. Surface wind speed is also a key factor for the exchange of carbon dioxide between the ocean and an essential information on the mass distribution of the atmosphere. One single surface wind observation can change the entire analysis of the mass structure in that particular location, which, in some cases, may lead to completely different forecasts. In the Southern Hemisphere, where only few conventional wind observations exist (see fig. 1.3), the introduction of scatterometer-derived winds has led to a significant improvement of the model analyses and,

to a somewhat less extent, of the forecast (Ingleby and Bromley (1991), Anderson et al. (1991), Hoffman, 1992, 1993, Gaffard and Roquet, 1995).

More recently it has been found that scatterometer data are also very valuable for land, snow and ice applications (e.g. Kerr and Magagi, 1993, Mougin et al., 1993, Wiesmann and Mätzler, 1993, Wismann and Boehnke, 1997, Boehnke and Wismann, 1997, Cavanie et al., 1997, Ezraty et al., 1997, Park, 1997, Woodhouse and Hoekman, 1997, Mougin et al., 1997). Parameters like surface moisture, sea ice concentrations, sea ice age and snow conditions could be successfully retrieved using scatterometer data. Particularly promising is the derivation of sea ice masks based on the polarisation ratios of the scatterometer data (for NSCAT) and on the different backscatter level behaviour at different incidence angles (for ERS scatterometer), which compare well to similar products derived from SSM/I data. These emerging scatterometer applications will be further developed in future. Also the applications of scatterometer data for climate studies have not been fully exploited. Scatterometer winds guarantee global, long-term monitoring of the winds on the oceans, which make them very valuable for climate studies.

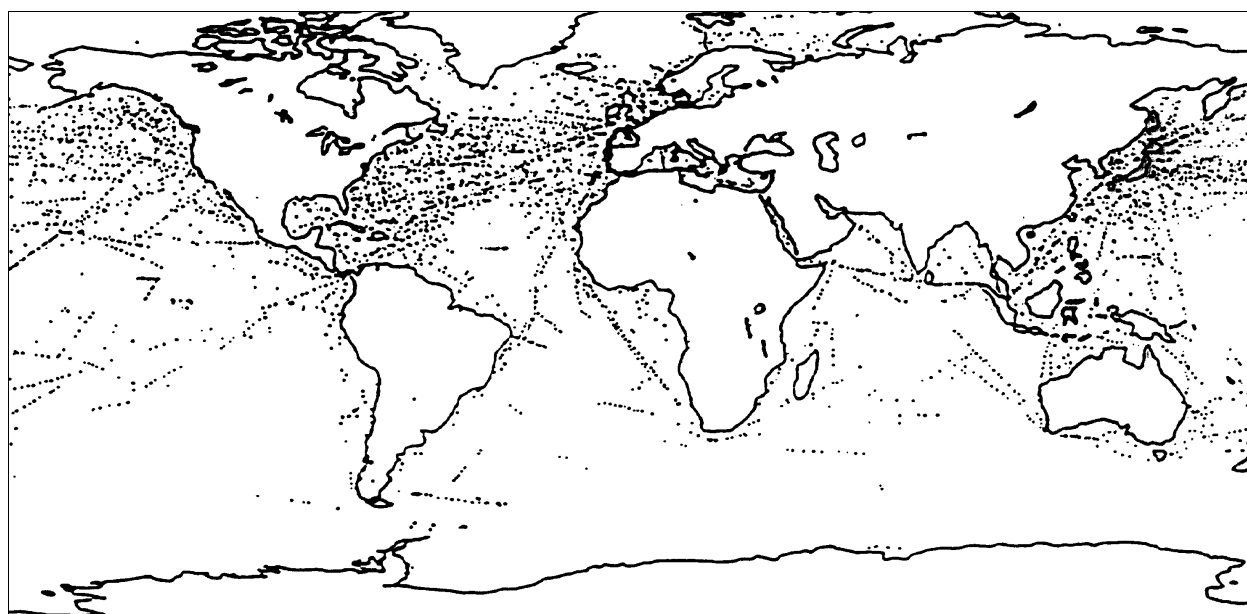


Fig. 1.3: Three-day coverage of the oceans by ship measurements.

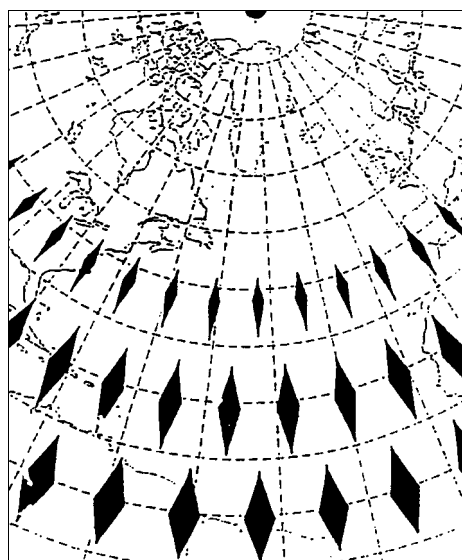


Fig. 1.4: Three-day coverage of the Atlantic Ocean by ERS-1 scatterometer measurements. The dark areas are not covered.

2

The scatterometer instruments

The first scatterometer instrument in space was the SEASAT-A Scatterometer System (SASS), on board of the experimental oceanographic satellite SEASAT-A that operated between July and October 1978. SEASAT-A measurements were ended by an abrupt power system failure less than four months after launch. SASS scanned the earth's surface on both sides of the satellite ground track with two independent antennae pointing in 45° (fore beam) and 135° (aft beam) direction (see fig. 2.4). The incidence angles θ of the radar beams varied from 25° to 55° resulting in a swath width of 475 km. SASS used a microwave Ku-band operating with a wavelength of 2.1 cm (14.599 GHz frequency).

Given these characteristics, each patch of the ocean was seen first by the fore beam and one to four minutes later by the aft beam (depending on the incidence angle). Successive orbits were separated by about 100 minutes in time and the outer edges of the swaths from successive orbits were separated by about 1200 km at the equator and swaths overlapped poleward of about 50° latitude.

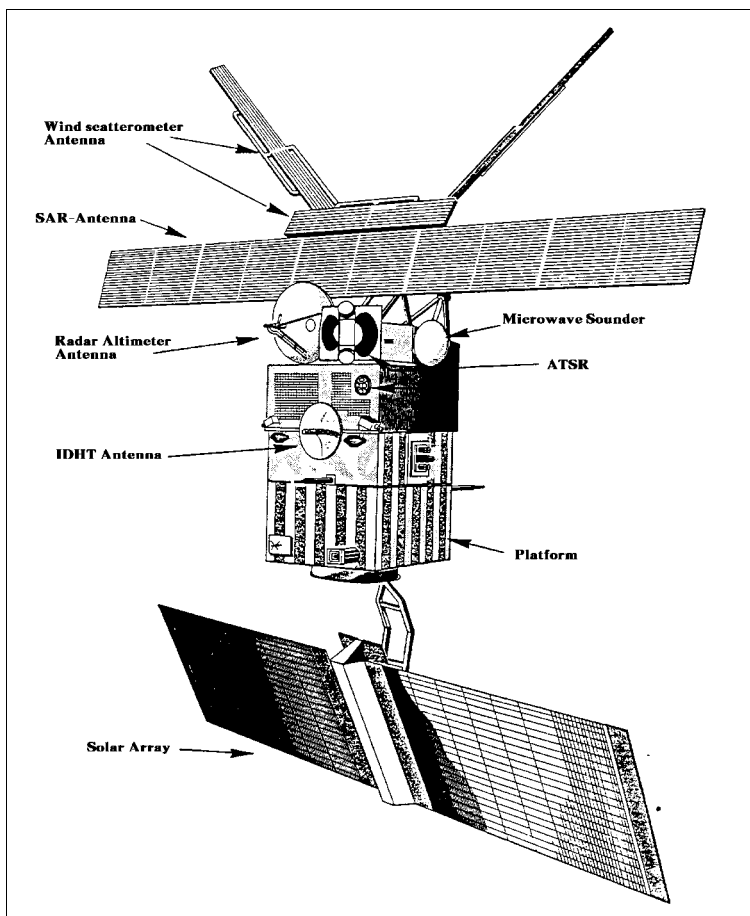


Fig. 2.1: ERS-1 instruments (from Oriol-Pibernat, 1990).

Thirteen years later, on 17 July 1991, ESA launched the remote-sensing satellite ERS-1, which carries a C-band scatterometer (wavelength of 5.7 cm, vertical polarisation). The satellite moves in a polar orbit at a height of approximately 800 km. The ERS-1 scatterometer differs from the

SEASAT scatterometer in that the radar antennae are mounted only on one side of the satellite illuminating a 500 km wide swath to the right side of sub-satellite track (see fig. 2.4). But instead of two, it has three independent antennae (see fig. 2.1, fig. 2.2 and fig. 2.4) pointing in 45° (fore beam), 90° (mid beam) and 135° (aft beam) direction with respect to satellite propagation. The incidence angle θ of the radar beam varies from 18° to 47° for the mid beam, and from 25° to 59° for the fore and aft beams.

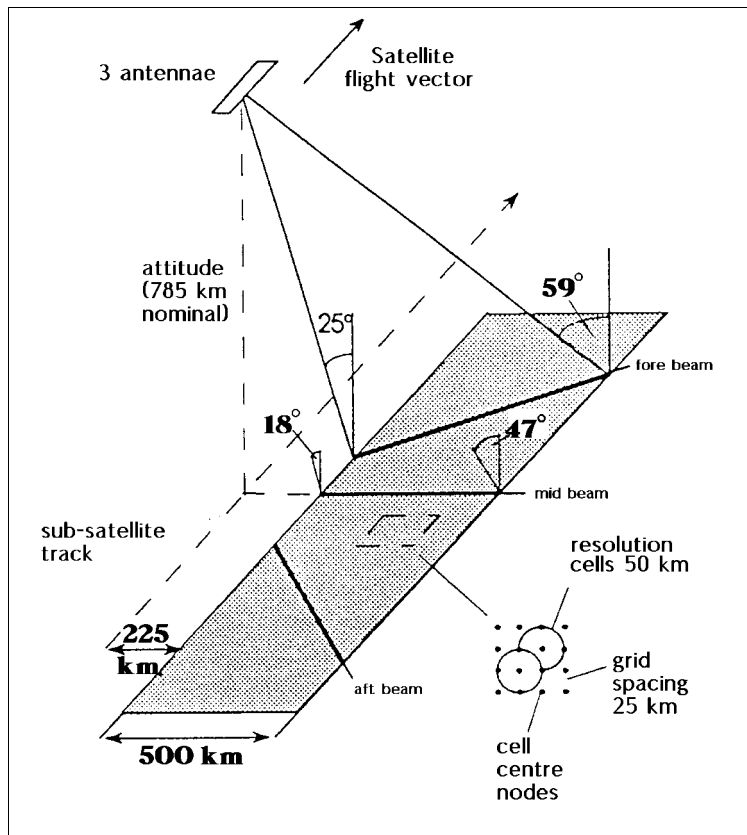


Fig. 2.2: ERS-1 wind scatterometer geometry (from ERS-1 reference manual, Royal Aerospace Establishment, U.K.)

The 500 km wide swath of the ERS scatterometer is sampled every 25 km resulting in 19 measurement nodes across the swath and about 160000 3-beam ocean nodes per day. The sampling distance along the swath is also 25 km. However, adjacent measurements across the swath are not independent due to the effective spatial resolution of the instrument of 50 km (overlapping footprints). The coverage of the swaths of the North Atlantic region over 1 day is shown in fig. 2.3. North of about 60°N most of the ocean area is covered, but south of 60°N large gaps can be seen.

The same type of scatterometer has been mounted on ERS-2, launched on 21 April 1995. ERS-2 follows ERS-1 on the same orbit with a delay of 24 hours. After the commissioning phase for ERS-2, which ended in March 1996, there has been a period of a few months when both ERS satellites were operated. Data from this period have been used to study the effect of an increased coverage of scatterometer data on the quality of weather forecast models (see chapter 10).

The American instrument NSCAT was launched into space on board of the Japanese Advanced Earth Observing Satellite (ADEOS) on 17 August 1996. Like the SASS instrument, it measured in the Ku-band (14 GHz) on both sides of the ground track (two 600 km wide bands separated by a gap of approximately 350 km). As mentioned in the introduction, the effects of rain on the measured signal are more important in this band than in the C-band. Compared to SEASAT

scatterometer, a third antenna had been added looking at 20 degrees from the aft/fore beam for the right/left side of the track, i.e. it was not a real mid beam (see fig. 2.4). The most important difference to the ERS scatterometer is that this mid beam was operating in two polarisations (horizontal, denoted HH, and vertical, denoted VV). All the other antennae and instruments operated in vertical polarisation.

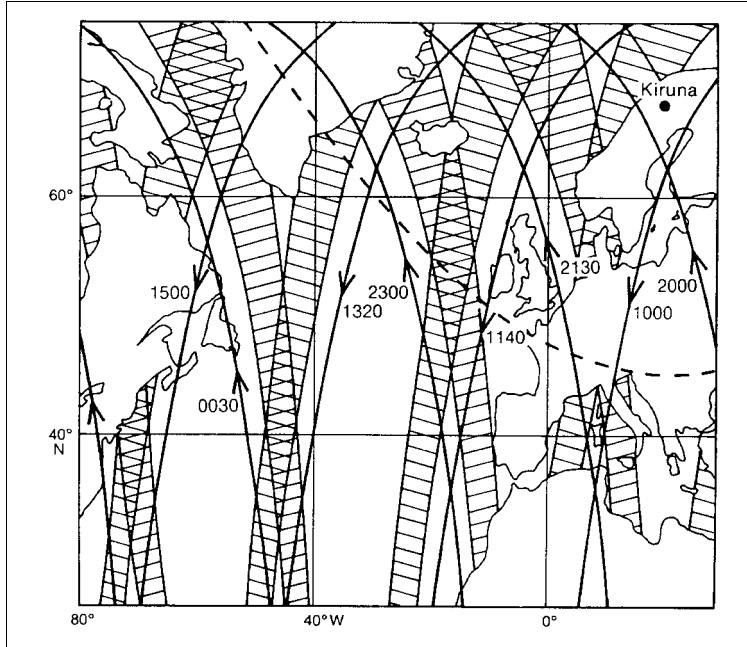


Fig. 2.3: ERS-1 sub-satellite tracks and wind scatterometer coverage of the North Atlantic region over one day. The large gaps are partially filled on subsequent days; nominally this occurs on a three-day cycle. The dashed line shows the limits of reception for the Kiruna ground station in Sweden (from Offiler, 1990).

Unfortunately, ADEOS-1 operations were terminated at the end of June 1997, after more than nine months of successful operations, due to a complete failure of the power supply system. This affected all eight instruments on board, including NSCAT. The 26 m long solar panel was the main cause for the ADEOS-1 failure. The thermal expansion of the bonding material in sunlight was larger than anticipated before launch, and the solar panel got unfixed. Nevertheless, the data collected will allow to study the impact of a three times greater coverage (as compared to ERS scatterometer) on analysis and forecasting.

After the dramatic loss of NSCAT, NASA is planning to launch QuickSCAT on a dedicated polar satellite at the end of 1998. QuickSCAT will help to fill the gap between the NSCAT on board of ADEOS-1 and SeaWinds on board of ADEOS-2, to be launched in the year 2000. Both instruments will operate at the same wavelength as NSCAT, with a total swath width of 1800 km (QuickSCAT) and 1600 km (SeaWinds). A major difference to NSCAT is the measurement geometry of these instruments. Indeed, QuickSCAT will be the first scanning scatterometer, as shown in fig. 2.4. The effect of such geometry is:

- Nodes on the subsatellite track will be illuminated from two exactly opposite directions, which makes the determination of wind direction very difficult.
- Nodes at the far ends of the swath will be illuminated from only one single direction. Therefore, no information on wind direction will be available towards the outer parts of the swath.
- Nodes in the middle of the swath will be illuminated from different directions, enabling the retrieval of wind speed and direction.

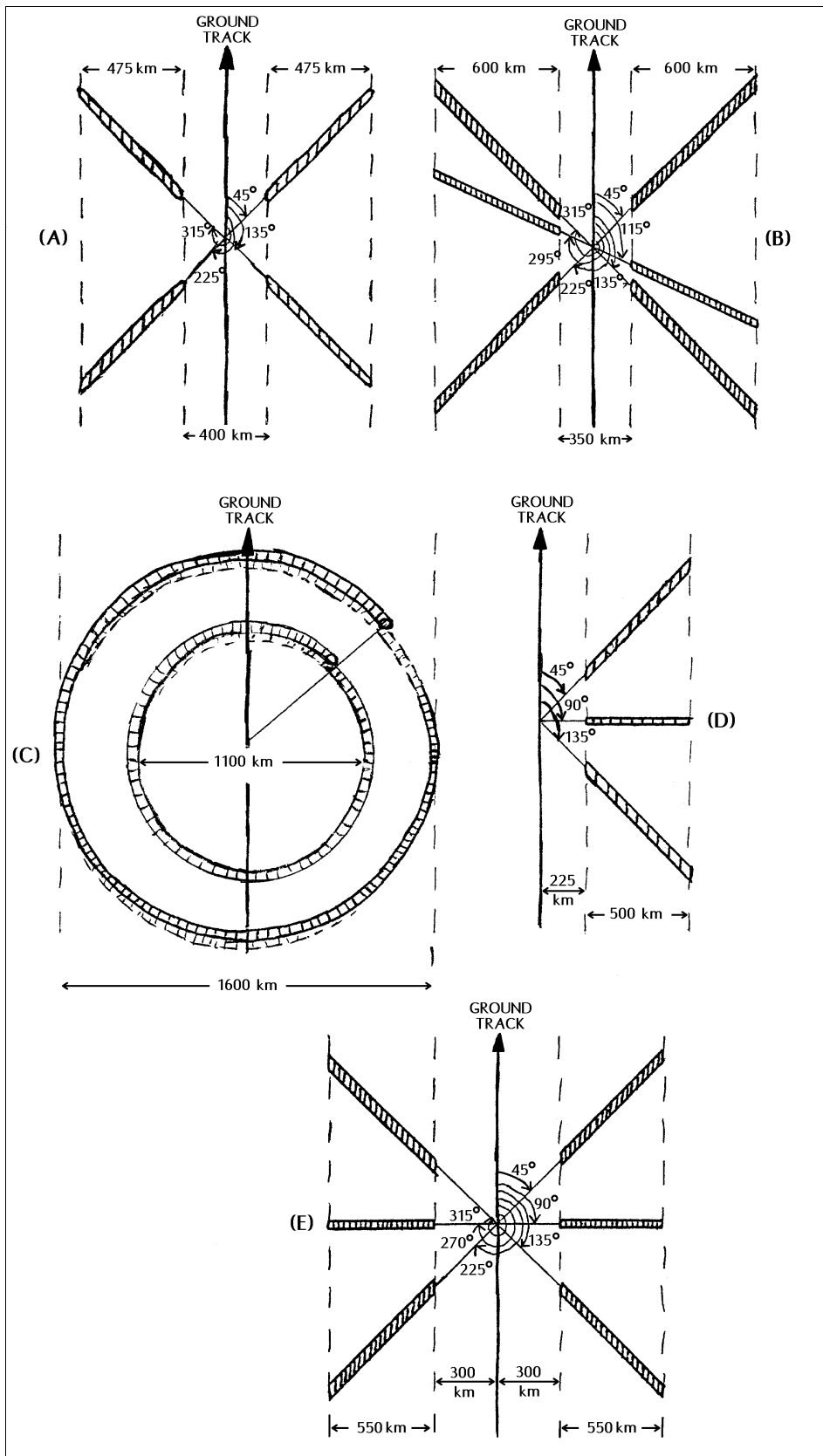


Fig. 2.4: Antennae geometry of SASS on board of SEASAT (A), NSCAT on board of ADEOS-1 (B), SeaWinds on board of ADEOS-2 (C), SCAT on board of ERS-1 and ERS-2 (D), ASCAT on board of Metop (E). The thin vertical lines denote the swath boundaries. Note that the ERS scatterometer has a swath only on one side of the satellite track with a significant smaller area coverage than the other instruments (from Stoffelen, 1998).

Finally, the advanced scatterometer ASCAT will be launched on board of Metop in the year 2003. ASCAT will be a real aperture C-band radar (5.7 cm wavelength, 5.255 GHz frequency) with high radiometric resolution and stability. The spatial resolution for the nominal operating mode will be the same as for the ERS scatterometer (50 km), but a research mode will be added with a resolution of 25 km. Like SASS and NSCAT, it will have a double swath (see fig. 2.4) to allow faster global coverage (see fig. 2.5). Since it will have a dedicated microwave source, i.e. there will also be no shared use with other instruments, the coverage will be about three times larger than for the ERS scatterometer. Another important change w.r.t. the ERS scatterometer is that the swath will be further outside with incidence angles ranging from 25 to 65°. It is expected that this will lead to a higher accuracy in the determination of the wind direction.

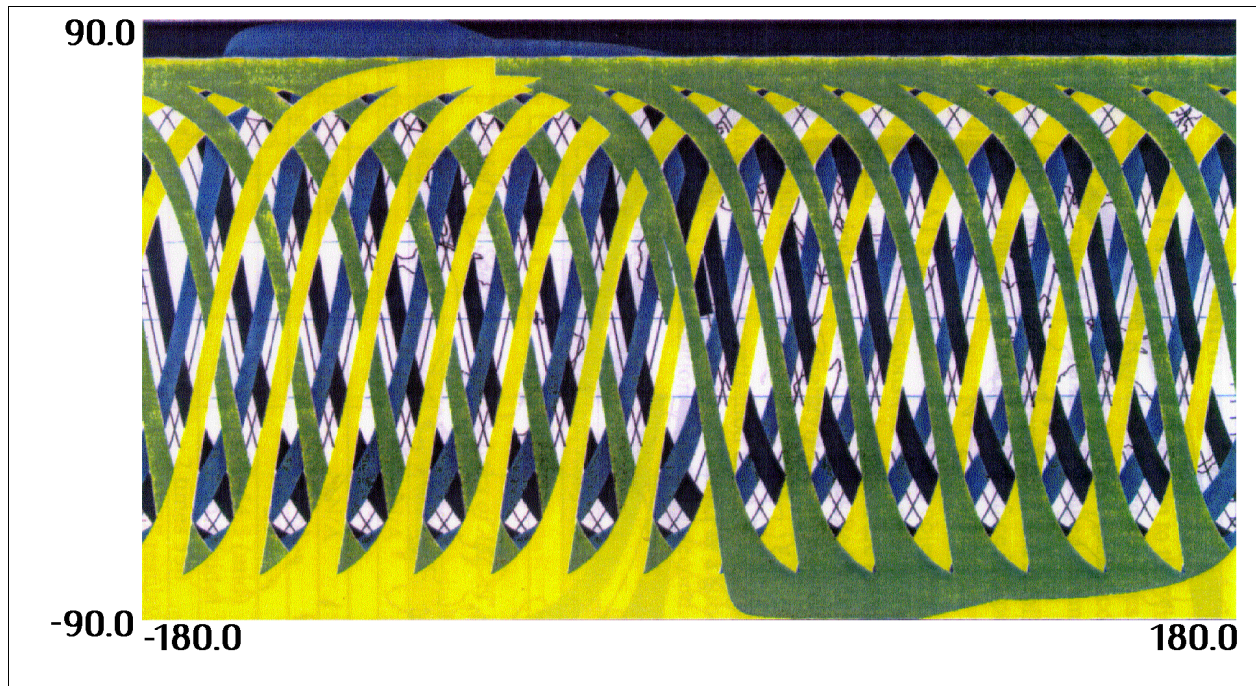


Fig. 2.5: ASCAT coverage for one day.

The hardware for ASCAT will not be identical to the one of the ERS scatterometer. A part of the processing of the data will already be performed onboard (e.g. some spatial filtering is done by averaging the spectra derived from successive echoes) resulting in a low data rate load on the telemetry link. It will not require on-board knowledge of satellite position/pointing and will be controllable by parameter setting from the ground station.

3

From raw data to sigma naughts

The Active Microwave Instrument (AMI) on ERS-1/2 combines the functions of two separate radars: the Synthetic Aperture Radar (SAR) and the Wind Scatterometer (WSC). The AMI can thus be operated in three modes:

- image mode;
- wave mode;
- wind mode.

The first two modes are related to the SAR instrument and will not be discussed here. The purpose of the third mode, the AMI wind mode, is to obtain information on wind speed and direction at the sea surface, which is sequentially illuminated by radar pulses from different angles, and the backscattered signal (σ° = sigma naught) is measured to determine the sea surface radar reflectivity.

The processing of the data provided by scatterometers can be divided into two steps:

- the calculation of a reflectivity triplet $\sigma^\circ_{\text{fore}}$, $\sigma^\circ_{\text{mid}}$, $\sigma^\circ_{\text{aft}}$ for each grid point in each swath (processing up to level 1.b);
- the determination of the geophysical parameter of interest (e.g. the wind vector) at a given grid point from the reflectivity triplet using a physical or empirical model function (level 2 and higher processing).

This chapter briefly describes the first step, while the following chapters deal with the second step.

For the ERS and ASCAT instruments, a part of the processing is already performed on board the satellite. As indicated in fig. 3.1, the instrument sends out 32 pulses in one block before switching from one beam to another. The Pulse Repetition Interval (PRI) is 10.21 ms and 8.7 ms for the fore/aft and the mid-beam respectively. Within this interval a noise calibration window and a target wind are defined where noise and response are measured respectively. Both response and noise are averaged over all PRI's in one block before sending the information down to the ground station.

For the mid-beam, the return echo is filtered and sampled in complex form I and Q, while for the fore and the aft beams, as the doppler variation is significant over the swath width (20 kHz near swath to 140 kHz far swath), a programmable doppler compensation law is applied to the received signal before filtering and complex sampling. The total steps performed on board are:

1. dechirping of received echoes (mapping of frequency components to echo time);
2. spectral analysis of dechirped signal;
3. spatial filtering by averaging the spectra from successive echoes;
4. packing of information into telemetry data including relative gain and background noise.

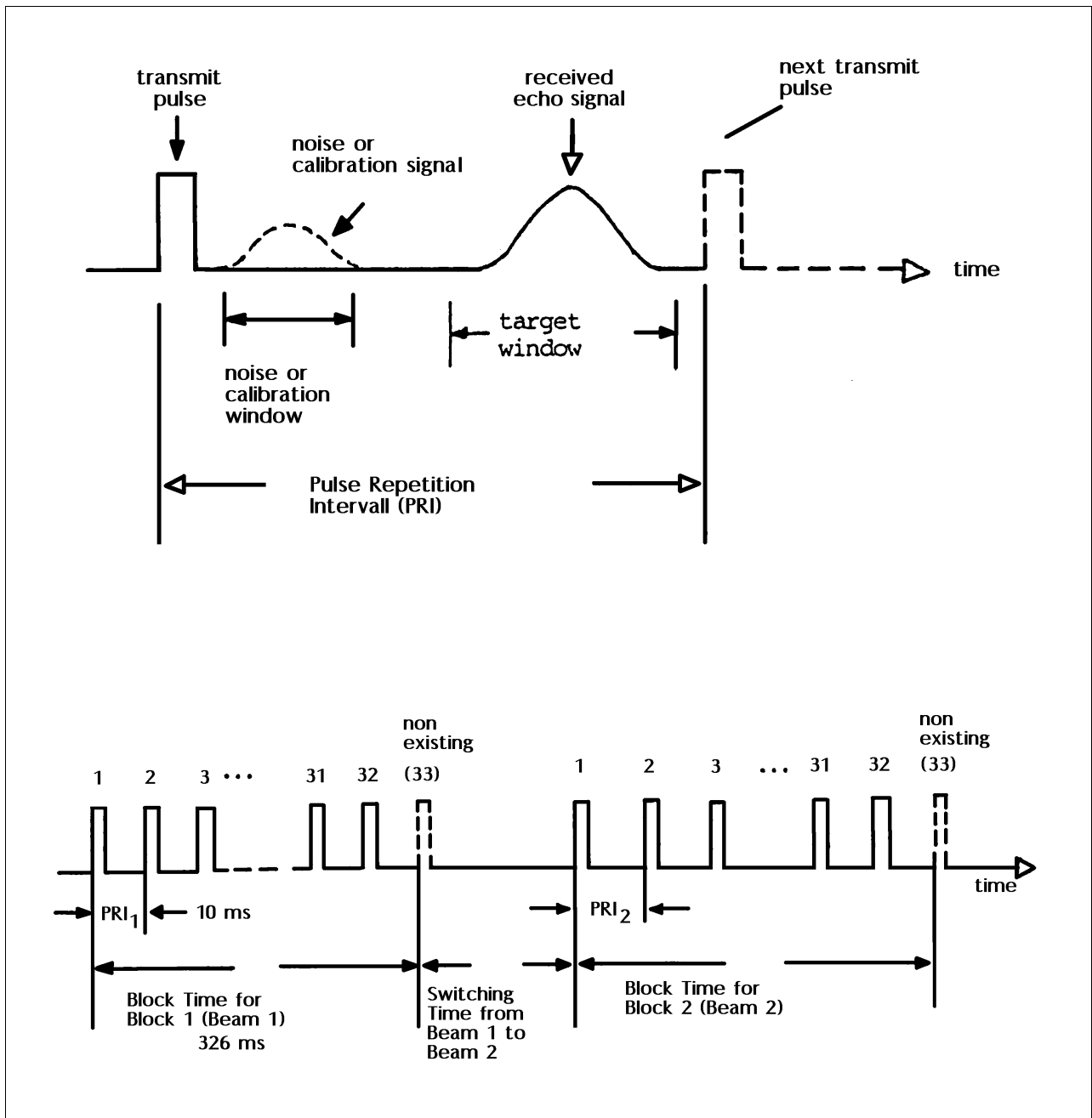


Fig. 3.1: Signal processing on board ERS for the wind scatterometer.

The main inputs received at the ground station are the Frequency Power Profile (FPP) and the noise measurement data given in an Orbit Time – Echo Frequency coordinate system. The first step of the ground processing is to subtract the average noise power from the Frequency Power Profile (see fig. 3.2). The value to be subtracted is calculated from the noise measurement data that are integrated over the frequency spectrum and time averaged over the noise integration time. Only noise data gathered from the same antenna as the measurement data are used for this. Next, the corrections for antenna gain variations and for power gain variations are applied to the data. The data needed for these corrections must come from internal (ancillary data in the measurement data stream) and/or periodical external calibration (e.g. transponders or measurements from standard targets) databases. After these corrections, a so-called deblooming can be applied (optional). This is to account for the weakening of the acquired signal in the vicinity of strong backscatters (causing for example low wind speed data in the vicinity of coastal lines).

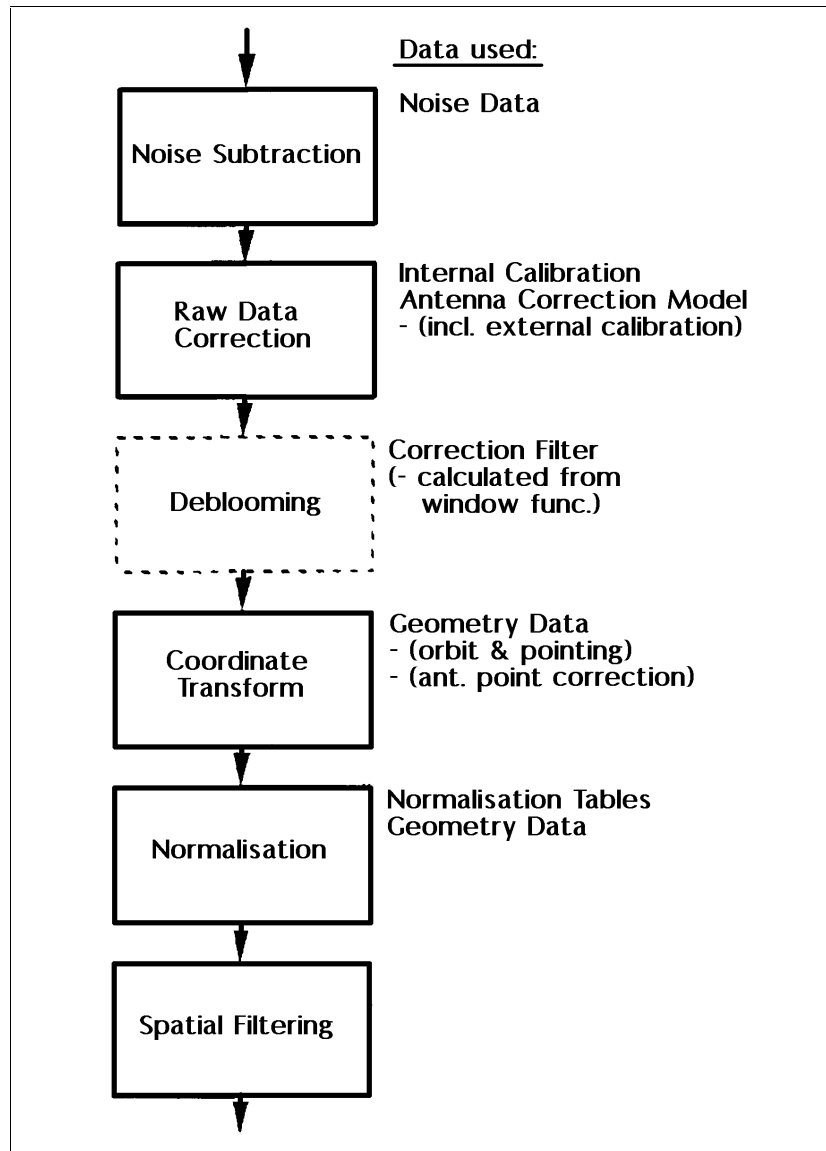


Fig. 3.2: Processing sequence on ground for ASCAT.

An important further step is the coordinate transformation from (frequency, time) to (x, y) coordinates, which requires the knowledge of orbit position and effective antenna pointing at the orbit time. The main step of the calculation of the σ° triplets in the ground processor is then the multiplication with the normalisation factor. This is done using precalculated tables. In the practical implementation, the node geometry and the sigma naught normalisation factors are in fact precomputed in the Scatterometer Simulator System (SSS) which generates some 50 tables, which are loaded in the station processing facilities to compute the sigma naughts.

The last processing step is the spatial filtering along each beam direction yielding the σ° triplets in the desired resolution. In principle the filtering, which produces a uniform spatial resolution, is possible before the conversion to sigma naughts (normalisation). However, the ground processor is more flexible if the normalisation is performed with the highest possible spatial resolution, that is before spatial filtering, because in this case outputs with different spatial resolution can be provided by simply changing the spatial filter function.

4

The physical problem (the wind connection)

Scatterometer instruments measure the returned radar power from an extended target area in terms of the “normalised radar cross-section”, or σ° (sigma naught), as defined in Long (1988). For given radar wavelength λ_r , slant distance to the target R_s , surface of the target A , antenna gain in viewing direction G and system losses L_s (including atmospheric attenuation), σ° is given by the ratio of the received to the transmitted power:

$$\sigma_{lin}^\circ = \frac{P_{received}}{P_{transmitted}} \frac{64 \pi^3 R_s}{\lambda_r^2 L_s G^2 A} \quad (4.1)$$

Since σ° is very small and covers a wide range of magnitudes, it is usually expressed in dB:

$$\sigma^\circ (dB) = 10 \log_{10} (\sigma_{lin}^\circ) \quad (4.2)$$

Two physical phenomena are responsible for returning a part of the emitted radiation into the satellite direction: specular reflection and backscattering at the surface (see fig. 4.1 and fig. 4.2). For incidence angles close to 0° (nadir looking), the specular reflection is dominating the returned signal and the intensity of the returned signal decreases rapidly with increasing incidence angle (see fig. 4.2). However, with increasing incidence angle, specular reflection gets less important and backscattering takes over the dominant role. This is reflected in fig. 4.2 by the fact that, for incidence angles from 20° to about 70° , σ° decreases more slowly forming a kind of “plateau” region. For incidence angles around 20° , i.e. at the inside part of the swath, both specular reflection and backscattering contribute to the returned signal. Shadowing effects and diffraction trapping cause again a rapid decrease of σ° for incidence angles higher than about 70° .

A tropical rain forest represents a homogeneous isotropic rough surface where backscattering is strong (many small surfaces (leaves) with dimensions similar to the radar wavelength). Rivers, towns and mountain areas have a lower echo than forests and show up as dark areas on a scatterometer image (see fig. 4.3), which means that scatterometer data can be used to identify some details of the surface type. This use is demonstrated in fig. 4.4, which shows an NSCAT image of the Amazon basin indicating a variety of different surface types such as rain forest and grassland.

The backscattering at the rough sea surface of the radar beam is principally due to in-phase (resonant) reflections from the small ripples (cat’s paws) and sea spikes generated by the instantaneous surface wind stress. As a wind gust rushes across the ocean surface, it leaves a path of easily observable ripples on the surface, which die away as soon as the gust has passed. These ripples are capillary gravity waves (Bragg waves) which have a typical wavelength of only some centimetres. They have a non-isotropic structure (they are longer in the crosswind direction), which allows the observer to estimate the wind direction.

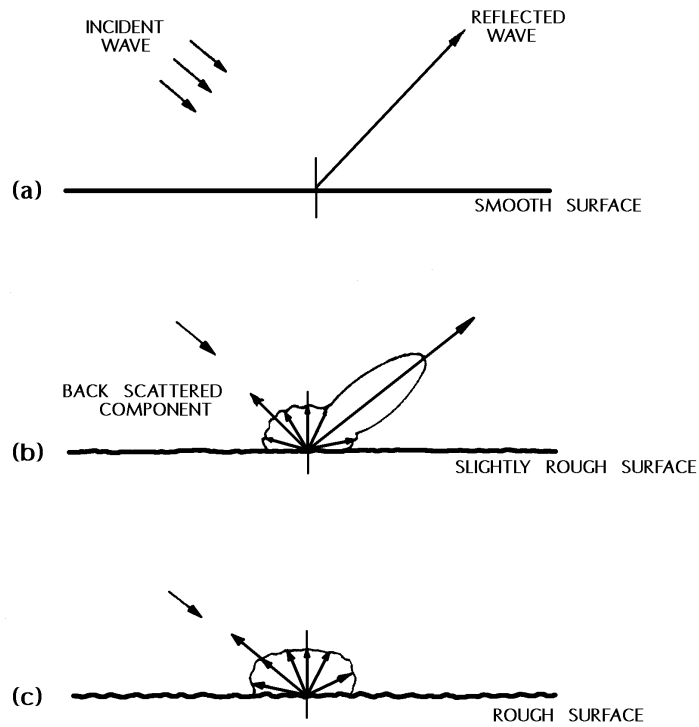


Fig. 4.1: Schematic representation of microwave scattering and reflection at a smooth (a), slightly rough (b), and rough (c) ocean surface. As the roughness increases more radar power is returned towards the direction of the radar source (from Stoffelen, 1998).

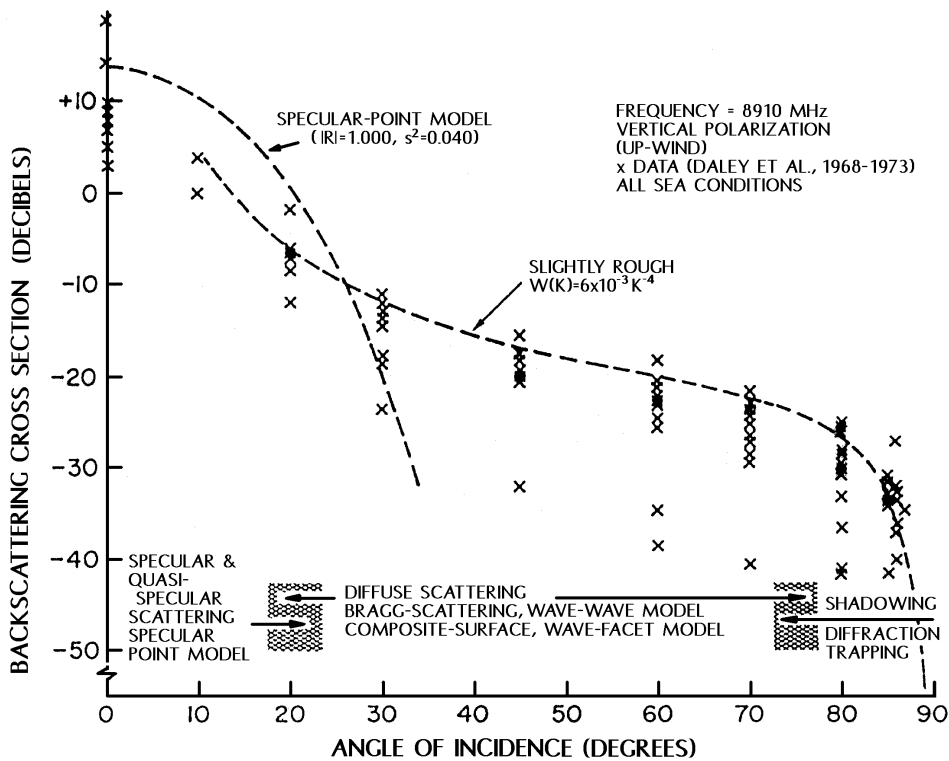


Fig. 4.2: Illustration of mechanisms which predominate in the radar backscatter from the ocean at the various angles of incidence.

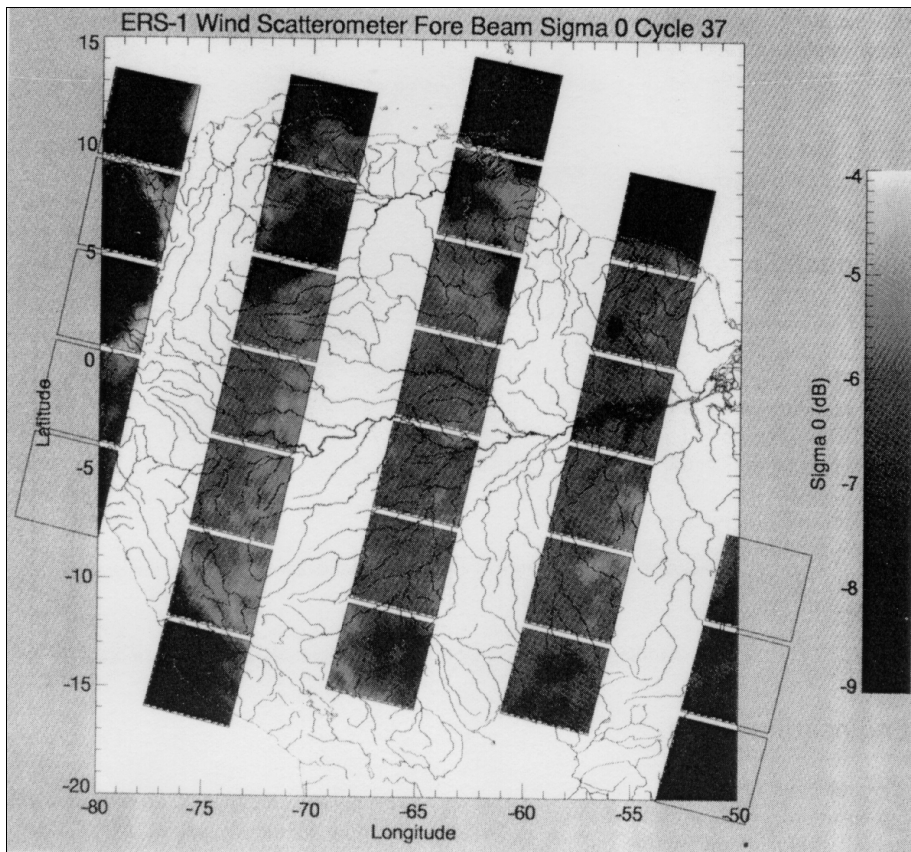


Fig. 4.3: ERS scatterometer image of the tropical rain forest (from Lecomte and Attema, 1992).

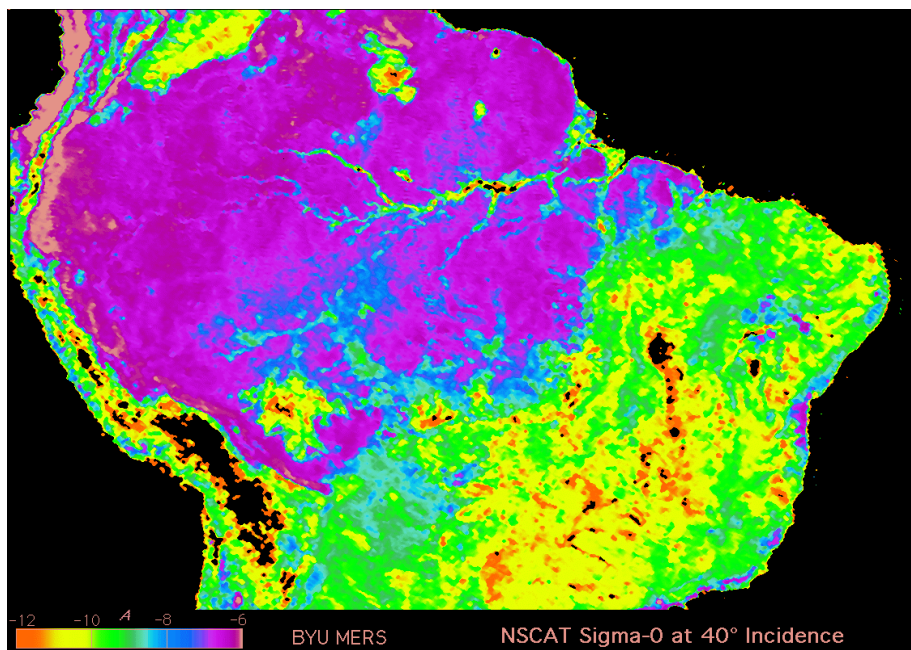


Fig. 4.4: False colour radar image of the Amazon rainforest in South America taken by NSCAT showing the sensitivity of the measurements to conditions on the earth's surface, such as the type and density of vegetation. Blue and purple areas are tropical rainforest, and green and yellow regions are woodlands and savannah. Mountains and degraded farmlands show up as black (image from Jet Propulsion Laboratory, Pasadena, California, USA).

The scattering of the radiation caused by Bragg waves (Bragg scattering) alone, however, does not explain the full characteristic of scatterometer images, particularly for high frequency radars (C-band, X-band). Tilting of the Bragg surface waves by longer surface waves modulates the basic Bragg scattering (Press et al., 1996).

It should be noted that the spectrum of the capillary gravity waves does not depend only on the local wind field. Non-linear three- and four-wave interactions, viscous dissipation and dissipation due to slicks also determine the spectrum (Janssen et al., 1996) When waves are sufficiently steep, longer gravity waves may, through the energy cascade, significantly influence the state of the short waves. The state of the long waves depends on factors such as coastal geometry, duration of storm system, currents and bathymetry, and therefore the backscattered signal may depend on these environmental factors as well.

Coming back to the Bragg waves, the condition for resonance is that the rays reflected at the equally distant waves have all the same phase. This is the case for:

$$\lambda_b = \frac{0.5n\lambda_r}{\sin \Theta} \quad (4.3)$$

where λ_b is the wavelength of the Bragg waves, n the order of the scattering (in practice 1), λ_r the wavelength of the radar beam and θ the incidence angle. The wavelength for resonant Bragg scattering for the ASCAT instrument ($\lambda_r=5.7$ cm) ranges from $\lambda_b=3.72$ cm (for $\theta=50^\circ$, outside part of the swath) to $\lambda_b=8.33$ cm (for $\theta=20^\circ$, inside part of the swath).

Summarising the above, σ° depends on wind speed V (it increases with V), on wind direction given by the azimuth angle ϕ (varies sinusoidal-like with ϕ with maximums for upwind/downwind directions and minimums for crosswind directions), on the polarisation of the radar beam (e.g. horizontal or vertical polarisation) and on the incidence angle θ defined to be the angle between the incident radiation and the local normal to the sea surface (σ° decreases with θ). It also depends on the transparency of the atmosphere (the atmosphere is nearly transparent for microwave radiation, but in the Ku-band rain may attenuate the signal). Finally, it depends on the SST (changing viscosity of the sea surface), wind waves, swell, slicks, currents, bathymetry and other factors that influence the short waves (see fig. 4.5), but these dependencies are small and difficult to be determined explicitly. Generally, only the dependencies on V , ϕ and θ are taken into consideration. Fig. 4.5 illustrates the major physical processes that contribute to a SAR (Synthetic Amplitude Radar) image of the ocean surface. Most of the processes shown are also contributing to scatterometer images.

With this assumption the problem consists of deriving wind speed and direction from σ° measurements, i.e. from the measure of surface roughness in terms of spectral density of the short capillary waves (only a small part of the wave spectrum around λ_b is considered). A large number of models have been published in literature, which solve this problem in an empirical way (e.g. Moore and Fung, 1979, Jones et al., 1982, Long, 1985, 1991, Offiler, 1987, Wentz, 1991, Freilich and Dunbar, 1992, Wismann, 1993, Stoffelen and Anderson, 1992, 1993, 1995, 1997).

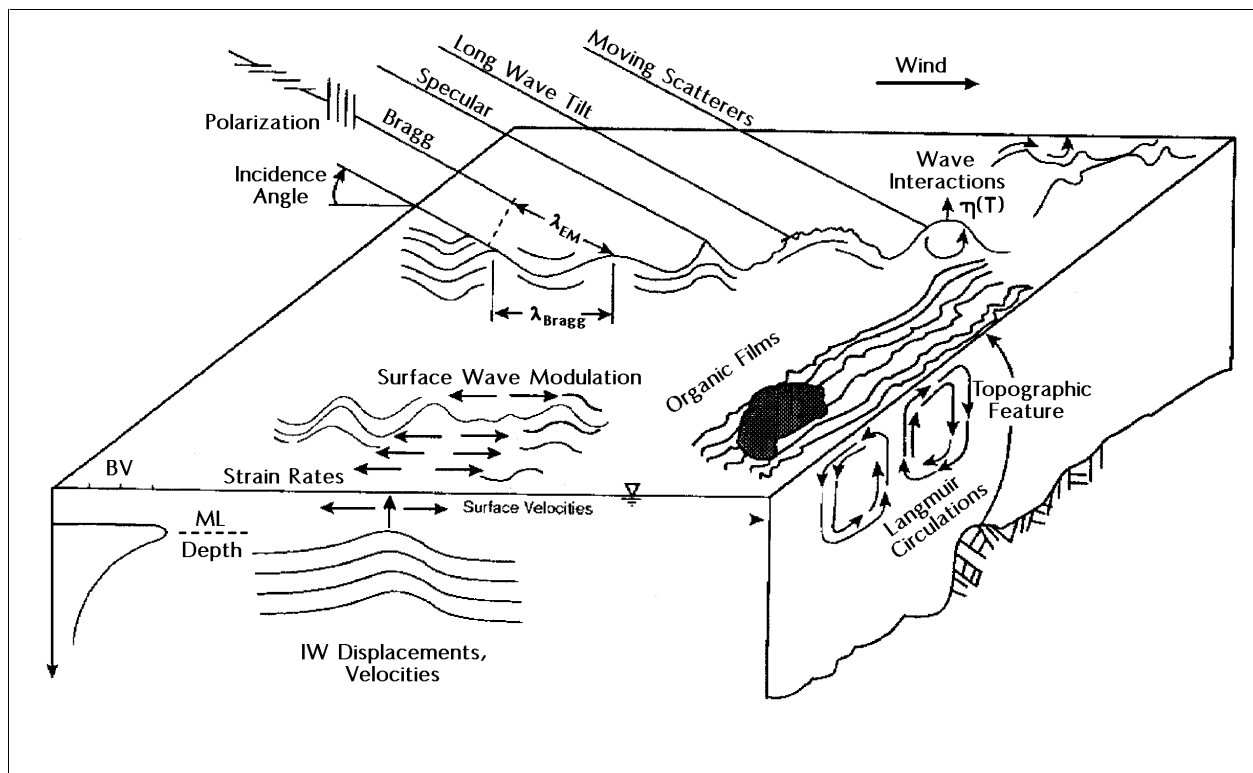


Fig. 4.5: Physical processes involved in SAR ocean imaging (adopted from Press et al., 1996). For low incidence angles both Bragg wave scattering and specular reflection contribute to the returned signal. For high incidence angles reflection effects are negligibly small. The Bragg scattering can be modified by interactions with longer waves (wind waves, swell). Organic films, topographic features and Langmuir circulations also contribute to a modification of the returned signal.

Only a few publications are known to the author where attempts have been made to find a physical solution to the problem (Donelan and Pierson, 1987, Janssen et al., 1996, Elfouhaily, 1997). This is probably due to the fact that three coupled physical models are required to resolve this problem analytically: 1) an electromagnetic scattering model that describes the radar measurements as a function of the wave spectrum of the ocean surface; 2) a model that describes the relation between wave spectrum and the wind stress; 3) an atmospheric boundary layer model that relates the surface wind stress to the wind speed and direction at a standard height.

There are several difficulties in deriving these analytical models.

- I. The mechanism of wind generation of water waves is a classic unsolved problem of fluid dynamics (Brown, 1990). Models for the short wave spectrum are generally based on the energy balance equation assuming steady state circumstances. Most of the terms in this equation, like the effects of the wind stress, the wave interactions, the dissipation due to wave breaking and the damping due to slicks, have to be parametrised and advection of short wave energy is usually disregarded.
- II. The electromagnetic models need to make a lot of assumptions regarding the random rough surface in order to be able to find a simple solution of the electromagnetic problem (Elfouhaily, 1997), and residual waves (swell) and shadowing effects are difficult to consider.

- III. The relationship between surface stress and wind at 10 m level depends on a large number of parameters so that solutions can be given only for very simplified cases (further discussion given below).
- IV. A physical algorithm is computationally very expensive and as such not feasible for routine applications. However, the operational computational costs may be reduced by generating tabulated values of the normalised radar backscatter σ° as a function of wind speed, wind direction and incidence angle (as done for the empirical methods). This costly exercise has to be done prior to the operational application of the algorithm. If other parameters of the physical model, like sea state, air-sea stability and the effect of surface slicks, are to be included, the tables become five, six or even higher dimensional.

As regards the atmospheric boundary layer, a variety of models for wind profiles exist that use as input information on the surface roughness length z_0 (the height where $V=0$, roughly at 1/10th of the mean height of the obstacles) and the so-called friction velocity u^* , which is a kind of a substitute for the surface stress, τ (Prandtl theory, e.g. Prandtl, 1952, Monin-Obukhov theory, e.g. Monin and Obukhov, 1971).

$$V(z) = \frac{u^*}{\kappa} \ln\left(\frac{z}{z_0}\right) \quad (4.4)$$

where κ is the von Karman constant ($\kappa \approx 0.4$).

The roughness length z_0 depends itself on the friction velocity u^* . For ocean surfaces it may be parametrised according to Smith et al. (1992):

$$z_0 = \alpha \frac{(u^*)^2}{g} ; \alpha = 0.48 \left(\frac{c_p}{u^*}\right)^{-1} \quad (4.5)$$

In equation (4.5) z_0 includes the effects of the sea state, where c_p/u^* is the age of the wind sea and c_p is the phase speed of the peak of the wind sea spectrum. The latter may be obtained from an ocean wave prediction model (e.g. the WAM model, Komen et al., 1994).

The third part of the geophysical problem (relation between surface stress and V) can therefore be solved with the aid of equations like (4.4, 4.5) and an ocean wave prediction model, but only for limited atmospheric conditions. For example, the logarithmic wind profile (equation 4.4) has been derived from land-based data of the surface layer and may not be valid for the oceanic boundary layer. Another critical point is the assumption of homogeneity and stationarity of the mean values (i.e. no horizontal gradients of wind and temperature, the mean V is only a function of z) which is necessary in deriving equation (4.4). Since homogeneity of temperature is related to barotropic conditions, i.e. no horizontal temperature gradient and no change of wind with height, this theory cannot be applied under baroclinic conditions, i.e. where large horizontal temperature gradients exist (like close to frontal zones).

Equation (4.4) is also only valid for neutral stratification. In cases with non-neutral stratification (highly unstable situations can be found on ocean surfaces), a correction term to this equation must be added, which comes from empirical studies. The model proposed by Ezraty (1985) has been used in several measurement campaigns to determine this correction term, including the RENE-91 campaign for the geophysical calibration of the ERS-1 scatterometer (Offiler, 1994, see chapter 8). In this model, the wind profile is assumed to take the form:

$$V(z) = \frac{u^*}{\kappa} \left[\ln\left(\frac{z}{z_0}\right) - \Gamma\left(\frac{z}{L}\right) \right] \quad (4.6)$$

where: L is the Monin-Obukhov stability length, z/L is a dimensionless stability length and Γ represents a stability-dependent modification to the logarithmic wind profile (Large and Pond, 1982, see also Businger et al., 1971):

$$\Gamma = \begin{cases} -5z/L, & \text{for } z/L > 0 \text{ (stable conditions)} \\ 0, & \text{for } z/L = 0 \text{ (neutral conditions)} \\ 2\ln\left(\frac{1+X}{2}\right) + \ln\left(\frac{1+X^2}{2}\right) - 2\tan^{-1}(X) + \frac{\pi}{2} \\ \quad \text{with } X = (1-16z/L)^{0.25} \\ \quad \text{for } z/L < 0 \text{ (unstable conditions)} \end{cases} \quad (4.7)$$

The difficulty in using the Ezraty model, which is strictly valid only for $-1.0 < z/L < 0.5$, lies in the determination of the stability length over oceans. Offiler (1994) determined z/L as a function of air-sea temperature difference and wind speed, with corrections for humidity and bulk estimates of the latent and sensible heat fluxes. The latter depended on the temperature and humidity profiles, which were determined using similar relationships. Since the temperature and humidity profiles in turn control the atmospheric stability, and hence the wind profile by means of equation (4.6), an iterative process has to be applied to solve the boundary layer wind profile (more details in Offiler, 1994).

The VIERS-1 scatterometer model (Janssen et al., 1996) uses a more simplified expression from Stewart (1985) to determine the stability length L over oceans:

$$L = \frac{-u^*V(z)}{g\kappa} \frac{T_{air}}{T_{sea} - T_{air}} \quad (4.8)$$

with g the acceleration of gravity, κ the von Karman constant, T_{air} the air temperature and T_{sea} the water temperature. Again, for given friction velocity u^* , phase speed of the waves, air and sea temperature the wind speed V can be solved from equations (4.5, 4.6, 4.7, 4.8) in an iterative manner.

Looking more closely at the connection of σ° measurements to the surface wind, it becomes clear that, the stronger the wind, the larger will be the fraction of the target area covered by Bragg waves, the higher will be their amplitude and the larger will be the returned signal. It has been shown that even at very high wind speeds, when probably all the target area is covered with Bragg waves, there is still an increase of the measured signal with increasing wind speed, which means that sea spray and breaking of waves contributes to the backscattered signal. At the lower end of the wind speed spectrum, a threshold value for the generation of capillary waves exists. Winds weaker than about 2 m/s are difficult to be inferred from scatterometer data.

As mentioned before, the Bragg waves have a unisotropic structure. This leads to a variation of the returned signal for different viewing angles. It is therefore possible to retrieve the wind direction from scatterometer data by pointing to the target from different azimuth angles. Two angles have been used for SASS on SEASAT, three angles for AMI on ERS-1 and ERS-2 and NSCAT on ADEOS-1. Data from radar altimeters, which have been flown/are flying on GEOS-C, SEASAT GEOSAT, ERS-1 and TOPEX/POSEIDON, are of no use for retrieving the wind direction because they look at the target area only from one azimuth angle (nadir-looking instruments).

Using three measurements (σ° triplets) to determine two geophysical parameters (V and ϕ) raises the question whether this leads to an overdetermined system. It does not (Stoffelen and Anderson, 1992). Multiple direction measurements are possible, because wind speed and direction are not iterated directly from the highly non-linear transfer function, but from minimising a residual function (Maximum Likelihood Estimator MLE). This will be explained in the following sections.

To summarise, a large number of problems arise when trying to relate σ° triplets to wind direction and wind speed:

- the relationship between surface wind stress and capillary waves is not solved;
- the relationship between surface stress and wind at 10 m level depends on local static stability, which is not known;
- there is no clear knowledge on unisotropic structure of capillary waves;
- in baroclinic conditions (close to surface fronts) there may be deviations from the logarithmic wind profile;
- in areas of rapidly changing winds or high wind speeds the sea state may have an effect on the measurements;
- at low incidence angles reflection from the surface adds noise to the measurements;
- the dependency on geophysical parameters like SST, sea state and surface slicks etc. is not clear.

5

The transfer function and the inversion problem

As shown in the previous section, the level of backscatter from the sea surface for the ERS scatterometer depends mainly on three parameters: wind speed V , wind direction (given by the azimuth angle ϕ) and incidence angle θ . The function that describes this dependency is called transfer or model function. Since θ is a known parameter, although different for the mid and the fore/aft beams, the wind speed and direction are the unknown variables of the transfer function. This doesn't mean that the functional dependency on θ is not important. For small incidence angles, for example, errors in θ can lead to substantial errors in σ° and must be taken into consideration (Stoffelen and Anderson, 1995).

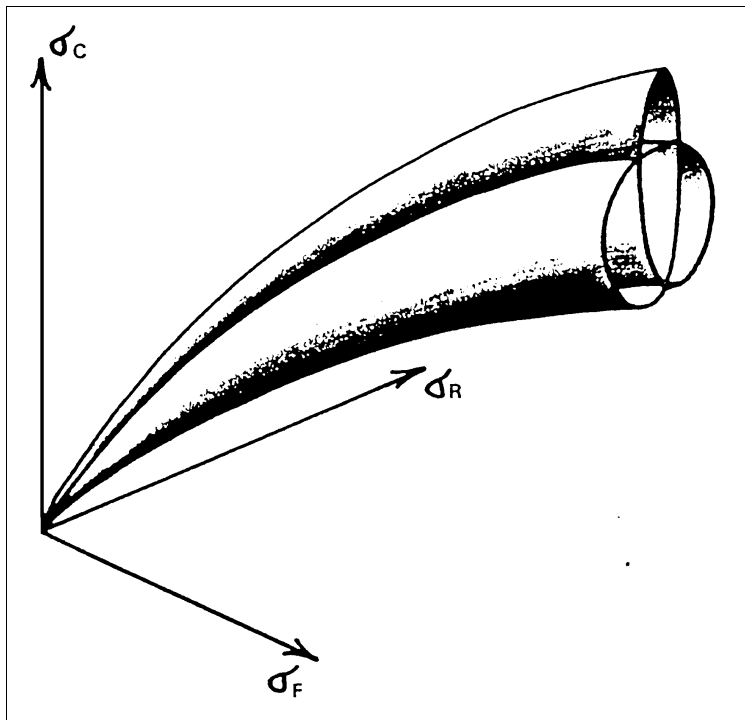


Fig. 5.1: 3D measurement space. Triplets of measured σ° s are expected to lie close to a cone-shaped surface (a cone with crossing leaves). The crossing points of the leaves represent triplets that do not have a unique solution of the inverse problem (from Cavanie et al., 1986).

The transfer function can be visualised by plotting the σ° triplets in the three-dimensional measurement space spanned by the σ° s of the fore, mid and aft beams respectively. This has been done by various authors (e.g. Cavanie and Lecomte, 1987, Stoffelen and Anderson, 1992, 1995) for different nodes of the swath. If the transfer function depended only on wind direction and speed and if there was no measurement error, then the triplets would lie on a surface in the 3D space (a cone, see fig. 5.1). The amount of scatter around this hypothetical surface is therefore a measure of the validity of the assumption. If the scatter is only within the measurement noise, the assumption is a good one. If a large part of the triplets lies far away from the hypothetical surface (they may lie inside or outside the cone), more than the distance given by the measurement noise, then other geophysical parameters probably play an important role.

Since the visualisation of such a cone is a rather difficult task, it has become common use to show cross sections of the cone, i.e. triplets situated close to the predefined section are projected on the section plane (the maximum allowed distance of the measured triplets from the projection

plane is defined from the measurement noise). In this way, reducing the space dimension by one, the plotted points should lie close to a line, which can be a double line, a circle, an ellipse or a Lissajous-type figure, depending on the position of the cross section (see fig. 5.2 and fig. 5.3). As could be shown by Stoffelen and Anderson (1995), the measured triplets clearly define such lines for most sections plotted. This proves that, for a given node, σ° depends in principle only on two variables (namely wind speed and direction). However, for low incidence angles (inside part of the swath), there is more scatter of the measured σ° triplets around the cone. At these angles the scatterometer is very sensitive to changes in the incidence angle (strong non-linear θ dependence of σ°). For the first nodes of the swath, the differences in the incidence angles between the mid, and the fore and aft beams may therefore lead to differences in the effective sampling area (Stoffelen and Anderson, 1995).

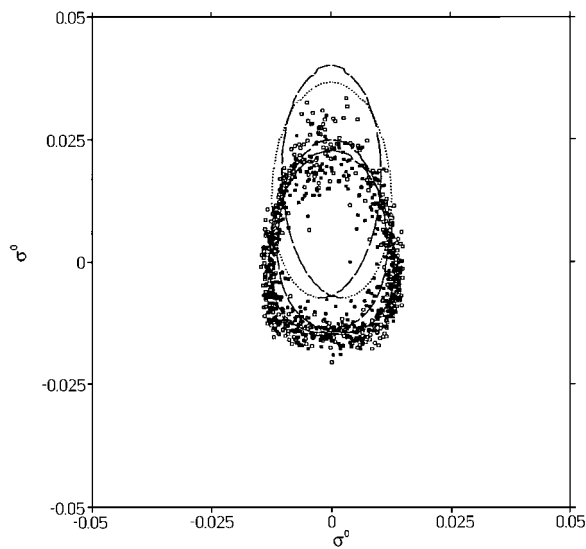


Fig. 5.2: Example of the distribution of measured σ° triplets in a cross-section across the cone. The expected cone surface can easily be identified. The collocated analysis wind speed for the triplets plotted is roughly 8 m/s. The two curves correspond to the transfer functions CMOD2 (upper curve) and CMOD4 (lower curve) (from Stoffelen, 1994).

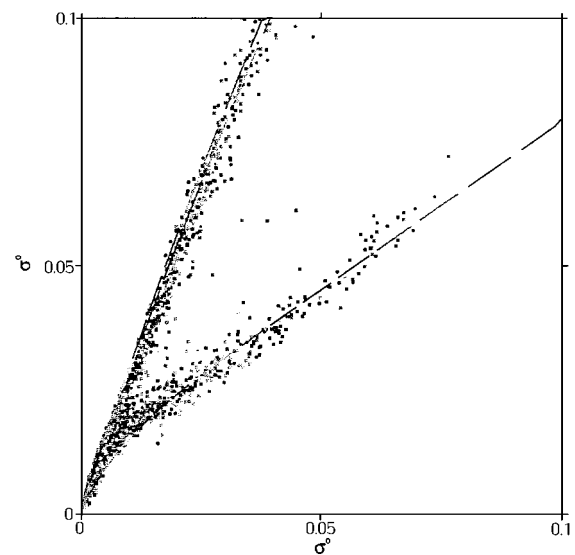


Fig. 5.3: Example of the distribution of measured σ° triplets in a cross-section along the cone. From the lower left to the upper right the wind speed is increasing. The curve represents the transfer function CMOD4 (from Stoffelen, 1994).

A cloud of points rather than a well-defined surface is also found for the part of the cone that corresponds to low wind speeds (the part of the cone close to the origin). This seems reasonable, since at low wind speeds backscattering is weak and other geophysical parameters may become more important.

The transfer function, when plotted together with the measurement triplets, should fit the scattered points. The periodicity with respect to the wind direction together with the non-linear increase of σ° with increasing wind speed suggest to use a truncated Fourier cosine series for the modulation of the ϕ dependence and to use an exponential function part for the V dependence. The determination of the coefficients can be done by a least squares regression using NWP data, wind measurements from an aircraft campaign or from wind buoys.

Several transfer functions have been derived so far for the SEASAT, ERS-1/2 and ADEOS-1 scatterometer. Most of them differ little in the functional approach. The most successful model for the SEASAT scatterometer was the Seasat-A Scatterometer System (SASS-1) model, which is based on the following function:

$$\sigma^\circ = A_0 + A_1 \cos(\phi) + A_2 \cos(2\phi) \quad (5.1)$$

where:

$$\begin{aligned} A_0 &= a_0 V^{\alpha_0} \\ A_1 &= (a_1 + \alpha_1 \log V) A_0 \\ A_2 &= (a_2 + \alpha_2 \log V) A_0 \end{aligned} \quad (5.2)$$

and a_0 , a_1 , a_2 , α_0 , α_1 and α_2 are implicit functions of polarisation ϵ and incidence angle θ . The coefficients of SASS-1 were tuned to a subset of true surface winds from the Joint-Air-Sea Interaction Experiment (JASIN, Schroeder et al., 1982). A comparison of SASS-1 winds with the JASIN data not used in the tuning (independent test) gave a favourable agreement, but a more detailed validation done by Woiceshyn et al. (1986) and Anderson et al. (1987) showed that SASS-1 winds were generally biased high at low wind speeds and biased low at high wind speeds.

Since NSCAT was using the same frequency band as the SEASAT scatterometer (Ku-band), the transfer function for NSCAT was based on the same functional approach as for SEASAT (i.e. equation 5.1). The pre-launch version, called SASS-2, had several drawbacks (see chapter 8), so that the tuning had to be repeated with real NSCAT data leading to the model function NSCAT-1 (coefficients not published).

Long (1985, 1991) derived two pre-launch versions of the transfer function for the ERS scatterometer, called CMOD1 and CMOD2. The CMOD2 function was obtained by calibrating measurements from airborne scatterometers against wind measurements from buoys, and is given by:

$$\sigma^\circ = 10^\alpha V^\gamma [1 + (b_1 + b_2 V) \cos \phi + (b_3 + b_4 V) \cos(2\phi)] \quad (5.3)$$

where α , γ , b_1 , b_2 , b_3 and b_4 were expanded as Legendre polynomials and functions of θ :

$$\begin{aligned} \alpha &= \alpha_1 + \alpha_2 X + \alpha_3 (3X^2 - 1)/2 \\ \gamma &= \alpha_4 + \alpha_5 X + \alpha_6 (3X^2 - 1)/2 \\ &\dots \\ b_4 &= \alpha_{16} + \alpha_{17} X + \alpha_{18} (3X^2 - 1)/2 \end{aligned} \quad (5.4)$$

$$X = \frac{\theta - 25}{40}$$

and the tuning coefficients $\alpha_1 \dots \alpha_{18}$ were determined from the data of the field campaigns.

The first term in equation (5.3), called the bias term, modulates the increase of σ° with wind speed. The second and third terms modulate the wind direction dependency. The factor $(b_1 + b_2 V)$

determines the differences in the σ° when looking at the target area from 180° opposite direction (upwind/downwind amplitude), and (b_3+b_4V) the differences when looking at the target area from angles differing 90° (upwind/crosswind amplitude).

After the launch of ERS-1, it became clear that the pre-launch model function CMOD2 had several drawbacks. The measurements did not exactly fit the model function (see fig. 5.2), and when comparing measured σ° s to simulated σ° s using ECMWF analysis winds, there was a bias across the swath. An interim model function called CMOD3 was developed shortly after launch, which fitted the measurements better than CMOD2, but which still resulted in a small bias. Therefore Stoffelen and Anderson (1995) introduced the transfer function CMOD4. The main changes with respect to CMOD2 and CMOD3 were the introduction of a correction factor depending on θ , a modification of the upwind/crosswind amplitude and a transformation in the measurement space, going from σ° to z , where:

$$z = (\sigma^\circ)^{0.625} \quad (5.5)$$

Offiler (1994) and Stoffelen and Anderson (1995) showed that the CMOD4 transfer function fits the σ° triplets much better than the CMOD2 function, and the CMOD4 function has become the baseline for the processing of scatterometer data from ERS. The validity for CMOD4 is the speed range from 2 to 20 m/s, although higher wind speeds can be retrieved. The CMOD4 transfer function is given by (Stoffelen and Anderson, 1997b):

$$\sigma^\circ = b_r 10^{\alpha + \gamma f_1(V + \beta)} [1 + b_1 \cos \phi + b_3 \tanh(b_2 \cos(2\phi))]^{1.6} \quad (5.6)$$

where:

$$f_1(y) = \begin{cases} -10 & \text{if } y \leq 10^{-10} \\ \log y & \text{if } 10^{-10} < y \leq 5 \\ \sqrt{y}/3.2 & \text{if } y > 5 \end{cases} \quad (5.7)$$

and:

$$\begin{aligned} \alpha &= c_1 + c_2 X + c_3(3X^2 - 1) / 2 \\ \gamma &= c_4 + c_5 X + c_6(3X^2 - 1) / 2 \\ \beta &= c_7 + c_8 X + c_9(3X^2 - 1) / 2 \\ b_1 &= c_{10} + c_{11} V + (c_{12} + c_{13} V) f_2(X) \\ b_2 &= c_{14} + c_{15}(1 + X) V \\ b_3 &= 0.42(1 + c_{16}(c_{17} + X)(c_{18} + V)) \\ f_2(X) &= \tanh[2.5(X + 0.35)] - 0.61(X + 0.35) \\ b_r &= \text{correction factor depending on } \theta \end{aligned} \quad (5.8)$$

$$X = \frac{\theta - 40}{25} \quad (5.9)$$

The transfer function CMOD4 is depicted in fig. 5.5, which shows the non-linear increase of σ° with wind speed (curves are not equally spaced) and the relative minima for crosswind observations. The transfer function IFR2, developed at IFREMER in Brest, is shown for comparison in fig. 5.6. The results achieved with this transfer function are quite as satisfactory as those achieved with CMOD4. Therefore both transfer functions can be regarded as valid for the

ERS scatterometer. Recently other transfer functions have been developed, like CMOD9 (by M. Crepon, not shown), a neural network derived model, or CMODA (by C. Rufenach, not shown), a buoy-based model, but an improvement over CMOD4 could not be demonstrated.

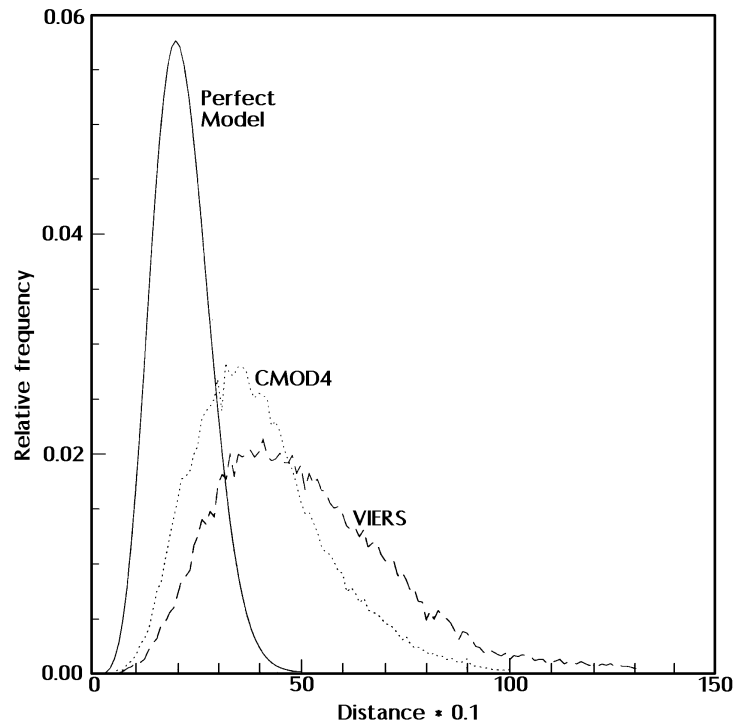


Fig. 5.4: Frequency distribution of the difference between observed σ° s and σ° s obtained from the CMOD4 and the VIERS model for 6 Nov 91, 12 UTC. The distribution for a perfect model is shown as well (from Janssen et al., 1996).

Janssen et al. (1996) have performed a statistical comparison of the results of the CMOD4 empirical model with the results from the VIERS-1 physical model (for three cases only). The statistics, i.e. bias and standard deviation against ECMWF analysed winds, were very similar with a slightly smaller rms error in wind speed for the CMOD4 winds. The latter also gave on average a smaller difference between observed and modelled σ° s (see fig. 5.4). However, Janssen et al. (1996) found that the VIERS algorithm performed better than CMOD4 for high wind speeds. Both models underestimate wind speeds in the high wind speed range, but the underestimation is more pronounced for the CMOD4 model function (see Table 5.1). Janssen et al. (1996) concluded that at the present stage it is difficult to decide which algorithm is better, pointing out that the VIERS model has many possibilities for further improvement.

Case (date)	Case 1 (6 Nov 91, 12Z)		Case 2 (7 Nov 91, 12Z)		Case 3 (10 Mar 92, 12Z)	
	VIERS	CMOD4	VIERS	CMOD4	VIERS	CMOD4
Number	1324	1324	1124	1124	1237	1237
Bias (m/s)	-0.89	-2.56	-2.18	-3.04	-0.14	-1.26
St. Dev. (m/s)	2.02	2.02	2.13	2.51	2.55	2.44

Tab. 5.1: Statistical comparison of VIERS and CMOD4 model winds against ECMWF analysis winds under the restriction that the ECMWF wind speed is higher than 15 m/s (from Janssen et al., 1996).

The above-mentioned transfer functions define a surface in the three-dimensional measurement space. Wind speed and direction V and ϕ can be obtained from minimising a Maximum Likelihood Estimator cost function (MLE, i.e. residual function):

$$MLE = \sum_{i=1}^3 \left[\frac{\sigma_{i,obs}^\circ - \sigma_{i,mod}^\circ}{Kp_i \sigma_{i,mod/obs}^\circ} \right]^2 \quad (5.10)$$

where $i=1,2,3$ stands for the fore, mid and aft beam, σ_{obs}° is the measured backscatter, σ_{mod}° is the backscatter derived from one of the transfer functions using an estimate of the wind vector, and Kp_i is a constant with a value determined by the instrument noise (typically 0.05, Stoffelen and Anderson, 1995).

$$Kp_i = \frac{1}{B \tau_{sn}} \left[1 + \frac{2}{SNR} + \frac{1}{SNR^2} \left(1 + \frac{\tau_{sn}}{\tau_n} \right) \right] \quad (5.11)$$

where: B = system bandwidth
 τ_{sn} = signal plus noise integration time
 τ_n = noise only integration time
 SNR = signal-to-noise ratio

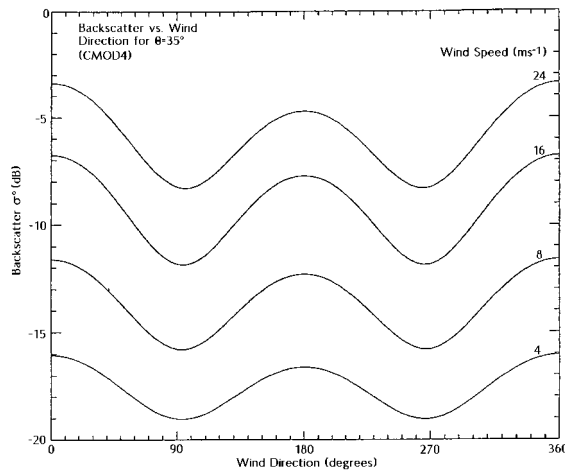


Fig. 5.5: Relationship between wind direction and σ° for different wind speeds for the transfer function CMOD4.

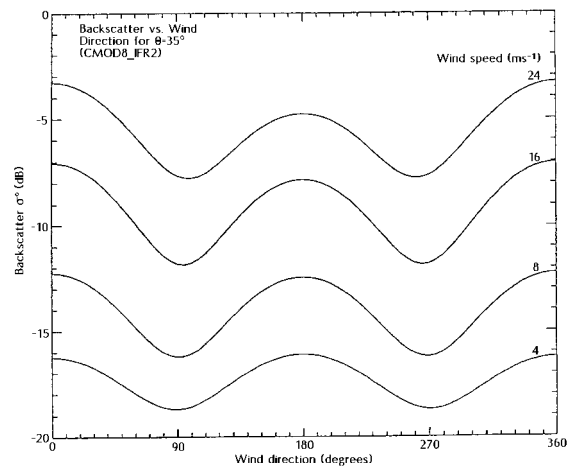


Fig. 5.6: same as fig. 5.5, for the transfer function CMOD8_IFR2.

The normalisation in MLE is a critical point. It may be done using either the observed or the modelled σ° values. Stoffelen and Anderson (1995) showed that, if the modelled values were used in the normalisation in equation (5.10), this would lead to problems in the retrieved wind directions. The frequency distribution of the retrieved wind directions showed unrealistic minima every 90° (some wind directions were practically "forbidden", see fig. 5.7). Therefore they reformulated equation (5.10) using a constant value for the normalisation and introduced a transformation to $Z=(\sigma^\circ)^{0.625}$. This was done to have the same probability for each angular segment of the wind direction. The resulting MLE is:

$$MLE = \frac{1}{SD^2} \sum_{i=1}^3 \left[(\sigma_{i,obs}^\circ)^{0.625} - (\sigma_{i,mod}^\circ)^{0.625} \right]^2 \quad (5.12)$$

where:

$$SD = 0.625 \left[\sum_{i=1}^3 (\sigma_{i,obs}^\circ)^{1.25} \right]^{1/2} g$$

$$g = 2 \left(1 + \frac{45 - \theta_m}{27} \right) \left(1 + \frac{5}{V} + \frac{1}{V^2} + \frac{5}{V^3} \right) h(V) \quad (5.13)$$

$$h(V) = \begin{cases} 1 & \text{for } V \leq 15 \\ 1 + (V - 15)^2 / 100 & \text{for } V > 15 \end{cases}$$

$\theta_m = \text{incidence angle of mid beam}$

In equation (5.13) V is derived a priori from the σ_{obs}° values of the fore and the aft beam and therefore SD is a constant during the minimisation of the MLE function.

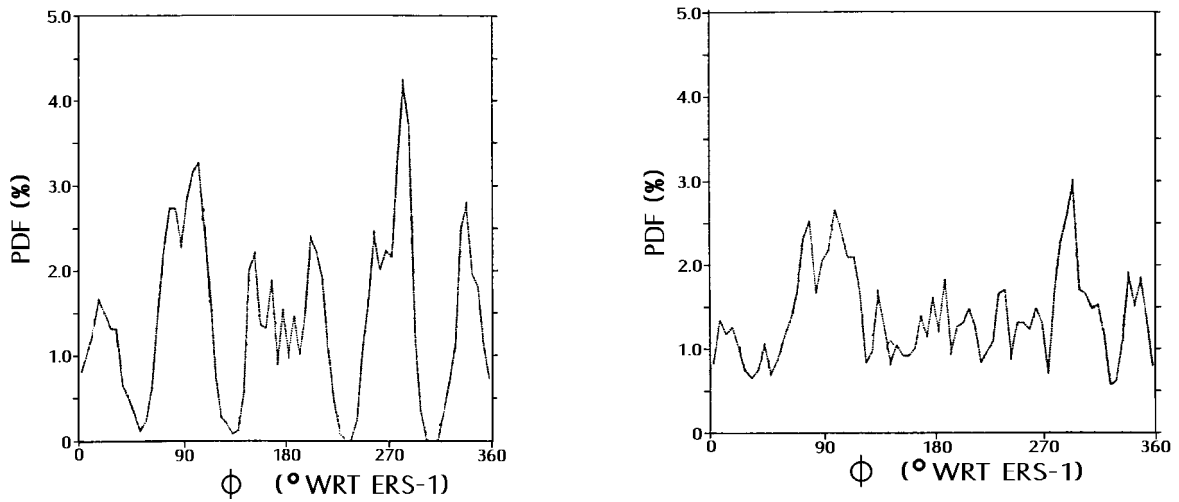


Fig. 5.7: Distribution of wind direction (rank 1 solutions) measured relative to the satellite movement with normalisation using the σ° s from the model function (left picture) or using a constant normalisation (right picture, from Stoffelen and Anderson, 1993).

6

Ambiguity removal

For each data location, the inversion process explained in the previous section may produce up to six ambiguous solutions. Due to the noisiness, the measurements do not lie on the cone of the transfer function and several possibilities exist to allocate the measurements to a point on the cone, especially for the triplets that lie inside the cone. But even if the measurements were noise-free, the determination of the wind direction would still not be unique for some special cases. Two noise-free ambiguities, approximately 180° apart, may arise due to the biharmonic nature of the transfer function with respect to the wind direction. This is valid for those points that fall on crossings of two leaves of the transfer function (see fig. 5.1).

The ambiguities are the minima of the MLE function, which is a function of wind speed and direction, measuring the difference between the observed σ° s and those calculated from the transfer function for a given wind speed and direction (examples are given in fig. 6.1). Four or six ambiguous solutions will arise from σ° triplets that lie close to the centre of the cone. On the contrary, only one solution (no ambiguity) is possible for triplets that lie far outside the cone or for weak winds. The retrieved wind vectors are very similar in wind speed, but vary considerably in wind direction. Therefore, the ambiguity problem may be considered as a problem for the wind direction only. In fact, the wind speed can be determined to a high precision from the sigma naughts from the fore and the aft beams.

The change from the two-beam (SEASAT scatterometer) to the three-beam (ERS scatterometer) configuration has reduced the number of ambiguous solutions (83% of all SASS wind measurements had four solutions, Chelton et al., 1989). In fact, the three-beam configuration often produces only two markedly different solutions, usually about 180° apart. Each solution is assigned a probability of being the closest to the true wind vector, and the solutions are ranked according to this probability (rank 1 has the highest probability). The probability is calculated using the distance to the cone, which is given by the value for the MLE function.

There are at least four different methods for removing the ambiguity:

- The subjective analysis by trained meteorologists.
- The so-called autonomous ambiguity removal scheme: this scheme uses only information from the scatterometer data (no other data). In this category there are several sub-categories: the ambiguity removal by using a Circular Median Filter (CMF) and the wind ambiguity removal by the use of Neural Network Techniques.
- A removal scheme that compares the ambiguous wind vectors to a background wind field.
- The assimilation of the ambiguous wind vectors in an NWP model: the ambiguity removal is performed implicitly within the 3D/4D-Var analysis.

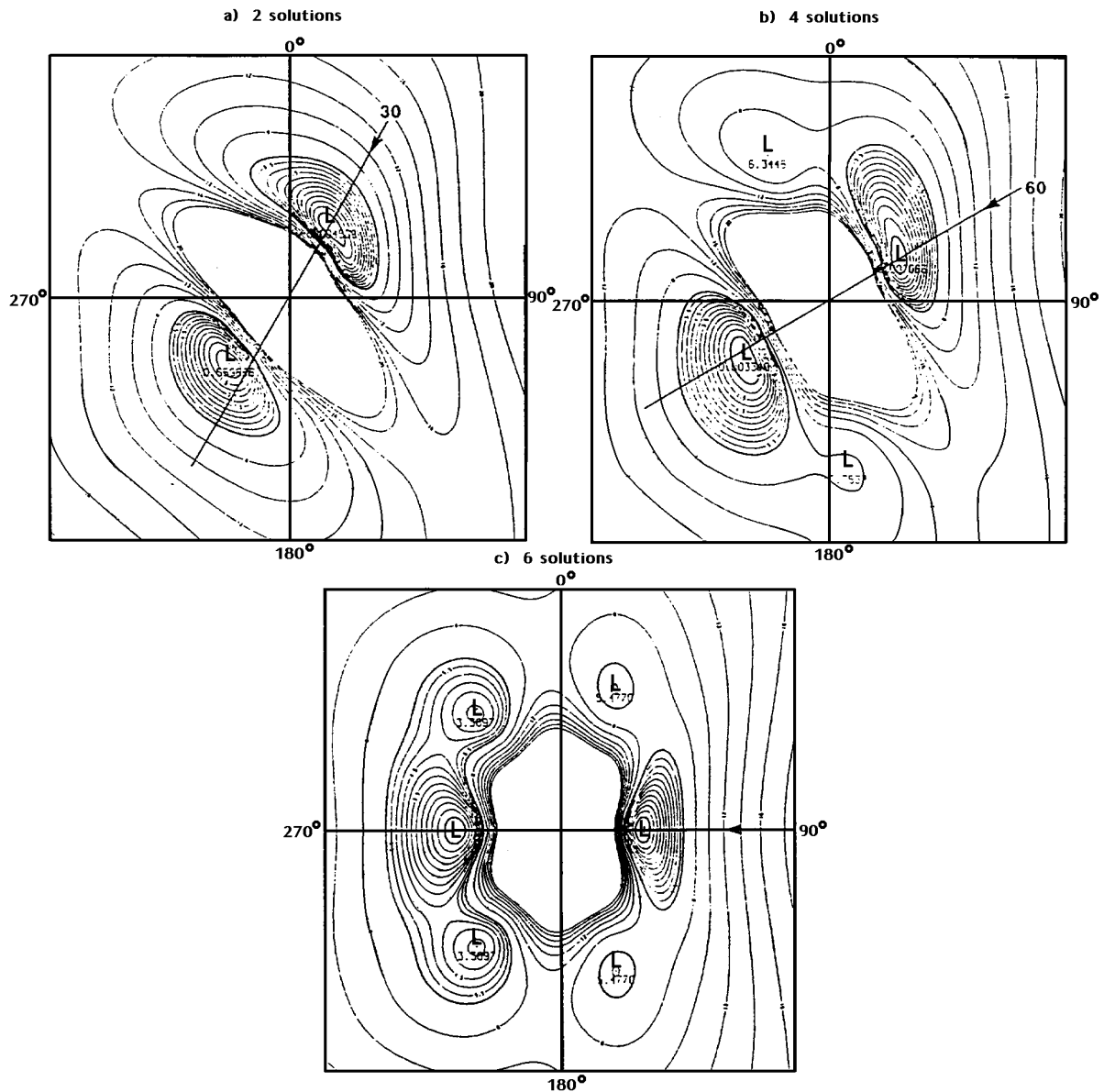


Fig. 6.1: The MLE function (cost function), as a function of wind components in the coordinate system defined by the satellite forward motion, for triplets of noiseless σ° measurements evaluated using CMOD1. The true wind speed is 10 m/s and the wind direction is from (a) 30° (b) 60° and (c) 90° measured clockwise from the satellite direction. Note that the contour interval is smaller near the minima and that no contours are drawn close to the origin where the MLE function is very high (from Hoffman, 1992).

6.1 THE SUBJECTIVE AMBIGUITY REMOVAL

A subjective analysis of ambiguous wind data from the SEASAT-A Satellite Scatterometer (SASS) was performed by the Jet Propulsion Laboratory (JPL) for 14 days in September 1978 (Chelton et al., 1989). Two independent teams of investigators, the University of California at Los Angeles and AES Canada, collaborated to produce a unique wind vector field. The multiple solution wind vectors were plotted for several orbits of the satellite, and streamline analysis of surface winds were constructed using subjective pattern-recognition techniques together with all available conventional ocean wind data. This streamline information was then used in an objective way to choose the vector with direction closest to the direction indicated by the

streamline analysis. The results from the two independent teams were then compared. If there were differences, the streamline analysis was repeated until a "consensus" dataset was produced in an iterative fashion.

The scope of this tremendous exercise was to check the quality of the wind vector solutions derived by an automated ambiguity removal scheme developed and applied to the complete SASS dataset (96 days) by the Goddard Space Flight Center (GSFC). This objective scheme used a three-pass iterative procedure to remove the directional ambiguity. The two methods agreed exactly in 73% of the ambiguous solutions. The differences for the cases when the two methods disagreed appeared to be random and hence averaged to near zero in spatial and temporal averages of the vector winds. It was therefore impossible for Chelton et al. (1989) to say which method was the better one.

6.2 AUTONOMOUS AMBIGUITY REMOVAL

In the autonomous ambiguity removal schemes the removal is done without use of any additional meteorological information. For each node, all possible solutions are ranked and stored, excluding relative minima not sufficiently small. The decision which solution has to be selected may then result from a consistency check with the neighbouring points or from filter techniques which eliminate noisy "outsiders".

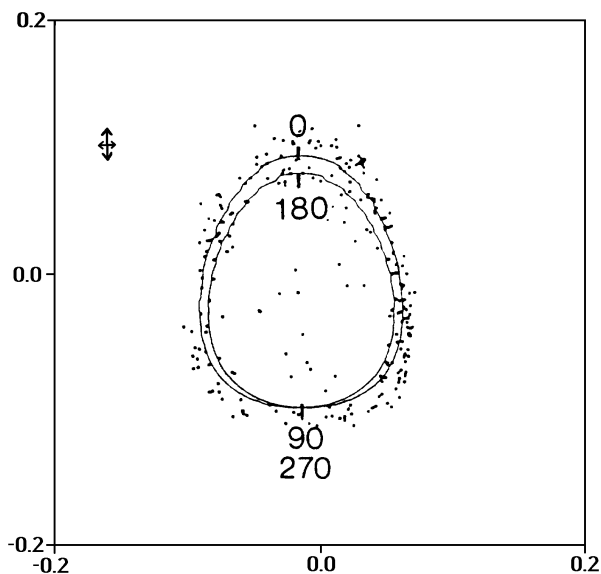


Fig. 6.2: Example of the distribution of measured σ^0 triplets in a cross-section through the cone for node 19. The collocated analysis wind speed is approximately 8 m/s. The crosses, of width $2K_p$, are estimates of the measurement noise (from Stoffelen and Anderson, 1993).

Concerning the transfer function (the cone, see fig. 5.1), the leaves can be fairly close together in measures of the noise (see fig. 6.2 for CMOD2 transfer function). The distance is generally smaller than the standard deviation of the noise. This implies that an autonomous ambiguity removal is not likely to be very successful (Stoffelen and Anderson, 1995). It could also be shown that the rank of the correct solution is horizontally correlated and that the probability of the two wind vector solutions is close to 50%. However, first results with the transfer function for NSCAT scatterometer, called SAS-2, suggest that the leaves of the cone are better separated (the upwind/downwind amplitude is larger, 40% compared to 10% for ERS), which will probably lead to better results for the autonomous ambiguity removal.

6.2.1 Ambiguity removal by simple horizontal filters

Using as input information the different solutions (mainly the rank 1 and rank 2 solutions) for each node, two “antiparallel” wind fields may be compiled for an area of approximately 500 x 3000 km with the main constraint of directional consistency. This can be achieved by applying horizontal filters. The ambiguity removal is accomplished by selecting one of the two fields, or the one with the lowest average MLE, or the one with the highest number of rank 1 solutions. Since there is no additional information used, wrongly ranked areas may be reinforced.

6.2.2 Ambiguity removal using a Circular Median Filter

The problem of detecting and correcting wind direction retrieval errors is analogous to the noise removal problem found in image processing applications (Schulz, 1990). In a uniform wind field a wind vector pointing in the opposite direction to the neighbouring points is easily detected. The same is true for an occasional bright pixel in an otherwise dark image area. An effective technique for removing this kind of “noise” is to use a median filter where each data value is replaced with the median of the surrounding data. For circular data such as the wind direction, a sequence of numbers may have multiple medians. A unique median can be defined by selecting the one closest to the circular mean.

The effect of a median filter is to replace a noise-contaminated value with the value of a noise-free neighbouring point, provided that less than half of the numbers within a window are “contaminated”. When applied to wind fields, median filters will not remove features such as convergence zones characterised by abrupt changes in wind direction. First, the most likely wind vectors, the rank 1 solutions, are selected within a window of $N \times N$ points (e.g. $N=7$). Then, the circular median filter is applied to the wind directions weighting the neighbouring points according to the mean wind speed of the aliases. As a result of the filtering, the selected wind vectors are updated by choosing among the aliases the direction closest to the median. The filtering and the updating are repeated until the selected wind vectors do not change from one iteration to the next or until a maximum number of iterations is exceeded.

6.2.3 Ambiguity removal by use of neural network techniques

Badran et al. (1991) presented a method for the ambiguity removal based on neural network techniques, which was one of the first applications of neural networks in oceanography/meteorology. The main objective was to draw attention to the performances of a new method and not to propose an operational scheme. The concept of the method is to determine the optimum topological filter to de-alias the wind direction, which makes the method similar to the circular median filter technique used by Schulz (1990). Two space filters (size of the window 5×5), one for the 180° ambiguity and one for the 90° ambiguity, are applied successively to the ambiguous wind field. The result of the filters is applied at the end of the computation in order to avoid possible propagation of errors. Three iterations of the filters (three stages of the relaxation) provided sufficiently good performances of the method.

The weights of the filters have been computed during a learning phase from a specific situation where the actual wind vectors were known. A quasi-linear multilayer network with one hidden layer was applied. One observation day (eight successive swaths of 18 August 1985) was used in the study resulting in 2000 elements for the training data sets. It may be questioned if this was enough for encoding the large variety of meteorological situations in the learning process.

Since no ERS-1 scatterometer data were available, σ 's have been simulated using ECMWF wind fields with 110 km resolution interpolated onto a 50 km x 50 km grid. A Gaussian noise was added to the direction and four estimates for the wind direction have been simulated (the true direction, and $\pm 90^\circ$ and 180° ambiguities). The validity of the method has not been shown for real scatterometer data. The main problems in applying the method to the complexity of real data are assumed to be: a) the creation of a representative training data set; b) the choice of the window size; c) the treatment of clusters and spatially correlated errors which can dramatically affect the skill of the method.

6.3 AMBIGUITY REMOVAL WITH A BACKGROUND FIELD

As an example of a removal scheme that uses a background wind field the revised procedure of the software package PRESCAT is presented (Stoffelen and Anderson, 1995, 1997). PRESCAT has been developed at the ECMWF for the processing (inversion and ambiguity removal) of the ERS scatterometer data. The background field is taken from a short-range forecast (e.g. ECMWF FGAT (First Guess at Appropriate Time) winds). In this scheme only two solutions coming from the inversion process are stored. From these solutions the one with the direction closest to the background wind field is initially selected. The so-produced initial field is quite reasonable, but in small regions (about 5% of the processed area) the solution appears to be unmeteorological, i.e. the wind directions are not consistent with the synoptic situation. In order to increase meteorological (i.e. directional) consistency a filter based on SLICE (Offiler, 1987) is applied. The filter consists of a box of 5x5 nodes, which slides over the wind field. At the edge of the path a box of 3x5 nodes is used. An along-track section of up to 2850 km (114 rows) is processed (filtered) at the same time. The box always slides over the area four times, regardless of how many points have been changed in a pass. The starting point and the propagation direction of the filter change from pass to pass (e.g. for the first pass, it starts at the inside part of the swath propagating in the direction opposite to the satellite propagation, see fig. 6.3). For every box a mean likelihood L is calculated:

$$L_i = \frac{1}{N} \sum_{j=1}^N C_j \exp\left(-0.5\left[\frac{(u_i - u_j)^2 + (v_i - v_j)^2}{q^2}\right]\right) \quad (6.1)$$

where:

- i is equal to 1 or 2 for the two ambiguous solutions;
- q^2 is the wind component variability ($q=2.5$ m/s);
- N is the number of surrounding points for the centre point (24 in a 5x5 box, when no data is missing);
- C_j represents the normalised confidence of the selected solution at the point j .

For the first pass of the filter, the confidence coefficients for each point are calculated from the MLE value for the rank 1 solution and the difference between the selected solution and the background wind vector. After each filter pass, the confidences C are updated according to:

$$C_{n+1} = C_n + (1 - C_n)L \quad (6.2)$$

A low/high confidence is identical to a weak/strong influence on the selection of the solution at neighbouring points.

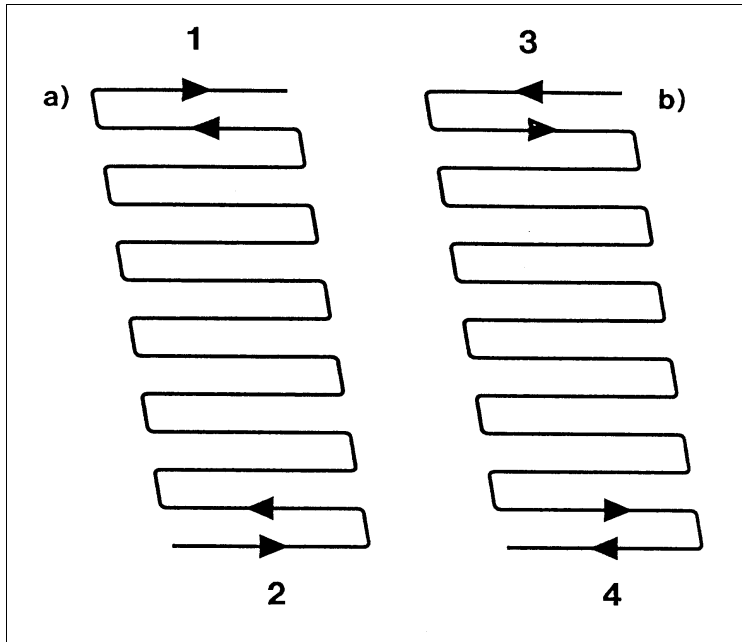


Fig. 6.3: Schematic of the way the filter SLICE slides along an ascending orbit in (a) the first two iterations and (b) the second two iterations (from Stoffelen and Anderson, 1995).

L is calculated for both possible solutions, and the solution with the highest value for L is selected. The result of the filter, i.e. the switching from one solution to the other (if necessary), is applied immediately to the selected wind field, so that information from a high confidence area can propagate quickly to low confidence areas.

6.4 AMBIGUITY REMOVAL BASED ON ASSIMILATION

For scatterometer data, Stoffelen and Anderson (1995) have shown that it is better to assimilate scatterometer winds, rather than assimilating directly backscatter measurements (using a complicated observation operator). The assimilation needs correct estimates of the error statistics of the assimilated variable, and adequate error statistics in the σ° -space are more difficult to specify (due to the strong non-linearity of the transfer function) than error statistics in the wind-space. Gaffard and Roquet (1995) described the assimilation procedure of scatterometer winds and assessed the quality of the 3D-Var ambiguity removal. Experiments with variational analysis of ocean surface winds based on ERS altimeter and scatterometer measurements are also ongoing at the Norwegian Meteorological Institute (Harald Schyberg and Lars-Anders Breivik, private communication). In the variational analysis, the ambiguity removal is performed implicitly using the two ambiguous wind solutions and all the additional information from background field and nearby wind observations. Additionally, in variational analysis, physical constraints on the estimated state of the atmosphere help to avoid the formation of fast growing gravity waves.

The wind solution selected in this way was found to be identical to the one selected by PRESCAT (ambiguity removal with a background field) in 99.3% of the cases for wind speeds higher than 4 m/s (Gaffard and Roquet, 1995). The differences are very small, but may be important in some specific cases. In Gaffard and Roquet an example is shown where the 3D-Var ambiguity removal performs clearly better than the PRESCAT scheme (see fig. 6.4).

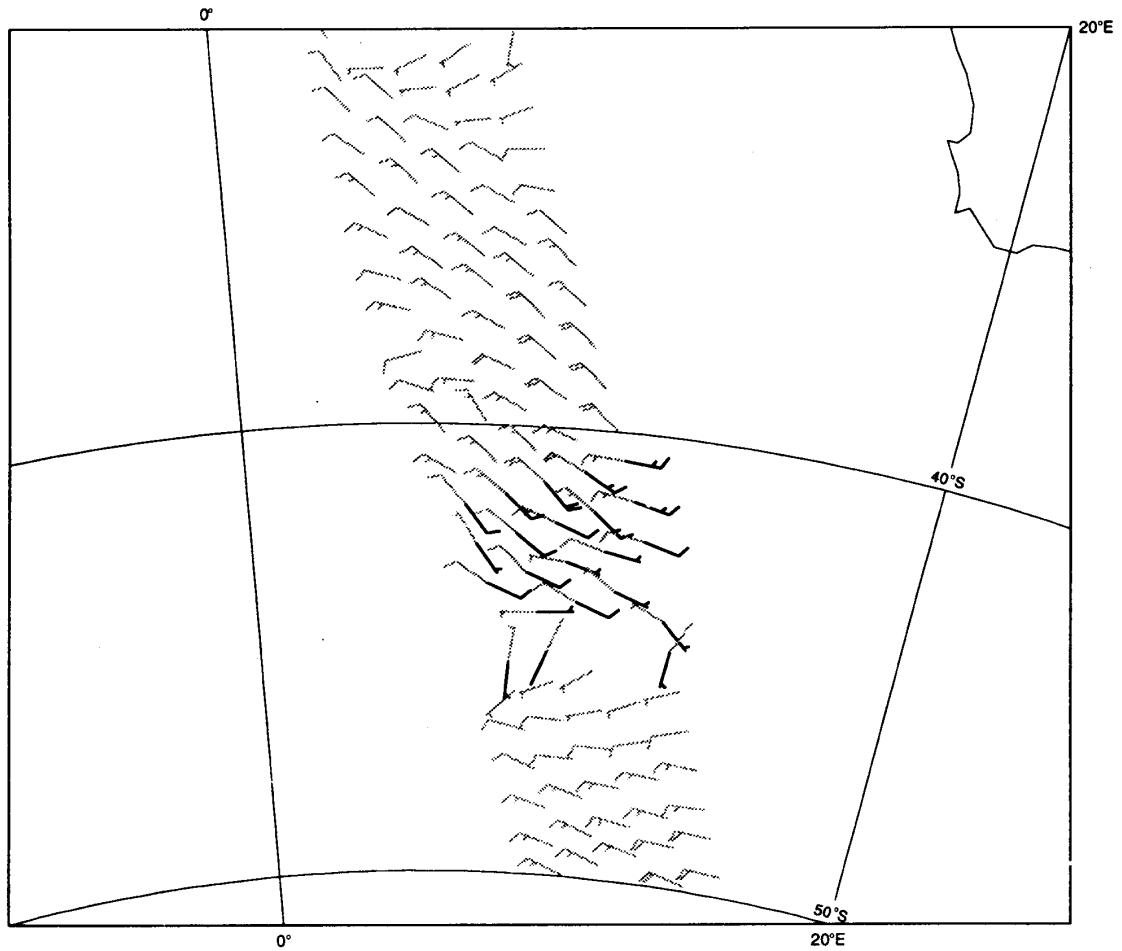


Fig. 6.4: Comparison of scatterometer winds de-aliased by PRESCAT (black wind flags, ambiguity removal with a background field) and by the 3D-Var assimilation system (grey wind flags), on 17 December 1994 at 00 UTC south-west of the African coast. PRESCAT solutions are visible only when they differ from the 3D-Var ones (from Gaffard and Roquet, 1995).

7

Quality control of retrieved wind data

Errors of retrieved scatterometer winds may be due to measurement (instrumental) errors, processing errors, incorrect ambiguity removal, sea ice contamination and geophysical errors (strong rain, changes in SST, sea state, slicks). Generally, the errors are larger at low incidence angles, i.e. at the inner edge of the swath (see fig. 7.1 and table 8.1).

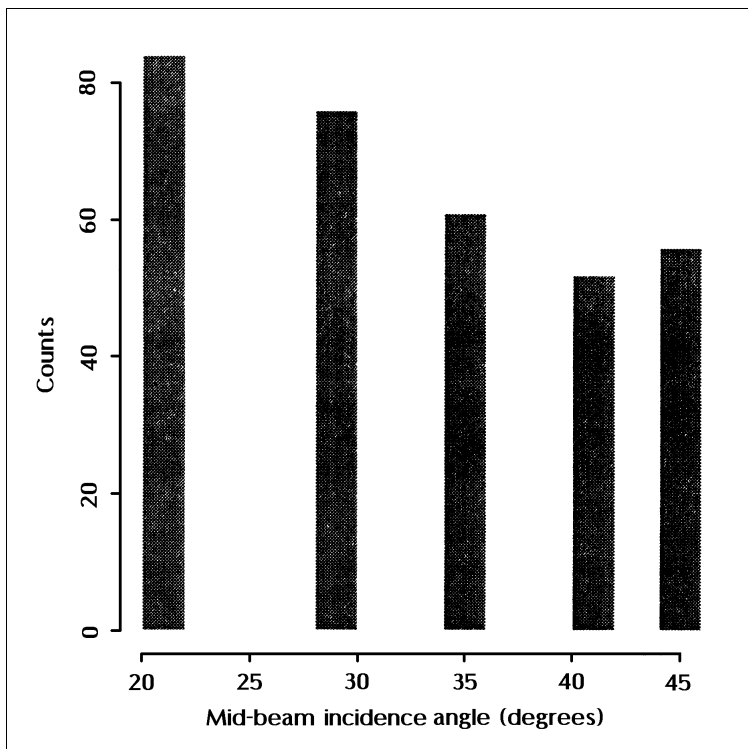


Fig. 7.1: The number of ERS-1 data failing the Optimum Interpolation (OI) quality control (buddy check) of the assimilation scheme of the ECMWF model as a function of incidence angle. Data are from 31 December 1991, 1200 UTC. Only five cells (nodes) are retained for the assimilation because of the 100 km resolution of the model (from Hoffman, 1992).

A first quality control comes from the quality flags that are operationally set by ESA for the data of the ERS scatterometer. These flags include information on transmission errors, antenna arcing, land contamination and signal-to-noise ratio contamination. A second quality control is done during the retrieval process. Gaffard and Roquet (1995) describe the quality control in the scheme used at ECMWF (PRESCAT). Data are rejected if too many σ° s in a cell are missing or if the signal-to-noise ratio is larger than 10% for one of the three beams. Data are also rejected for areas where SST is less than 0°C (possible sea ice contamination). Another significant number of σ° triplets is rejected if the distance to the cone exceeds three times the σ° scatter estimate (between 1% and 2% of triplets fail this test, Stoffelen and Anderson, 1997b). The triplets that fail this test are usually in areas of strong winds, close to intense fronts or low pressure systems. Finally, the calculation of the mean normalised distance to the cone over a period of six hours gives important information on the quality performance of the scatterometer data (see fig. 7.2).

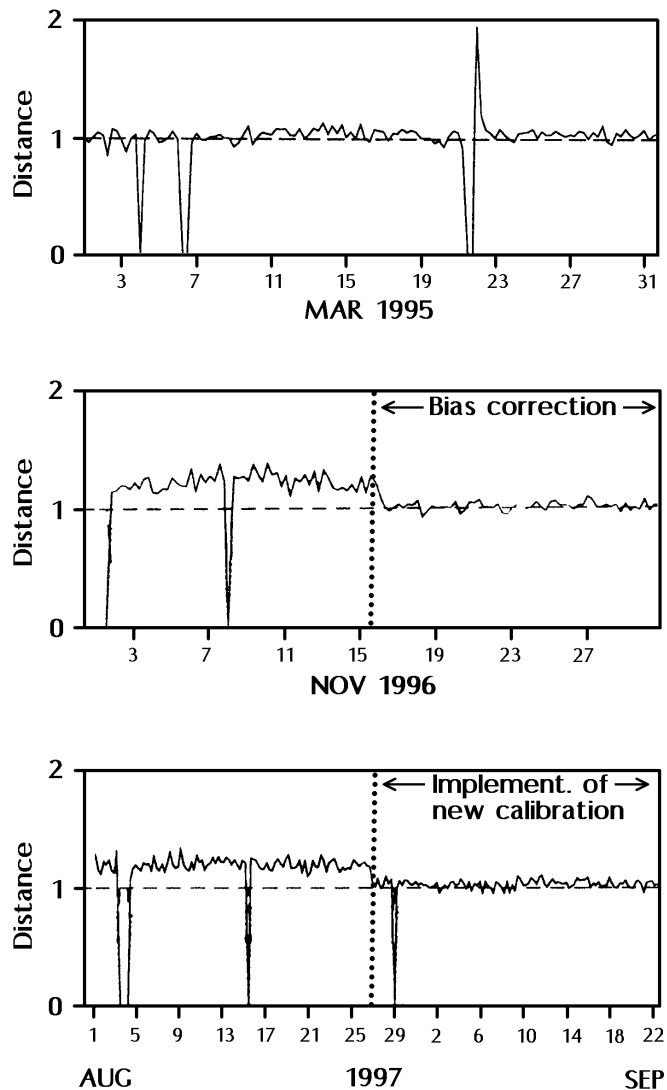


Fig. 7.2: Monitoring of the mean normalised distance of the σ^o s to the cone averaged over a period of six hours for the nodes 3-4. In the absence of instrumental problems, this distance should be close to one. On 22 March 1995 00 UTC (top panel), a problem was detected, which was due to ERS-1 orbital manoeuvres. Bias corrections and implementations of new calibrations, as in November 1996 and August 1997 respectively, become clearly visible (top panel from Gaffard and Roquet, 1995, other panels courtesy D. Le Meur).

Prior to assimilation, a third check of the retrieved and de-aliased scatterometer winds may be performed by:

- Checking if the values are physically reasonable;
- Comparing the values to a more timely background field (a first guess field);
- Comparing the observation to an analysis made without the observation in question (the so-called OI-check or buddy-check). If the difference is large, the value is rejected. Stoffelen and Anderson (1997) report that typically about four PRESCAT winds are rejected every analysis by the buddy-check out of about 3000 measurements presented.

Finally, quality control (i.e. the filtering of remaining incorrect aliases) can also be done by putting constraints on the observed divergence (Bell and Holt, 1993).

8

Geophysical calibration and validation of scatterometer winds

Scatterometer winds are specified to be those equivalent to a measurement at a reference height of 10 m in a neutrally stable atmosphere. Therefore, prior to comparing in situ measurements to scatterometer winds, they must eventually be adjusted to a height of 10 m. This can be achieved by using a boundary layer model where the relation between wind vector and height is given as a function of stability, surface stress and surface roughness (see chapter 4).

Various methods for the geophysical calibration of the ERS scatterometer have been proposed prior to the launch of the satellite, including the comparison against buoy measurements, NWP data and dedicated aircraft campaigns. In the end, all these data sources were used for the RENE-1 calibration campaign for ERS-1, which took place off the coast of Norway during the period mid-September to mid-December 1991. Extensive in situ measurements of winds were made to calibrate the wind product derived from the ERS-1 scatterometer. In particular, the UK Meteorological Research flight C-130 aircraft measured low-level winds beneath the scatterometer swath. Together with data from other aircraft (a Do-228), ships and buoys, the measured in situ data were objectively analysed to form a unique calibration data set (see example in fig. 8.1). By this an optimised relationship (model function) between the σ° s and the local wind vector could be determined. It could also be verified that the ERS scatterometer winds met their accuracy requirements of 2 m/s rms (or 10%, whichever is higher) for wind speed and 20° for wind direction (to be met over the range 4 to 24 m/s). Using only a subset of the RENE-91 data, which was taken to most closely represent the “true” neutral-stability wind conditions at a height of 10 m, the accuracy of the ERS scatterometer winds was even better than specifications: 1.5 m/s for wind speed and 8° for wind direction.

The most common method for validating scatterometer-derived winds is comparing them to buoy or ship measurements. As mentioned before, the buoy/ship wind speed has to be adjusted to a height of 10 m and a collocation process has to be performed. Typically, observations within 50 km in space and 30 minutes in time from the scatterometer wind are used. Another possibility is to compare winds from very small islands with nearly contemporaneous measurements taken by the scatterometer during overpasses of the island (see e.g. Davison and Harrison, 1989, 1990).

Several validation experiments have been performed by UKMO, IFREMER and JPL. Jones et al. (1982) and Offiler (1984) validated the SASS winds against surface observations, revealing a quite good agreement between these two data sets. They concluded that SASS met its design target of rms errors less than 2 m/s in wind speed and 20° in wind direction (the accuracy requirements for SEASAT were essentially the same as those defined for the ERS scatterometer, see Grantham et al., 1977). Woiceshyn et al. (1986) and Anderson et al. (1987) found that SASS wind speeds were usually biased low at high speed and slightly high at low speed.

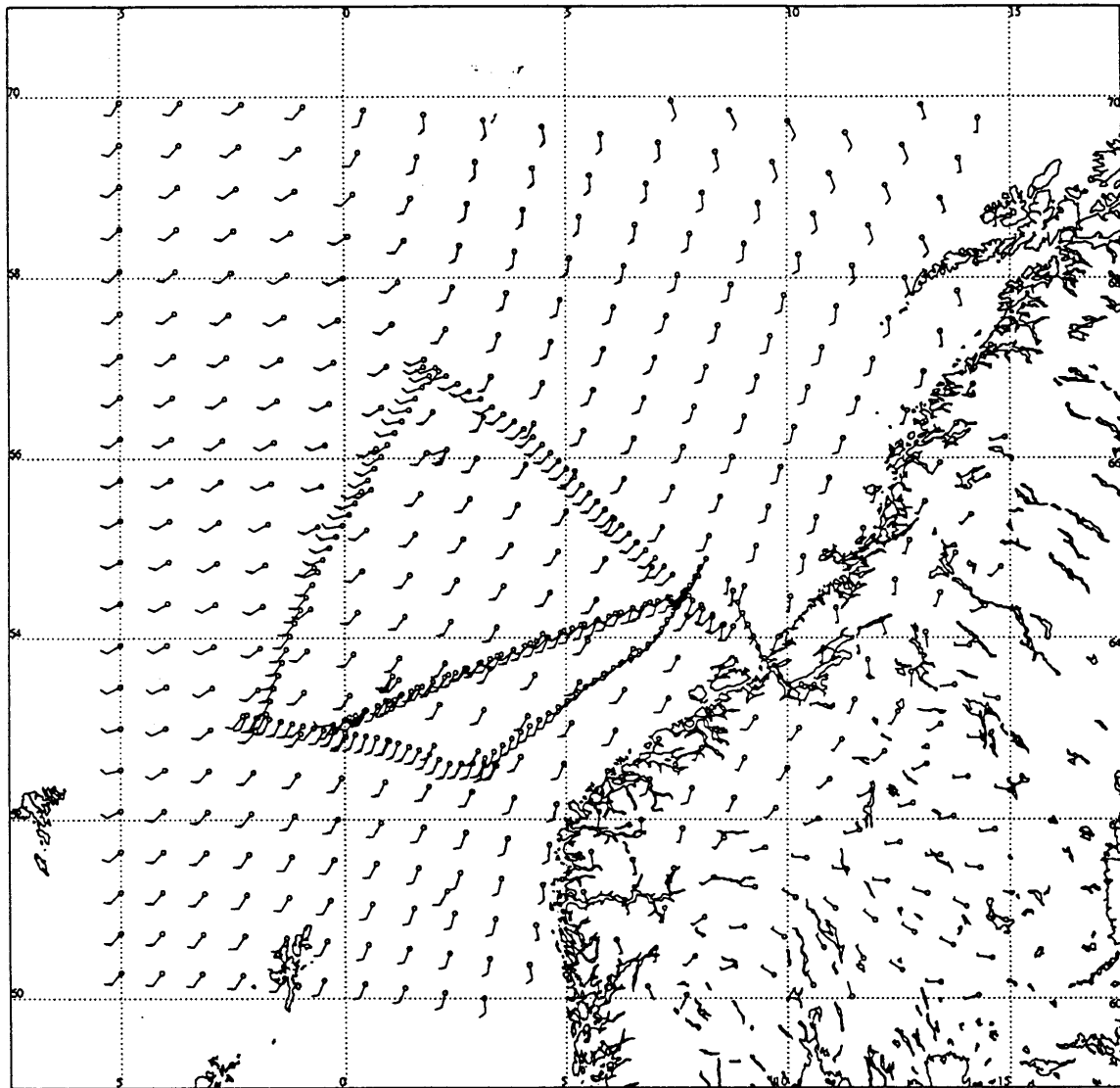


Fig. 8.1: Example of the data inputs (aircraft measurements, ships, buoys and NWP background field) for the RENE-91 analyses in the Haltenbanken area off the coast of Norway. Data were used within three hours of the ERS-1 overpass at 1049 UTC 2 December 1991 (from Offiler, 1994).

During March 1992 the UKMO performed a validation of ERS-1 scatterometer winds against reliable ship observations (Bell and Holt, 1992). This was shortly after the final engineering calibration of ERS-1 scatterometer winds. The comparison was broken down into four speed bins (<5, 5-10, 10-15, 15-20 m/s). The number of ship observations was much smaller (some thousands in each class) than the scatterometer wind observations (up to one million in a class). The result was that, for all wind classes, the ship winds were slightly higher than the scatterometer winds (about 1 m/s higher). This was tentatively explained with the fact that ship winds are taken at a height which is somewhat higher than 10 m. The standard deviations of observed wind speed and wind direction from model background is smaller for the scatterometer winds compared to the ship observations (see table 8.1). Therefore, Bell and Holt (1992) came to the conclusion that scatterometer wind data are of “substantially higher quality” than ship data.

		<5 m/s	5-10 m/s	10-15 m/s	15-20 m/s
Wind speed	Scat – model	1.6	2.3	2.8	3.0
	Ship – model	2.1	2.5	3.1	3.5
Wind direction	Scat – model	37.7	23.4	18.5	15.4
	Ship – model	53.7	32.4	22.5	17.5

Tab. 8.1: Standard deviations of observed scatterometer and ship wind speeds and wind directions from model background (UKMO operational global model) for different speed classes (from Bell and Holt, 1992).

In a recent experiment, David Halpern from JPL (Halpern, 1997) compared three different scatterometer wind products (ESA product using CMOD4, IFREMER product using IFR-2 and JPL product) to measurements from a sophisticated buoy positioned in the Arabian Sea. The IFREMER wind product gave the best result with a mean difference of 0 m/s and a slope slightly different from 1.0. An additional test was performed by checking the capability of the scatterometer data to estimate the onset of the monsoon (defined by winds higher than 7.5 m/s from south-west direction for more than six days) in the area under investigation. For the IFREMER winds a perfect agreement with the buoy data was found (for the year 1995), whereas the ECMWF analysis data gave the onset with a delay of four to five days.

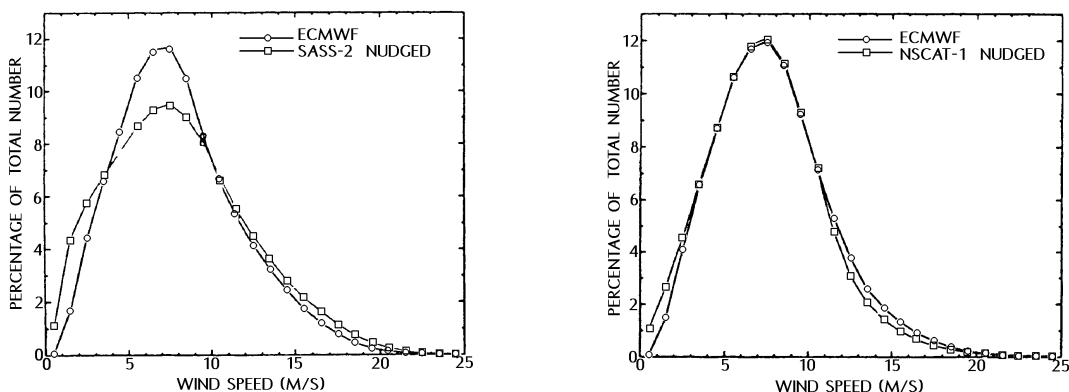


Fig. 8.2: Histograms of the globally observed wind speeds for NSCAT winds and for the ECMWF analysis in bins of 1 m/s (left using the SASS-2 model function, right using the newly developed NSCAT-1 model function). The data are from the area 52°S to 52°N for the period 15 September to 29 October 1996 (about 3.3 million wind vectors, from Ebuchi, 1997).

Another validation commonly used is comparing the scatterometer winds to NWP model data (see e.g. tab. 9.1 and fig. 9.1). Histograms of global wind speed and wind direction data easily show systematic biases in the scatterometer data (compared to model data). An example was given by Ebuchi (1997) who found that the histograms of the preliminary NSCAT winds (using the SASS-2 model function) were quite different compared to ECMWF winds (see figs. 8.2, 8.3 and 8.4). The NSCAT SASS-2 winds showed markedly higher frequencies for low wind speeds (fig. 8.2a), the histogram depended on the incidence angle (fig. 8.3), which it should not do, and there was a peak in the wind direction distribution, i.e. a preferred wind direction (fig. 8.4). This led to the formulation of a new transfer function for NSCAT data, called NSCAT-1, which gives much better results (see fig. 8.2b). Ebuchi also showed how the wind direction of the ERS scatterometer winds distribution improved progressively when changing from CMOD2 to CMOD3 and CMOD4 transfer function. At ECMWF, ERS scatterometer winds are routinely

compared to model winds, and, if systematic biases are found, the model function is eventually changed (assuming the model wind to be the true wind).

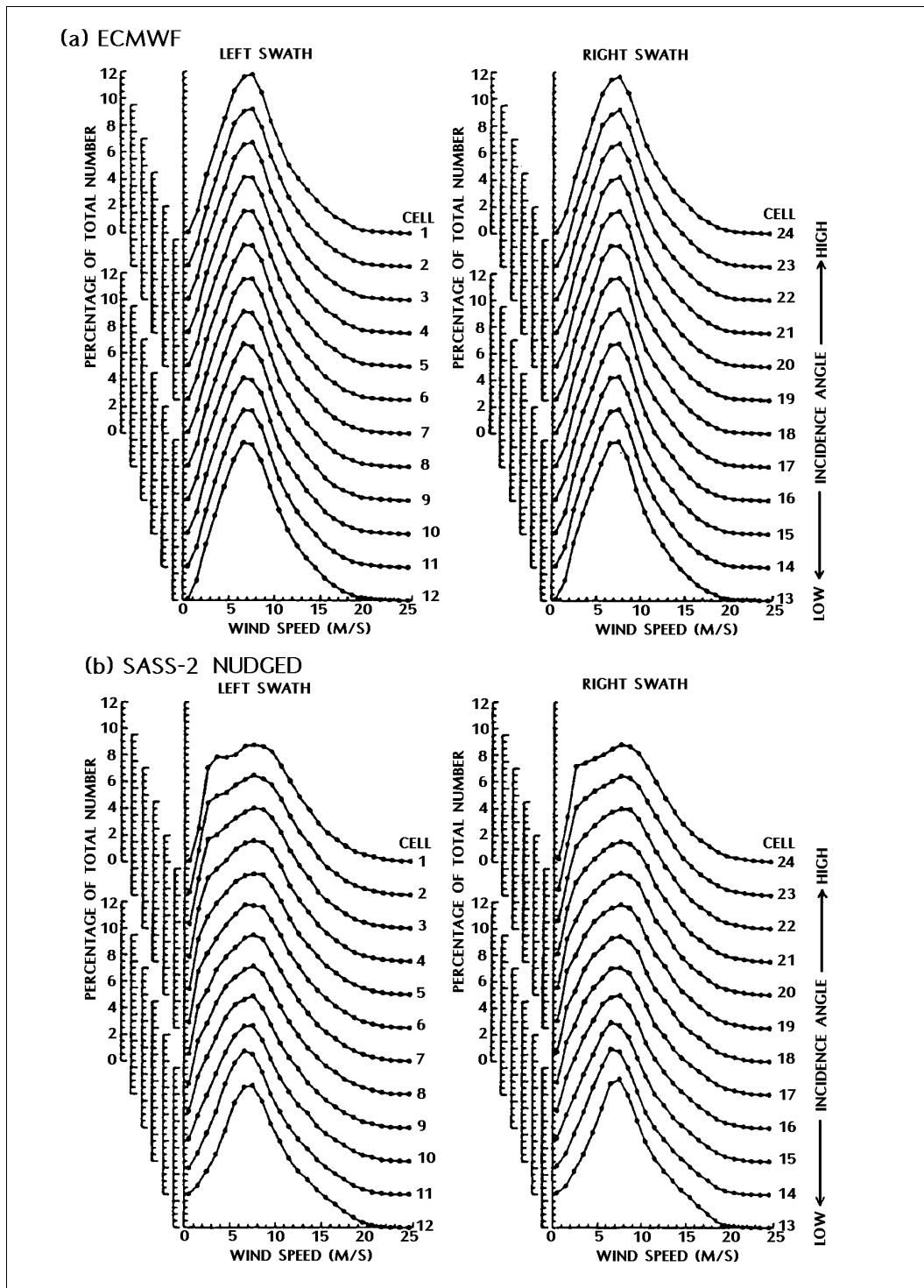


Fig. 8.3: Variation of wind speed histograms with the cell location: (a) ECMWF analysis winds, (b) NSCAT winds retrieved with the preliminary model function (SASS-2). The same data as for fig. 8.2 were used (from Ebuchi, 1997).

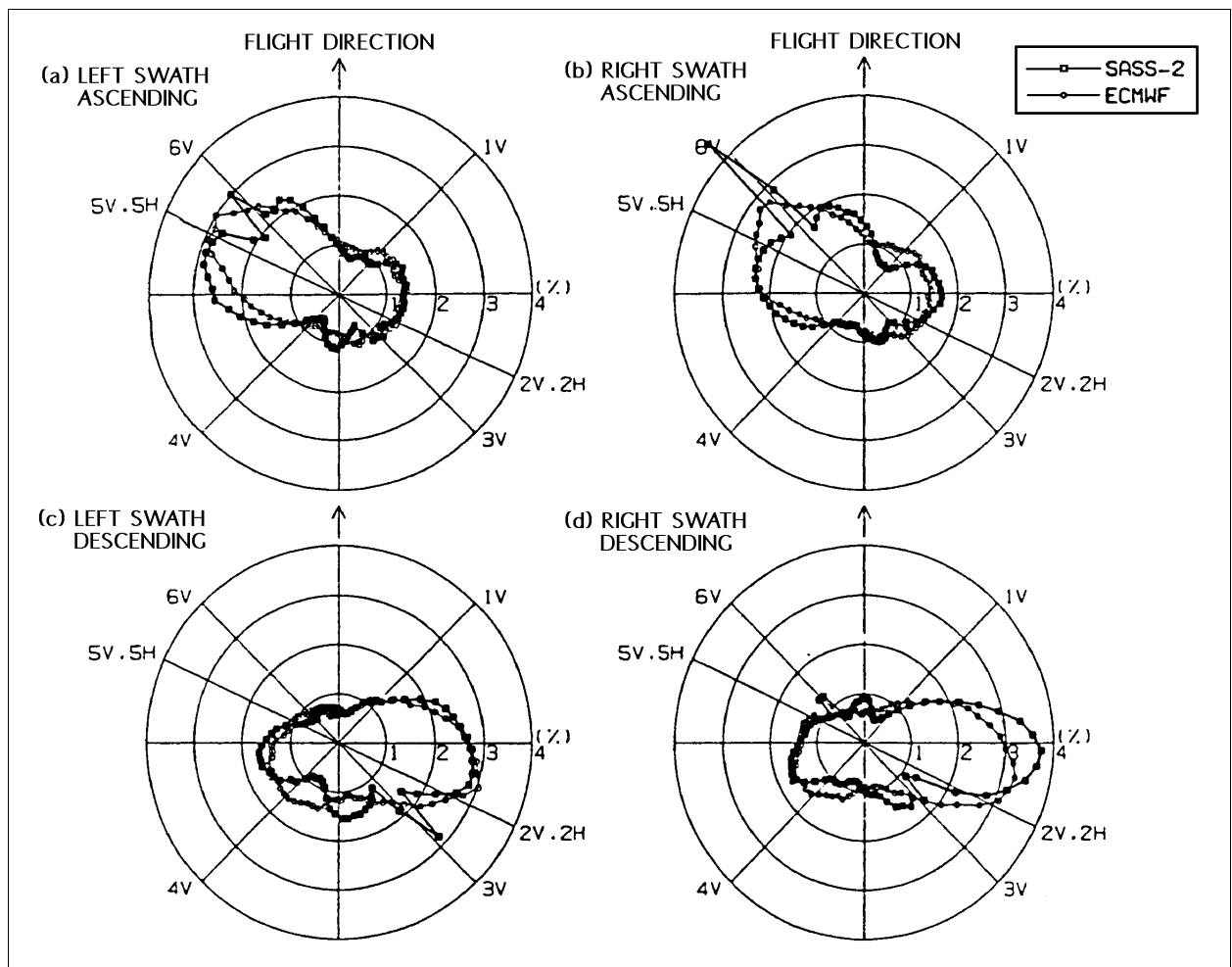


Fig. 8.4: Distributions of the SASS-2 NSCAT and ECMWF wind directions relative to the spacecraft flight direction. The number densities of bins of 5 degrees are shown as percentages of the total number of data. Only those wind vectors with speeds ranging from 5 to 15 m/s were used. (a) left swath and ascending paths, (b) right swath and ascending paths, (c) left swath and descending paths, (d) right swath and descending paths (from Ebuchi, 1997).

9

Assimilation of scatterometer winds in NWP models

Scatterometer winds are more accurate than any other operationally available surface wind observations over the oceans. When plotting the components of scatterometer winds against NWP forecast winds, correlations of up to 97% are achieved (Stoffelen et al., 1993, see also fig. 9.1), higher than for conventional data sets like moored and drifting buoys, automatic and non-automatic ship observations and island stations. Table 9.1 shows some statistics of scatterometer minus ECMWF analysis winds. It can be seen that the departure standard deviation for the wind speed increases slightly with increasing node number, whereas for wind direction it decreases. The vector rms decreases with increasing node number, indicating that the overall errors of scatterometer winds are smaller at high incidence angles.

Node	Wind direction				Wind speed			
	Nbr.	Bias	Sd	Vrms	Nbr.	Bias	Sd	Vrms
1	9168	0.88	23.81	3.73	10883	-0.48	1.93	3.54
3	9511	0.92	21.13	3.37	11008	-0.41	1.94	3.24
5	9717	1.26	19.89	3.21	11199	-0.30	1.96	3.10
7	9783	1.46	19.17	3.16	11355	-0.28	1.97	3.05
9	9794	1.10	19.07	3.17	11472	-0.26	1.99	3.05
11	9762	1.42	18.86	3.15	11480	-0.24	1.98	3.02
13	9700	1.48	18.69	3.15	11526	-0.25	2.00	3.01
15	9656	1.29	18.71	3.15	11545	-0.25	2.05	3.02
17	9638	1.11	18.31	3.14	11564	-0.24	2.07	3.00
19	9677	0.98	18.36	3.11	11616	-0.24	2.04	2.98

Tab. 9.1: Departure statistics of ERS-1 scatterometer winds minus ECMWF analysis wind speeds (right) and directions (left), for all odd nodes. Direction statistics are only made when the average wind speed exceeds 4 m/s. Nodes are numbered from inside swath. Nbr = number of observations used in the collocation experiment, Sd = standard deviation, Vrms = vector rms (from Stoffelen et al., 1993).

Given the high accuracy of the retrieved scatterometer winds, it certainly is worthwhile to assimilate the data into NWP models. Early tentatives to assimilate scatterometer data in a model have been made by Baker et al., 1984, Duffy et al., 1984, Yu and McPherson, 1984, Duffy and Atlas, 1986, Anderson et al., 1987, Atlas et al., 1987, and Ingleby and Bromley, 1991. The assimilation schemes involved in these experiments are mostly based on statistical methods (e.g. Successive Correction (SC), Cressman, 1959, Optimum Interpolation (OI), Gandin, 1963). They require a precise knowledge of the correlation (or structure) functions of the errors of scatterometer winds.

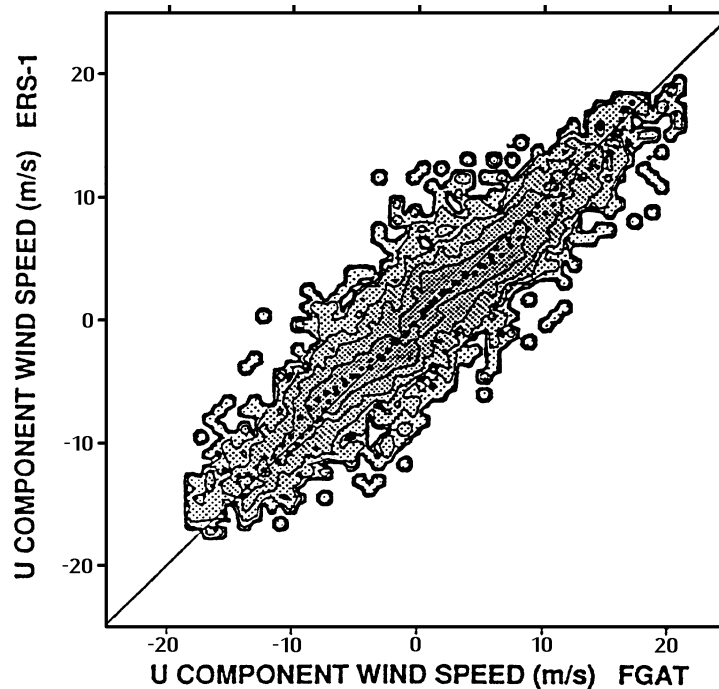


Fig. 9.1: Collocation histogram (scatterplot) of the component of the wind in the direction of the mid beam for node 11 (from inside swath): ECMWF FGAT winds against winds retrieved from the ERS-1 scatterometer selecting the closest of the two available solutions to the short-term forecast (from Stoffelen et al., 1993).

In the assimilation scheme of the UKMO (a 3-D univariate optimum interpolation scheme) the SASS observations were processed like Cloud Motion Vectors (CMVs) and assigned a pressure value corresponding to 19.5 m above the surface (Ingleby and Bromley, 1991). The rms error of the wind components were assumed to be 4.5 m/s and the error correlation for u-u, v-v was estimated to be a function of distance only, namely $\exp(-400D^2)$, where D is the separation of the observations measured in radians at the centre of the earth. The u-v correlation was set to zero. Scatterometer winds with a large difference from the background field (first guess) were rejected by the assimilation scheme. At each gridpoint up to seven observations were selected for the analysis. This means that the radius of influence of a single SASS observation was limited to about 150 km, approximately the model grid spacing. No mass or temperature increments were included for wind observations (due to the univariate scheme), including scatterometer winds. Instead, high frequency oscillations created by the unbalanced introduction of wind observations were damped at all points of the model grid. Nevertheless, the abrupt wind speed change in the first analysis (with scatterometer winds) led to a marked 12-hour oscillation in the area south of 30°S, which died out after 36 hours simulation time.

Ingleby and Bromley (1991) pointed out that, in general, it is not efficient to have observations on a finer resolution than the model. Therefore all backscatter measurements within a square should be combined to form so called “superobservations” on 100-km squares.

Bell and Holt (1992) pointed out that observed scatterometer winds have different characteristics compared to conventional ocean wind data (geographical distribution of the data, high data density along the swaths, winds at 10 and not 20 m, unreliability of directions in light wind regimes). Revisions to the UKMO data assimilation system were introduced to account for these

differences. For example, tuning of the horizontal correlation scale (the scales were reduced) was necessary, and below a threshold of 4 m/s the assimilation used only the speed information.

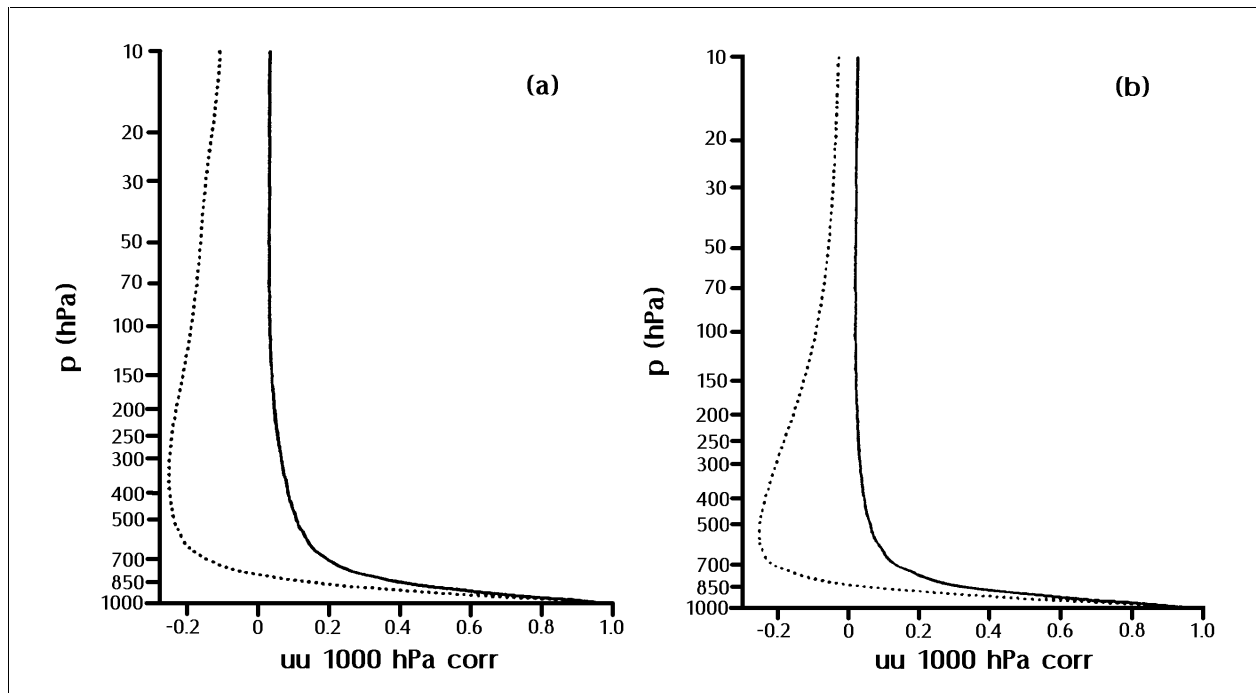


Fig. 9.2: Vertical correlation function in the OI analysis system of the ECMWF model to extent surface forecast error correction in the vertical: (a) mid-latitudes; (b) tropics. Continuous line: non-divergent wind component covariance. Dotted line: divergent covariance (from Undén, 1989).

Several experiments of assimilating scatterometer data in the ECMWF model have been carried out (at discrete six-hour intervals of the ECMWF analysis). Since the ECMWF model resolution (~ 125 km for T106, ~ 60 km for T213) is lower than the resolution of the scatterometer data, the data presented to the analysis were thinned to a coarser resolution before handing them to the analysis (to 100 km for the T106 model). Until January 1996, the ECMWF analysis used Optimum Interpolation (OI) where data and the model forecast were combined into a balanced analysis. In contrary to the UKMO model, the analysis was multivariate, which means that measurements of the winds influenced also the mass field through a latitude-dependent application of geostrophy (Stoffelen and Anderson, 1997). In addition, vertical correlation functions in the OI system extended the surface forecast error correction caused by the scatterometer wind data in the vertical (see fig. 9.2). This projection was strictly vertical (assuming a barotropic atmosphere) and limited mainly to the lowest layers (the correlation fell below 0.2 already at 700 hPa level, see fig. 9.2). The horizontal spreading of the information from the data points was determined by the structure (correlation) functions of the observation errors. All error correlations were considered, namely the u-u, u-v, u-z, v-v, v-z, z-z correlation functions, where u, v are the horizontal wind components and z the geopotential. In the ECMWF model, these functions depended on latitude (e.g. the spatial scale for the tropics was twice that at 60°N).

A major change was made in the ECMWF assimilation system in January 1996, when the OI analysis scheme was replaced by the 3D-Var method. In 3D-Var, all observations are merged with the model first guess through the minimisation of a cost function:

$$J = J_O + J_B + J_C \quad (9.1)$$

where J_B and J_O are quadratic terms measuring the distance from the model state to its background estimate (i.e. the first guess) and the observations respectively, and J_C is a penalty term expressing physical constraints on the model state (e.g. no fast growing gravity waves).

Compared with OI, one main advantage of 3D-Var is that it allows to handle data that are non-linearly related to the analysed quantities. This means that for instance satellite measurements can be directly assimilated. Moreover, the control of gravity waves is done implicitly within the cost function (J_C term). In the OI analysis, a separate initialisation step was necessary to control the fast growing gravity waves.

As mentioned before, for scatterometer data Stoffelen and Anderson (1995, 1997a) have demonstrated that it is better to assimilate scatterometer ambiguous winds, rather than assimilating directly the σ° measurements. In the wind domain, the error characteristics have a gaussian structure and can be described quite easily. In the σ° domain, the description of the error characteristics (structure functions) is much more complicated due to the high non-linearity of the transfer function.

Scatterometer data are assimilated in the 3D-Var system as pairs of ambiguous wind vectors, through a two-minima cost function of the following form (Le Meur et al., 1998):

$$J_O^{scat} = \frac{J_1 \times J_2}{[J_1^p + J_2^p]^{1/p}} \quad (9.2)$$

with:

$$J_i = \frac{(u_i - u)^2}{\delta u^2} + \frac{(v_i - v)^2}{\delta v^2}, \quad i = 1, 2 \quad (9.3)$$

where u and v are the model state wind components, u_i and v_i ($i=1, 2$) the two ambiguous scatterometer wind solutions, δu and δv the associated standard deviation of the scatterometer observation error and p an empirical exponent set to 4. Stoffelen and Anderson (1995) found that the two ambiguous solutions have almost equal probability of being chosen by the assimilation system. Therefore, both solutions have a priori the probability of 0.5.

Since the transfer function relates the backscatter measurements to an equivalent wind at a height of 10 metres in neutral stratification, the model state wind components in equation (9.3) also have to be taken at 10 metres. Depending on the model layers, it may be necessary to perform an extrapolation of the model wind to the 10 metre height, taking into account the atmospheric stability as outlined in chapter 4. An alternative assimilation procedure would be to assimilate scatterometer observations as wind stress vectors (Gaffard and Roquet, 1995).

As mentioned before, the two ambiguous solutions provided by the inversion scheme, before presenting them to the assimilation system, may have to be thinned to a coarser resolution (to 100-km resolution in the ECMWF model). Furthermore, a speed bias correction scheme may have to be applied to remove the underestimation of the high winds produced by the transfer function CMOD4. The bias correction for high winds is important to make good use of scatterometer data in the 3D-Var assimilation system. Assimilation experiments have shown that

without this bias correction there is a tendency to “fill” mid-latitude lows because of too low wind speeds inferred from the backscatter measurements (Le Meur et al., 1998).

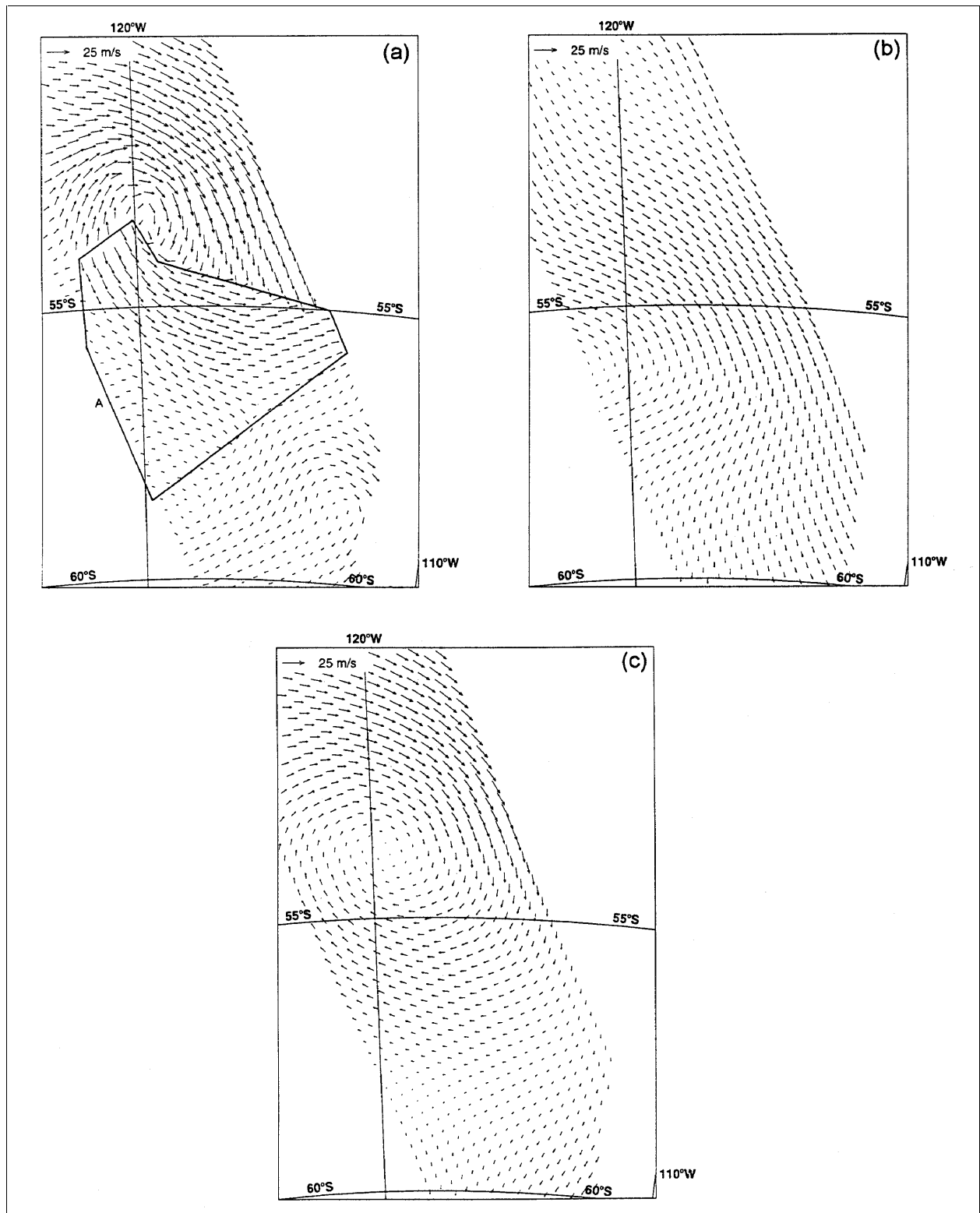


Fig. 9.3: Assimilation of scatterometer winds in the ECMWF model: (a) ESA scatterometer winds at 08 UTC 17 August 1993 over the South China Sea. Note the failure of the ambiguity removal scheme in the area A; (b) short-range forecast used as background field in the analysis; (c) 3D-Var analysis using PRESCAT winds and the forecast shown in (b) as input (from Stoffelen and Anderson, 1997a).

The assimilation of scatterometer winds in the ECMWF model using 3D-Var has led to a clear improvement of the analysed and first guess surface fields (Le Meur et al., 1998). Ambiguity removal is done accurately with 3D-Var, and a large scale compromise is found even in complicated situations, as shown in fig. 9.3 (Stoffelen and Anderson, 1997a). Despite these positive impacts, Le Meur et al. (1998) point out that the 3D-Var scheme does not allow for an optimum use of the scatterometer observations because fixed error correlation structures are assumed. This will be improved with the 4D-Var assimilation system that will bring a variation of the structure functions dynamically consistent with the meteorological situation.

10

Impact of scatterometer winds on NWP and Ocean Forecasting

The impact of scatterometer winds on the NWP model analysis depends to a high degree on the geographical area and on the synoptic situation. Ingleby and Bromley (1991) showed that in the area north of 30°S the differences between the two analyses, the CONTROL analysis without scatterometer data and the SEASAT analysis with scatterometer data, were small (16 analyses were compared). The mean differences in the pressure at mean sea level (MSL) were less than 1 hPa almost everywhere. At 700 hPa level the differences were found to be slightly larger.

However, in the area south of 30°S the differences were very large because of the scarcity of non-scatterometer observations. The analyses seemed almost unrelated. The differences in the pressure at MSL exceeded 10 hPa in the south-eastern Pacific and rms differences in the winds were large at all levels, particularly in the Pacific to the west of the Antarctic Peninsula and to the south of Australia (see fig. 10.1, rms vector differences of up to 12 m/s at 700 hPa level). Concerning the spin-up time, the analysis wind fields spun up within 6 or 12 hours, whereas the mass fields took about two days.

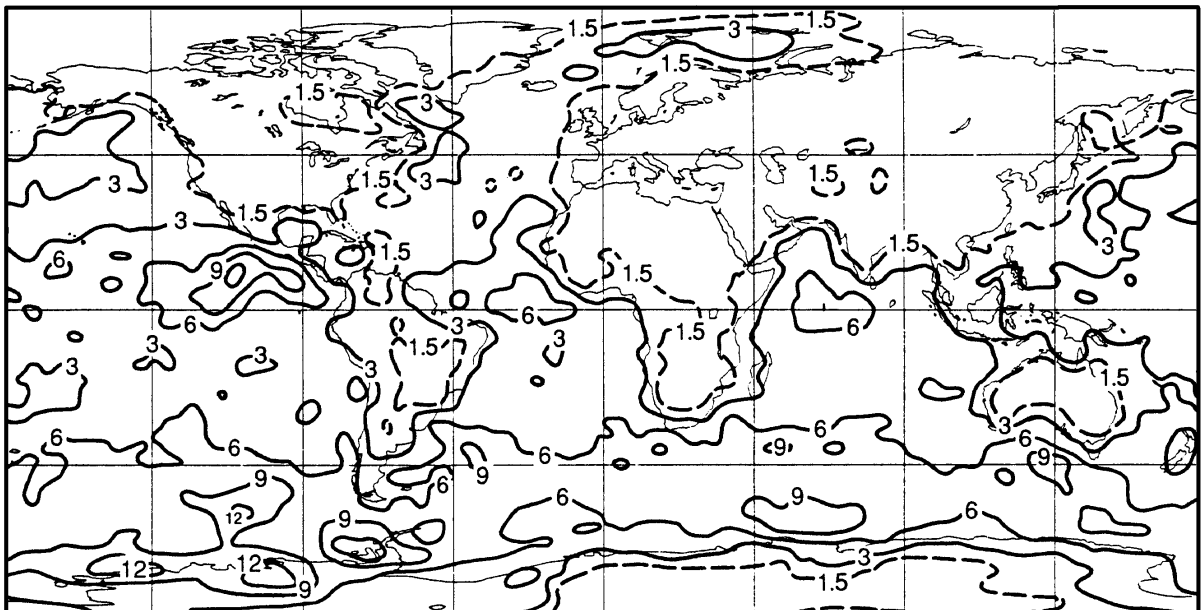


Fig. 10.1: Rms vector differences at 700 hPa, 0 UTC 9 September minus 18 UTC 12 September 1978, 16 analyses with SEASAT data minus 16 analyses without SEASAT data. The analyses were performed with the UKMO NWP model at six-hour intervals, starting from an interpolated analysis for 0000 UTC 3 September 1978 obtained from the NMC in Washington. The UKMO data assimilation is based on 3D univariate optimum interpolation scheme. Contours every 3 m/s, dashed contour at 1.5 m/s (from Ingleby and Bromley, 1991).

The impact of scatterometer winds on weather forecasts can be studied by so-called Observing System Experiments (OSEs) (e.g. Undén et al., 1997). OSEs are data assimilation experiments where one can assess the impact of an operational observing system by deleting its observations from the operational network and then running extended data assimilation and regular forecasts with the reduced system to assess the contribution of the deleted system to the total operational system. OSEs can also be used to assess the value of a new or experimental observing system by running extended data assimilation followed by regular forecasts (10-days at ECMWF) with and without the new observations. Undén et al. (1997) point out that the interpretation of OSEs is not always straightforward. The value of an observing system is easier to demonstrate by adding it to a minimal base-line system, than by deleting it from a maximal baseline system. The stand-alone value of a new observing system may be masked if there are overlaps in the observations. This can easily happen in a complex 3D or 4D-Var assimilation system, which uses all kinds of conventional and satellite observations and which makes use of multi-variate relations between the different variables of the model. Therefore the statistical results of OSEs should be supported by case studies analysing the synoptic aspects of the results of the different forecasts.

The impact of SEASAT winds on the weather forecast has been studied at several centres, some with global models, including the National Meteorological Centre in Washington (Yu and McPherson, 1984), the Goddard Laboratory for Atmospheres (Duffy et al., 1984; Baker et al., 1984), ECMWF (Anderson et al., 1987), and the UK Met Office (Ingleby and Bromley, 1991). The response was generally small, being largest in the Southern Hemisphere. Anderson et al. (1991) found that SEASAT scatterometer data in the T106 ECMWF model had a neutral impact in both Southern and Northern Hemisphere. This was confirmed by Ingleby and Bromley (1991) who stated that the impact of scatterometer data on the forecast was generally small, being largest in the Southern Hemisphere. It was also found that a conflict might arise when introducing scatterometer-derived winds together with data from other satellite instruments. For example, Baker et al. (1984) found a larger beneficial impact on the forecast when satellite temperature soundings from TOVS were excluded. The inclusion of the satellite soundings eliminated the positive impact of the scatterometer winds.

The impact of ERS scatterometer winds on global-scale weather forecasts has been studied at ECMWF (e.g. Undén et al., 1997, Isaksen, 1997). The results of the OSEs showed that scatterometer data improve the scores for the Northern Hemisphere in both 3D-Var and 4D-Var but that it is most pronounced in 4D-Var (reduced rms error, increase in the reliability of the forecasts, see figs. 10.2 and 10.3). This suggests that in future scatterometer data may have a greater impact on the forecast when the 4D-Var assimilation scheme will become operational at ECMWF. Undén et al. (1997) found out that the positive impact in 4D-Var came from better assimilation of some low pressure systems in the North Pacific where scatterometer data were particularly valuable.

For the Southern Hemisphere the results were not equally encouraging. As demonstrated in figs. 10.2 and 10.3, the use of scatterometer data for the test period (the last two weeks of January 1996) had a neutral impact on the scores in this area, both in 3D-Var and in 4D-Var. Undén et al. attribute this result to the less intense weather systems in the Southern Hemisphere during the summer period. Additional OSEs are necessary to come to a final conclusion.

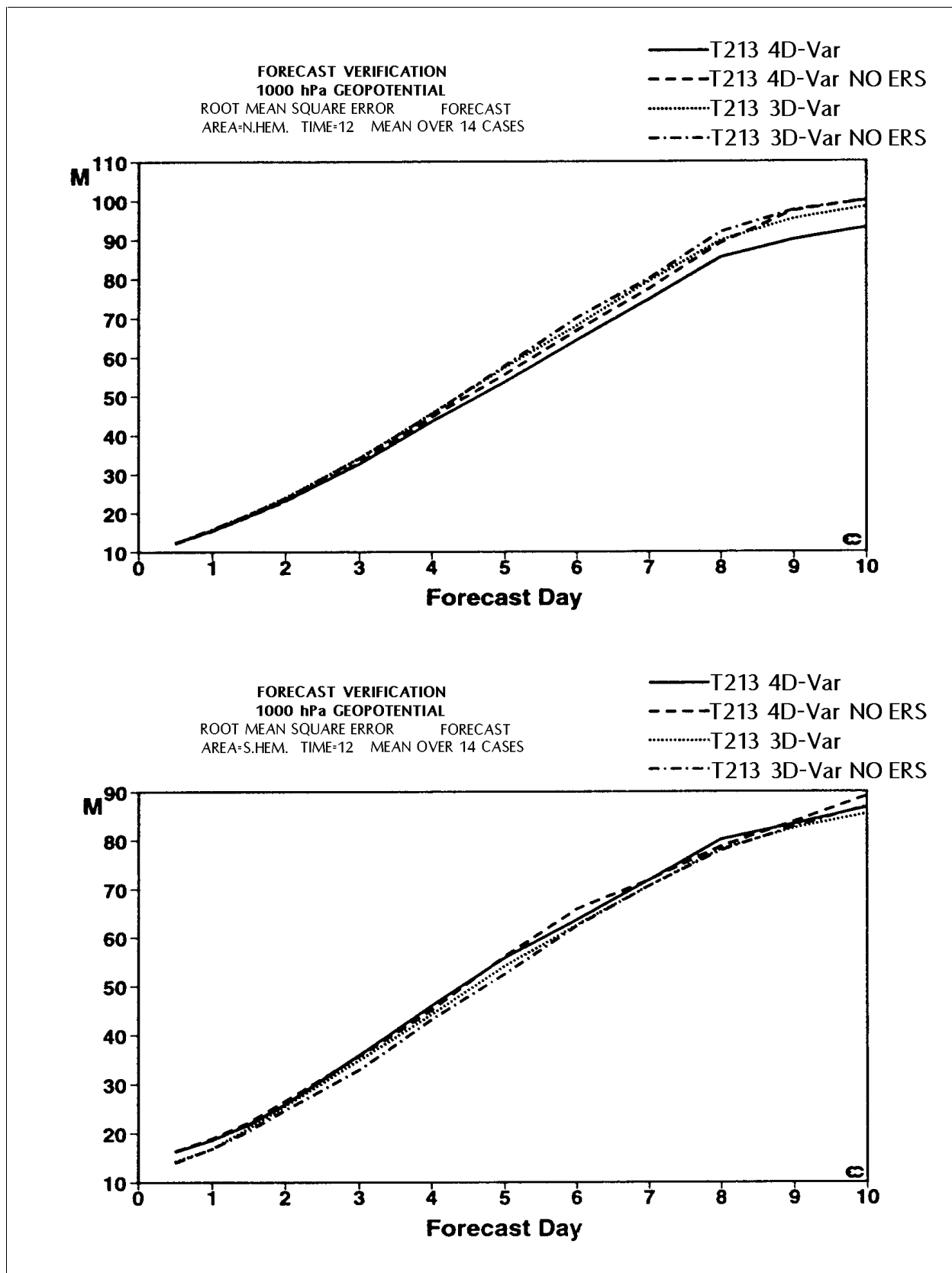


Fig. 10.2: 1000 hPa height forecast rms errors for Northern (top) and Southern Hemisphere (bottom) from 4D-Var and 3D-Var assimilations with and without scatterometer data (from Undén et al., 1997).

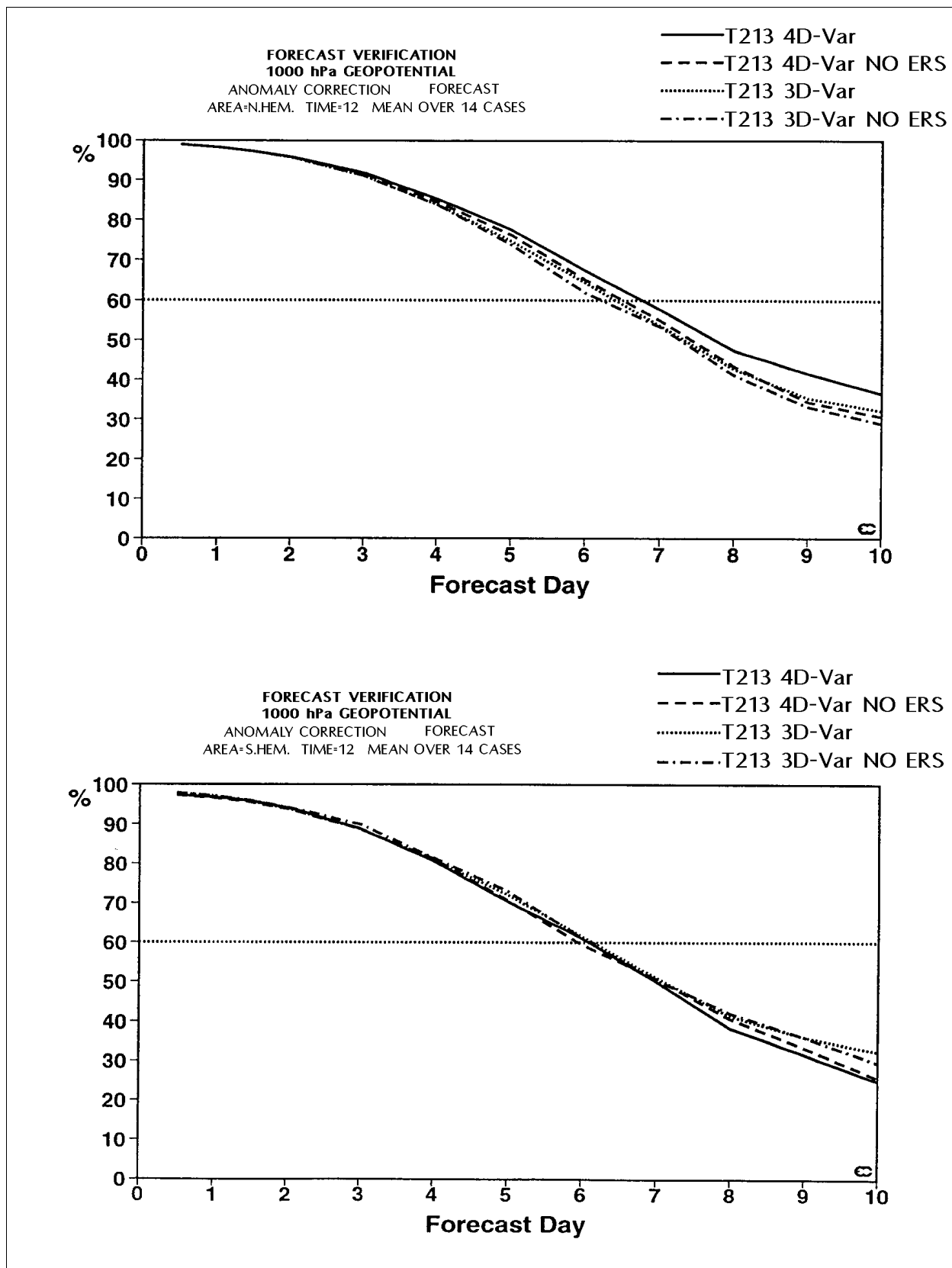


Fig. 10.3: Mean 1000 hPa height forecast anomaly correlations obtained over the Northern (top) and Southern Hemisphere (bottom) from 4D-Var and 3D-Var assimilations with and without (NO ERS) scatterometer data (from Lars Isaksen, ECMWF).

Undén et al. (1997) performed an additional study taking the tandem operations of ERS-1 and ERS-2 scatterometers in April-May 1996 as an opportunity to investigate the impact of increased area coverage of scatterometer data. Four parallel assimilation experiments in 3D-Var were performed: using no scatterometer data (NOSCAT), using ERS-1 or ERS-2 data only, and using both ERS-1 and ERS-2 data (ERS1+2). Table 10.1 summarises the results of the impact on the surface wind analysis. The departures between first guess and scatterometer observations are given for each experiment. The vector rms difference is reduced by 0.1 and 0.08 m/s when using ERS-1 and ERS-2 data respectively, and by 0.15 m/s when using both ERS-1 and ERS-2 data. With this and other experiments Undén et al. could demonstrate a good complement between both scatterometers, their separate benefits being juxtaposed without particular overlap when using them together. This was confirmed by a tandem ERS impact study made at KNMI (A. Stoffelen, private communications), which showed an improvement of the forecast when data from both ERS satellites were used. The assimilation of data from ERS-1 only had led to a neutral forecast.

Experiment	Vector rms (m/s)	Difference w.r.t. NOSCAT
NOSCAT	3.40	/
ERS-1	3.30	-0.10
ERS-2	3.32	-0.08
ERS1+2	3.25	-0.15

Tab. 10.1: RMS departures between the first guess and scatterometer observations obtained using no scatterometer data (NOSCAT), ERS-1 or ERS-2 data only, and both ERS-1 and ERS-2 data (ERS1+2) (from Undén et al., 1997).

Summarising the above, the impact of scatterometer winds on the analysis are very large in the S. Hemisphere where conventional observations are sparse. In the N. Hemisphere the impact on the analysis is much smaller. As regards the impact on the forecast, a neutral or small positive impact has been found depending on the geographical area and the time period chosen for the experiments. The conflict between the earlier results from Ingleby and Bromley (1991), i.e. positive impact in the S. Hemisphere and neutral impact in the N. Hemisphere, and those from Undén et al. (1997), i.e. the opposite results, is probably due to the different time periods selected for the experiments. Generally, a positive impact was found whenever strong cyclones were observed in the area of investigation. The results from Undén et al. (1997) also indicate that scatterometer data may have a greater impact on the forecast when 4D-Var assimilation schemes will be used for the analyses.

Several studies exist that document the impact of ERS-1 scatterometer and satellite cloud motion wind data on analysing and forecasting Atlantic tropical cyclones. Case studies have been performed from various assimilation experiments over the 1995 hurricane season (Tomassini et al., 1997), showing that the consistent coverage offered by satellites over the ocean can be essential for improving the monitoring of tropical cyclones. An example is given in fig. 10.4, where a Meteosat visible image reveals four tropical storms over the Atlantic at the same time. For this case, conventional wind reports (not shown) were rather sparse and almost absent from the large area where the storms formed. Thus the potential benefit of the scatterometer winds as shown in fig. 10.4 is obvious.

Tomassini et al. (1997) performed a systematic comparison of the analysed and reported centre position of North Atlantic tropical cyclones for 32 cases during a 16-day period in summer 1995. The location of the cyclones in the ECMWF analysis, which was estimated from the position of the maximum in the relative vorticity field at 850 hPa, was compared to the reference position as

reported from the National Hurricane Center. Only those cases when the cyclones were located south of 30°N were considered. Two runs of the ECMWF model were carried out: the operational assimilation run with T213 resolution (CON), which at that time used the OI assimilation scheme with no scatterometer winds, and a 3D-Var assimilation run with the scatterometer winds (SCAT/3D). Out of the 32 cases considered, 22 had a better position in SCAT/3D. The mean positional error for all cases could be reduced from 173 km (CON) to 111 km (SCAT/3D), and the difference in the means was found to be significant at the 95% confidence level. The remaining positional error (111 km) is very small, if one considers that the maximum precision achievable with the model is 90 km.

The improved analysis also led to better forecasts in the short range. An improvement was also found in the 72 hour forecast. At this range the CON forecasts only detected seven tropical storms out of a total of 21, whereas the SCAT/3D forecast was able to forecast 17, with a mean positional error of 266 km. As for the analysis, a tropical storm was considered to be detected when the maximum vorticity was lower than the threshold of $5 \times 10^{-5} \text{ s}^{-1}$. In two cases (hurricanes Iris and Luis) the improvements in the analysed position of the hurricane due to the scatterometer data led to a significant better forecast of the track and the intensity of the hurricane. Furthermore, the cyclone structure appeared to be better described in the SCAT/3D experiment with stronger winds at shorter distances from the hurricane centre (Le Meur et al., 1998). A rather dramatic example of the impact of scatterometer winds on a five-day forecast is given in fig. 10.5. Fig. 10.6 shows the verifying analysis corresponding to the five-day forecasts in fig. 10.5. The CON forecast (top panel) completely fails to detect the hurricane Luis. The 4D-Var forecast shows a clear improvement with the storm nearly in the right position, but it underestimates its intensity. Finally, the 4D-Var forecast with scatterometer winds reflects the real intensity of the storm, although it predicts the cyclone to be further to the east than its actual position.

Bansal et al. (1994) reported a case where scatterometer winds derived from ERS-1 were available directly over a tropical cyclone over the Bay of Bengal. The inclusion of the scatterometer data in addition to the usual GTS data in the assimilation system of the NWP model described the cyclone much better than those obtained without use of scatterometer data. The centre of the storm could be exactly located, but the intensity was not properly defined. Bansal et al. attributed the intensity error to the tendency of scatterometer wind speeds to underestimate the true wind speed (Lorenc, 1993). The storm could be tracked with the inclusion of scatterometer winds, although the precise location of the landfall could not be predicted correctly.

The resolution and sampling of scatterometer measurements (50 km resolution and 25 km sampling in the case of the ERS scatterometer) is generally too coarse to measure the mesoscale wind structures in the vicinity of tropical cyclones (TCs). Quilfen et al. (1998) experimentally produced a few sets of ERS-1 scatterometer measurements at $25 \times 25 \text{ km}^2$ resolution (12.5 km sampling). Enhancing the resolution by a factor of two allowed a more precise location of the wind maxima and minima and of the positions of the TCs. Figure 10.7 gives an example of high-resolution surface winds for TC Elsie for four ERS-1 passes where the TC centre was identified. One striking feature is the asymmetric structure of the wind field with respect to the TC centre. The maximum winds are on the right side of the TC moving north-westward on 3 and 5 November. The knowledge of these small-scale structures is relevant for the forecasting of TCs.

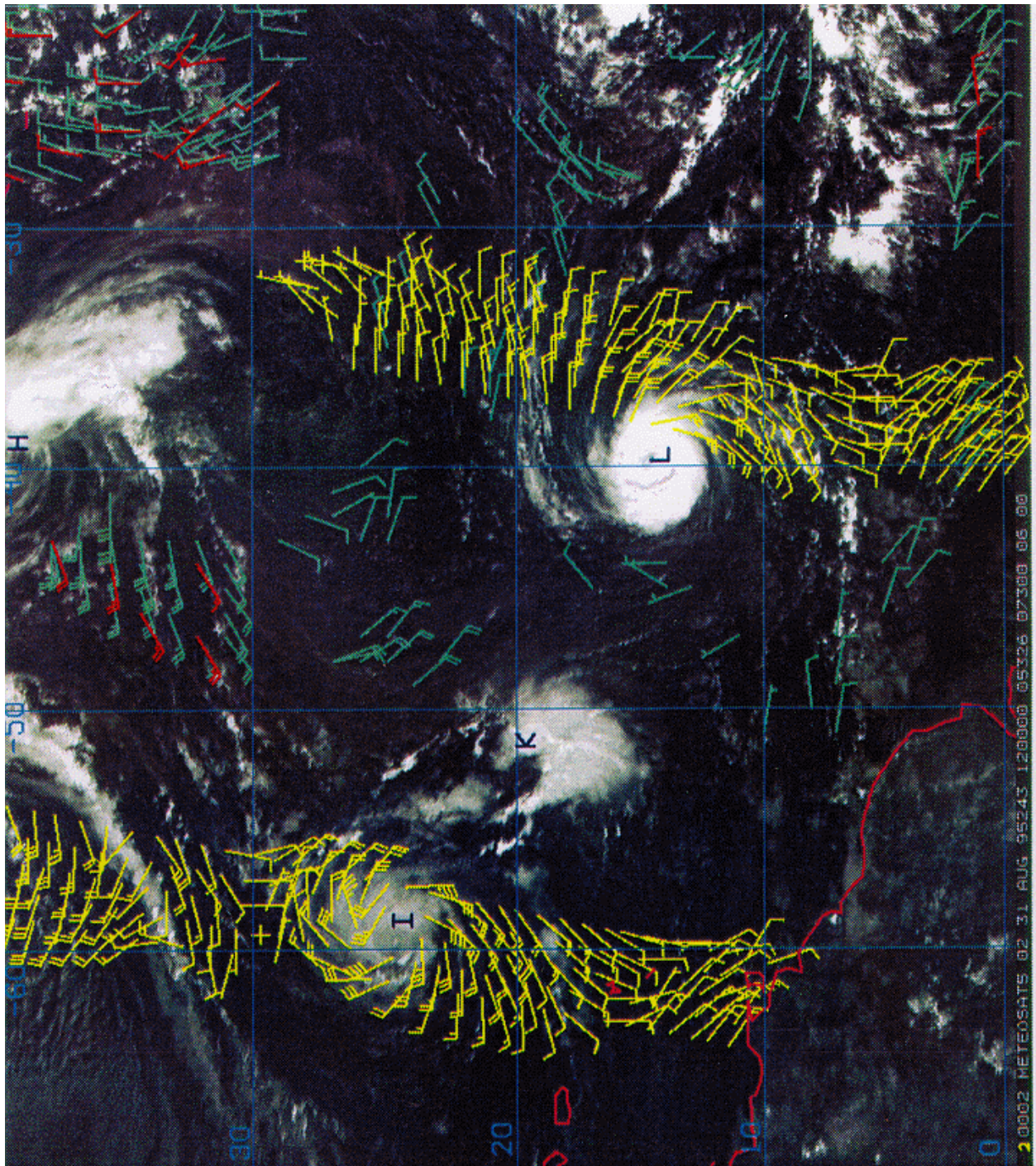


Fig. 10.4: Data coverage for 31 August 1995 at 12 UTC of satellite wind observations. ERS-1 scatterometer winds (yellow), Meteosat VIS (green) and IR (red) cloud motion vectors below 700 hPa are overlaid on a Meteosat visible image (from Tomassini et al., 1997).

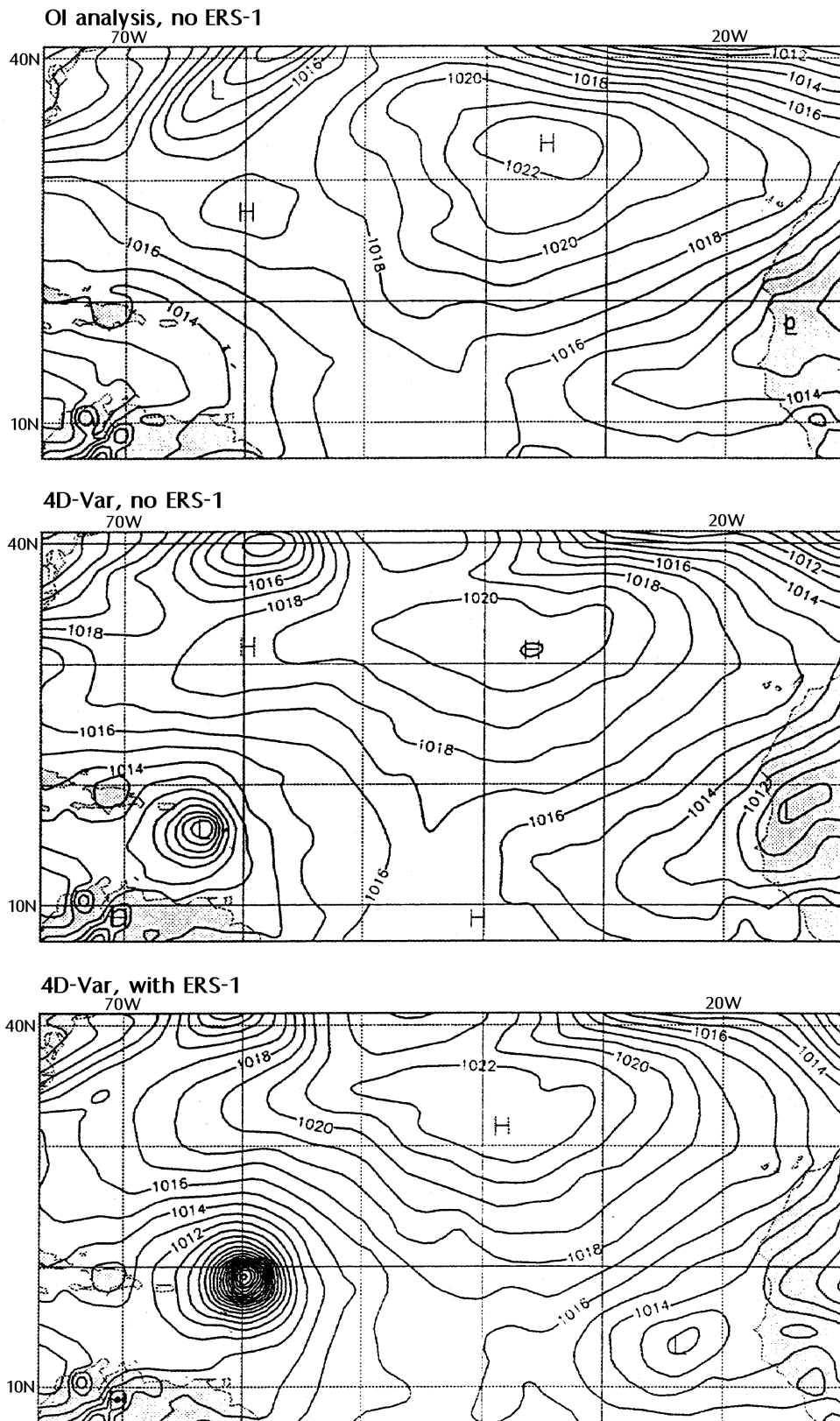


Fig. 10.5: Mean sea level pressure five-day forecast with the ECMWF model valid at 6 September 1995, 12 UTC. Upper panel: forecast from the old assimilation system (Optimum Interpolation, OI) without scatterometer data. Middle panel: forecast using the 4D-Var assimilation system without scatterometer data. Bottom panel: forecast using the 4D-Var assimilation system with scatterometer data (from Le Meur et al., 1998).

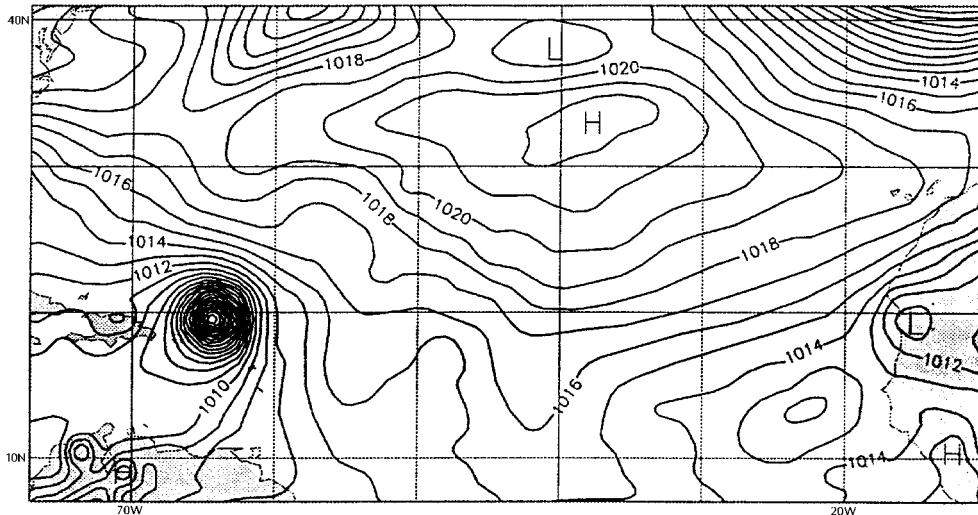


Fig. 10.6: Analysed mean sea level pressure field for 6 September 1995, 12 UTC, corresponding to the five-day forecasts shown in fig. 10.5 (from Le Meur et al., 1998).

Quilfen et al. (1998) come to the same conclusion as Bansal et al. (1994) as regards the underestimation of the wind speeds for winds above 20 m/s. It is one of the major challenges for the future to extend the validity of the C band backscattering models to higher wind speeds in order to better define the intensities of TCs. One possibility could be to apply a correction factor depending on the distance to the centre of the TC. Another possibility would be to directly modify the model function in a way that better reflects the strong increase of the wind speed at the high end of the σ^0 spectrum. The problem with this is that only a few measurements exist at very high wind speeds, which makes the fit of a model function very uncertain.

Scatterometer winds can also help to detect polar lows or rapidly moving cold air lows. In single cases it could be shown that reruns with scatterometer winds had a beneficial impact on short period forecasts. For instance, rapidly moving mesoscale lows in cold air could be detected in time leading to a better forecast of heavy showers (Bell and Holt, 1992). There are many other examples of applications of scatterometer winds in the area of mesoscale meteorological features over the oceans, including the monitoring of katabatic winds around the Antarctic (e.g. Marshall and Turner, 1997) and the monitoring of airflow around mountainous islands (Laing and Revell, 1997, see fig. 10.7). Scatterometer winds are often the only data source capable of resolving the fine scale structures, thus contributing significantly to the understanding and the prediction of these mesoscale features.

Another application area for scatterometer wind data is operational ocean forecasting (marine winds, waves/swells, tides, ocean currents, etc.). It could be shown that the integration of wind and wave data from the ERS-1 scatterometer and altimeter in the ocean models added quality to the forecasting of marine winds and wave features, but only to a limited extent (Guddal, 1992). The reason seems to be that the models have already achieved a high accuracy. However, for the immediate real-time monitoring of some products, like significant wave heights, there was a quality improvement (Guddal, 1992). Equilibrium wave heights calculated by an ocean wave model are particularly sensitive to changes in the surface wind field. This is because wave height is proportional to wind speed squared, and wave models retain a memory of the past wind field through the swell energy. In a case study that compared wave heights from a six-day NWP model run with and without the assimilation of scatterometer-derived winds, the largest pointwise differences were about ± 1 m, whereas mean differences amounted to 0.013 m (Bell and Holt, 1992). The largest differences occurred in regions with discrepancies in the storm positions. Away from the storm tracks, differences in wave height were very small.

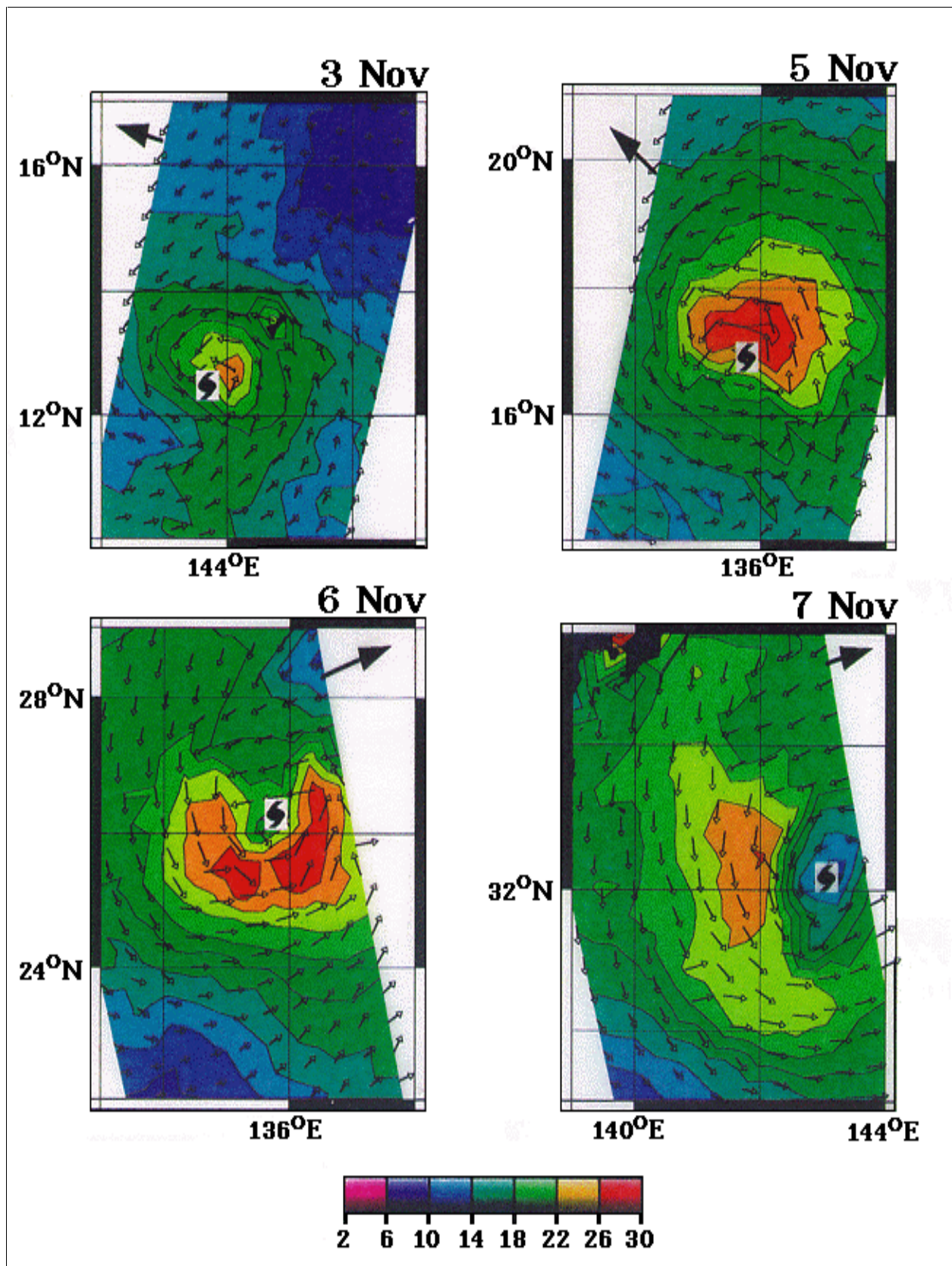


Fig. 10.7: High resolution surface wind field from the ERS-1 scatterometer of tropical cyclone Elsie for 3, 5, 6 and 7 November 1992. The location of the centre of the tropical cyclone and the direction of its movement are indicated. On the bottom: wind speed scale in m/s (from Quilfen et al., 1998).

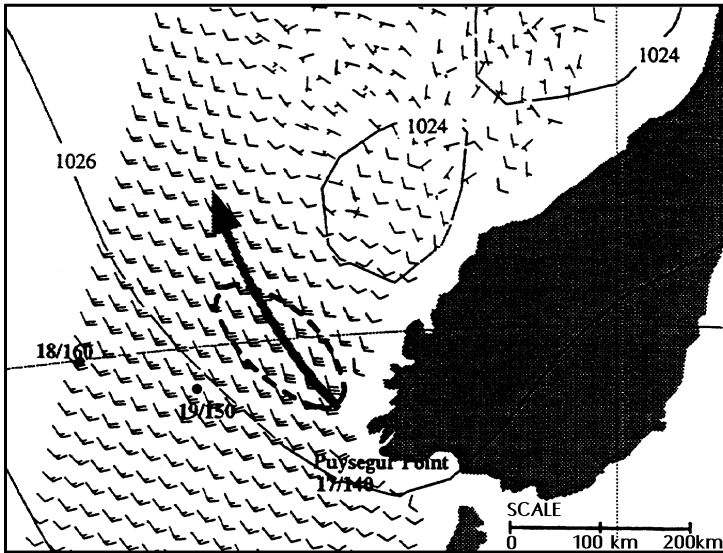


Fig. 10.8: Scatterometer winds for the ERS-1 pass at 22:30 UTC on 5 September 1993. Shown are the 14 m/s isotach (grey dashed line), the line of the wind maximum (thick arrow), the wind observations at Puysegur Point and two concurrent ship observations (formatted as knots/direction, from Laing and Revell, 1997).

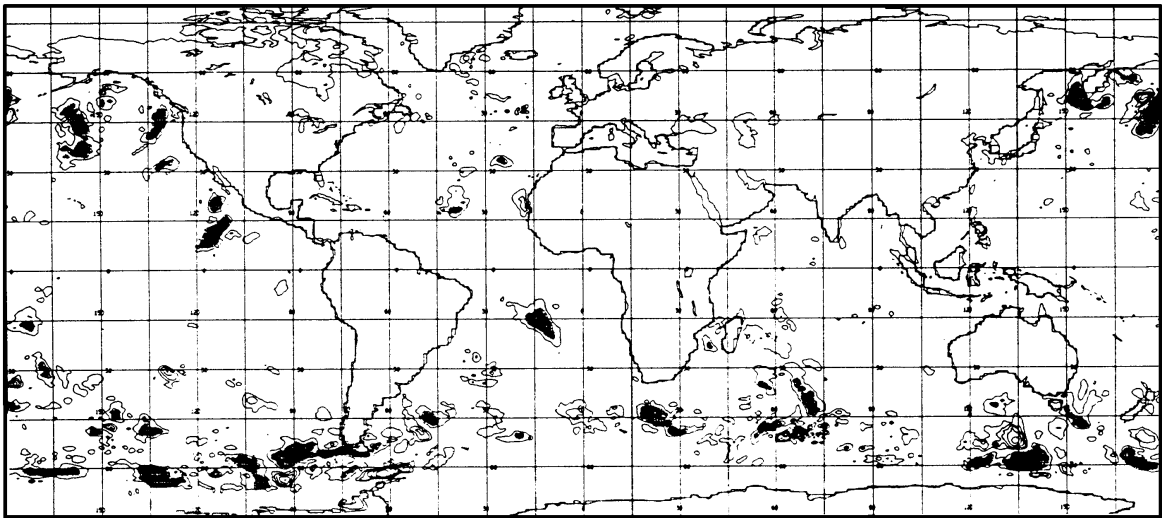


Fig. 10.9: Wave height difference at 0000 UTC 29 September 1992 (with and without ERS scatterometer data) after six-day forecast derived from the UKMO global wave model. Shaded 0.2-0.4 m, 0.4-0.6 m and >0.6 m. Contour interval 0.1 m omitting the zero contour. The largest differences are of the order of +/- 1 m (from Bell and Holt, 1993).

11

Perspectives for ASCAT

The Advanced Scatterometer (ASCAT) on Metop is intended as follow-on to the ERS scatterometer on-board ERS-1 and ERS-2. ASCAT is a real aperture C-band radar (5.255 GHz frequency) with high radiometric resolution and stability. The beam directions (see fig. 11,1), the radar frequency and the polarisation (VV) are the same as for the ERS scatterometer. Spatial sampling (25 km) and horizontal resolution (50 km, i.e. overlapping footprints) will also be identical to the ERS scatterometer, but a research mode will be added with 25 km resolution (12.5 km sampling). Since ASCAT will have a dedicated microwave source (i.e. there will be no shared use with a SAR) and a double swath of 550 km width, the area coverage will be about three times greater than for the ERS scatterometer (see fig. 2.5 on page 8). The double swath coverage is provided by 6 antennae arranged in 3 pairs of V-shaped assemblies. In order to improve the skill in the retrieval of the wind direction, the swath has been moved to higher incidence angles (mid beam 25° to 54.5° ; fore/aft beam 33.7° to 65.3°). This implies an increase in the standoff distance between each wind swath and the sub-satellite track as compared to the ERS scatterometer.

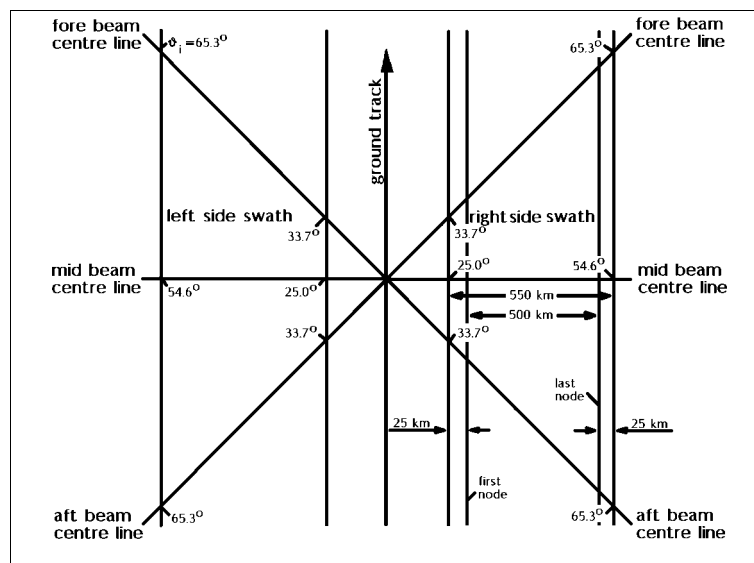


Fig. 11.1: ASCAT system geometry: ground projection showing dimensions and local incidence angles.

The prime objective of the ASCAT mission is to measure the wind field at the ocean surface in the range of 4 to 24 m/s with an accuracy of 3 m/s vector rms. Other objectives that are supported by the ASCAT mission are:

A. Measurements over the oceans:

- Sea ice boundaries
- Sea ice concentration and type

B. Measurements over land:

- Soil moisture
- Snow cover
- Snow/ice liquid water content

The hardware for ASCAT will not be identical to the one of the ERS scatterometer. A part of the processing of the data will already be performed onboard (e.g. some spatial filtering is done by averaging the spectra derived from successive echoes) resulting in a low data rate load on the telemetry link. It will not require onboard knowledge of satellite position/pointing and will be controllable by parameter setting from the ground station.

The following table summarises the characteristics of ASCAT.

Characteristics	Value	Unit
Scan rate	3.763	s
Sampling interval	continuous	-
Grid cells/scan	44	-
Swath	25.0-54.5 (mid) 33.7-65.3 (side)	deg
Swath width	2 times 550	km
Cell resolution	50/25	km
Along track grid spacing	25.0/12.5	km
Across track grid spacing	25.0/12.5	km

Tab. 11.1: Scanning characteristics of ASCAT.

11.1 CHANGES WITH RESPECT TO THE ERS SCATTEROMETER

The most obvious change of the ASCAT instrument with respect to the ERS scatterometer is the increased coverage due to the double swath, the slightly increased swath width and the dedicated microwave source. This will significantly improve the monitoring of tropical cyclones as the cyclones will be more frequently "hit" by the scatterometer. In addition, the gaps in the coastal zones caused by switching the Active Microwave Instrument (AMI) on ERS from one mode to another will disappear. This will be an advantage for the monitoring of the early stage of tropical cyclones in the Eastern Pacific, close to the coast of Mexico and the U.S., where a large number of tropical cyclones are borne.

The impact of greater area coverage of scatterometer measurements on numerical weather forecasts has been studied, among others, by Undén et al. (1997). The tandem operations of ERS-1 and ERS-2 scatterometers in April-May 1996 provided an ideal opportunity to investigate this impact. Table 10.1 on page 51 summarises the results of the impact on the surface wind analysis. The vector rms difference is reduced by 0.1 and 0.08 m/s when using ERS-1 and ERS-2 data respectively, and by 0.15 m/s when using both ERS-1 and ERS-2 data, demonstrating a good complement between both scatterometers, their separate benefits being juxtaposed without particular overlap when using them together.

As already mentioned the shifting of the swath towards higher incidence angles will help to improve the retrieval of the wind direction from the σ° triplets. From tab. 9.1 on page 41 it can be seen that the departure standard deviation for the wind direction decreases with increasing node number. Also the vector rms decreases with increasing node number, indicating that the overall errors of scatterometer winds are smaller at high incidence angles.

The high resolution mode (research mode) of the ASCAT measurements will be particularly beneficial for studying the mesoscale wind structure in tropical cyclones and polar lows and for the estimation of the surface wind in closed or semi-enclosed seas. Quilfen et al. (1997, 1998) have experimentally produced a few sets of ERS scatterometer measurements at $25 \times 25 \text{ km}^2$ resolution (12.5 km sampling). They illustrated that the high resolution will provide more consistent wind fields in coastal areas allowing to use the measurements up to a few tens of kilometres from the coast. They also showed that enhancing the resolution by a factor of two allows a more precise location of the wind maxima and minima and of the position of tropical cyclones (see fig. 10.7 on page 56).

As regards NWP applications, the current resolution of global models is lower than the resolution of scatterometer data. Therefore, the data are thinned to about 100 km before handling them to the assimilation system. However, the upper limit for the horizontal resolution set by the hydrostatic approximation, i.e. 10 km, is by far not reached. It can be expected that the resolution of global NWP models will improve during the next decade. In addition, scatterometer data are also assimilated into regional NWP models, which need high resolution surface data.

11.2 OPERATIONAL APPLICATIONS AND RESEARCH REQUIREMENTS

There are a number of operational applications of scatterometer data that have developed as a result of ERS research and demonstration. Scatterometer winds are routinely used for the monitoring of tropical cyclones over the worldwide oceans as well as for climate monitoring. For Oceanography, scatterometer data are one of the driving input data, whereby the data are used in two ways: by assimilation in the ocean models or by direct use of the wind product. Also sea ice maps are operationally produced from scatterometer data on a weekly basis. Fig. 11.2 depicts a comparison if the sea ice edge product for the Antarctic derived from ERS scatterometer data with the same product derived from SSM/I data.

The assimilation of scatterometer data in NWP models remains so far the main operational application of scatterometer data. The impact of scatterometer winds on the analysis is generally very large in the Southern Hemisphere where conventional observations are sparse. In the Northern Hemisphere the impact on the analysis is much smaller. As regards the impact on the forecast, a positive impact is found whenever strong cyclones are observed in the area of investigation.

The recent switch from the 3D-Var to the 4D-Var assimilation system at ECMWF has led to a significant increase of the impact of scatterometer data on the forecast. First tests with the high resolution ECMWF model (T639) also show an improvement in the use of scatterometer data as compared to the current model (T319). However, the assimilation of scatterometer data into NWP models needs still to be improved (sharper structure functions, situation dependent structure functions) and the underestimation of the wind speed in the vicinity of tropical cyclones needs to be resolved.

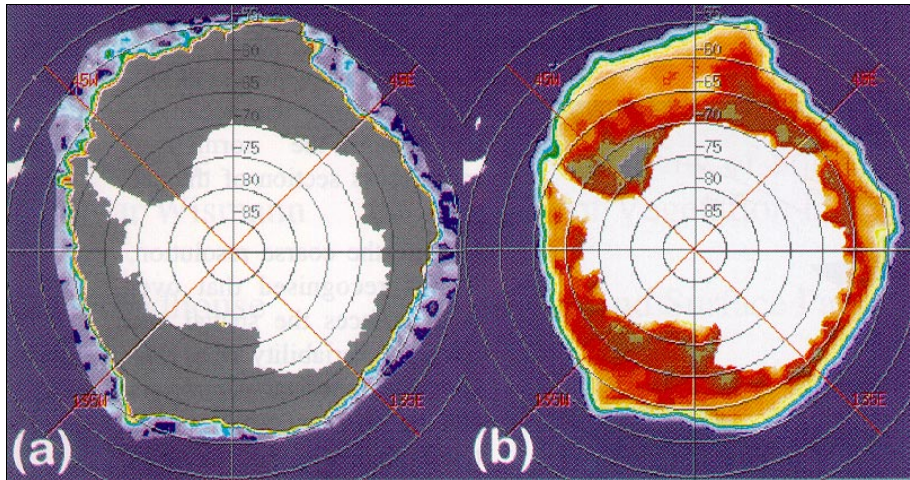


Fig. 11.2: Comparison of the ice edge mask for the Antarctic derived from: (a) ERS-1 scatterometer data; (b) SSM/I passive microwave data (from Cavanié et al., 1997).

In combination with other scatterometer instruments (e.g. SeaWinds) and altimeters, ASCAT will give the forecaster a wealth of information on the ocean surface and contribute significantly to climate monitoring. Concerning the tropical circulation, ASCAT data will be particularly useful for the prediction of El Niño – Southern Oscillation (ENSO) events and other upwelling events (e.g. Boehnke and Wismann, 1993, Freilich et al., 1997, Chen, 1997, Nakazawa, 1997) and the onset of the Indian summer monsoon.

To reach these goals, research and development is needed to improve the transfer function and the ambiguity removal scheme, to extend the transfer function to higher incidence angles, to check and possibly include the sea state dependency, to get a better flag for the sea ice edge and to improve the quality control of the measurements.

11.3 EMERGING APPLICATIONS

Beyond the original mission of scatterometers, intended to provide measurements of the wind vector over the oceans, a large number of new unforeseen applications have emerged. These applications cover not only the ocean, but also land surfaces and continental or sea ice with frequent global coverage.

As regards land applications, new methods for the retrieval of soil moisture and vegetation type/coverage have been developed. Comparison of soil moisture retrieved from scatterometer data with in situ measurements reveal a good agreement for both, the 0-20 cm layer and the 0-100 cm layer. Concerning vegetation types, it has been shown that most of the information from scatterometer data comes from the higher incidence angles, i.e. "vegetation types start to emerge at 30 degrees incidence angle". Vegetation types have so far been successfully retrieved for the Sahel area and for Siberia. An example for the fractional vegetation cover for the Sahel area is given in fig. 11.3. The seasonal variability can clearly be seen, with the September retrievals showing significantly more Sahelian vegetation coverage than in December.

As regards snow and ice applications, several years of backscatter time series from Greenland and Antarctica ice sheets have shown that there is a clear impact of the dry snow on the scatterometer measurements, suggesting that it is possible to estimate the snow accumulation rate

from scatterometer data. It has also been demonstrated that it is possible to identify and locate the percolation zone (and its temporal variation) and the ablation regions. Furthermore, it could be shown that the anisotropy pattern of the scatterometer data over Antarctica correlate well with the location and orientation of sastrugi, as developed in response to katabatic winds. Finally, ice features can be well tracked on a monthly basis with scatterometer data. Even the tracking of large icebergs (larger than 180 km²) is possible on a single pass basis, allowing the determination of ocean currents.

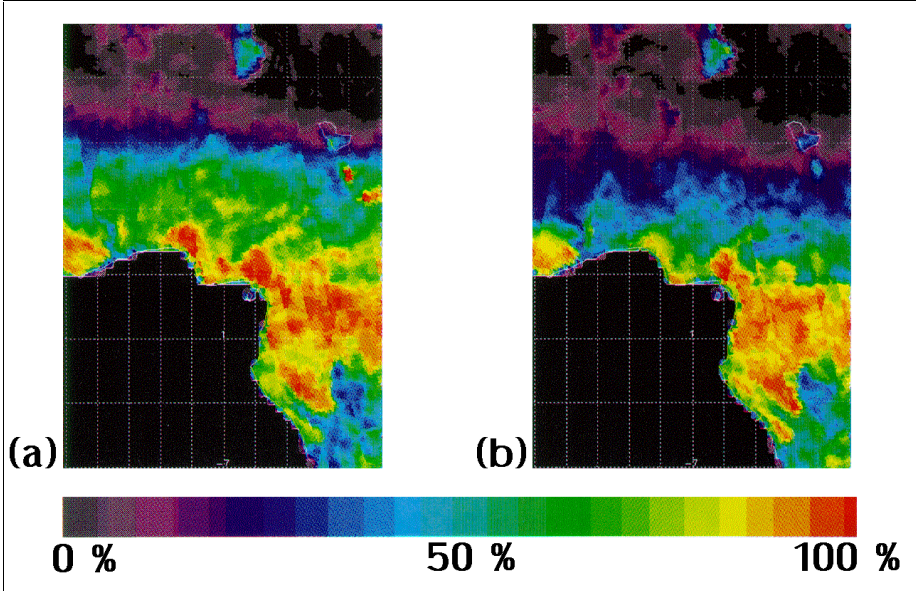
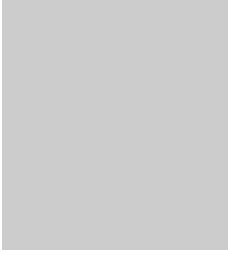


Fig. 11.3: Equivalent fractional vegetation cover over Africa (Hapex Sahel) for September 1992 (a) and December 1992 (b) retrieved from ERS-1 scatterometer data (from Woodhouse and Hoekman, 1997)



Bibliography

- ANDERSON, D., HOLLINGSWORTH, A., UPPALA, S. and P. WOICESHYN, 1987: A study of the feasibility of using sea and wind information from the ERS-1 satellite. Part 1: Wind scatterometer data. ESA, ECMWF contract report, No. 6297/86.
- ANDERSON, D., HOLLINGSWORTH, A., UPPALA, S. and P. WOICESHYN, 1991: A study of the use of scatterometer data in the European Centre for Medium-Range Weather Forecasts Operational Analysis-Forecast Model: 1: Quality assurance and validation. *J. Geophys. Res.*, 96, No. C2, 2619-2634.
- ARABINI, E., BOCCOLARI, M., PUGNAGHI, S. and R. SANTANGELO, 1997: Wind field over Lampedusa island in the Mediterranean Sea by ERS-1 scatterometer implemented by wind observation at ground. *Proceedings of the Third ERS Symposium, ESA SP-414, Volume III*, 1201-1204.
- ASKNE, J., 1990: General principles of relevant satellite systems. In: *Microwave remote sensing for oceanographic and marine weather forecast models*, edited by R.A. Vaughan, NATO ASI Series, C, Vol. 298, 23-44.
- ATLAS, R., BUSALACCHI, A.J., KALNAY, E., BLOOM, S. and M. GHIL, 1987: Global surface wind and flux fields from model assimilation of SEASAT data. *J. Geophys. Res.*, 92, 6477-6487.
- BADRAN, F., THIRIA, S. and M. CREPON, 1991: Wind ambiguity removal by the use of neural network techniques. *J. Geophys. Res.*, 96, No. C11, 20.521-20.529.
- BAKER, W.E., ATLAS, R., KALNAY, E., HALEM, M., WOICESHYN, P.M., PETEHERYCH, S. and D. EDELMANN, 1984: Large-scale analysis and forecast experiments with wind data from the SEASAT-A scatterometer. *J. Geophys. Res.*, 89, 4927-4936.
- BANSAL, R.K., KRISHNAN, R., KISHTAWAL, C.M., SIMON, B., JOSHI, P.C. and M.S. NARAYANAN, 1994: Impact of ERS-1 scatterometer data on the analysis and prediction of a severe cyclonic storm in the Bay of Bengal. *Vayu Mandal*, 24, 59-66.
- BAUER, E., 1997: Statistical comparison of winds from ERS-1 scatterometer and ECMWF model in time and wavenumber domain. *Proceedings of the Third ERS Symposium, ESA SP-414, Volume III*, 1195-1200.
- BEAUDOIN, P.T., LEGLER, D. and J.J. O'BRIAN, 1996: Information content in the ERS-1 three-day repeat orbit scatterometer winds over the North Pacific from January through March 1992. *Mon. Wea. Rev.*, 124, 583-601.
- BELL, R.S., 1993: Operational use of ERS-1 products in the Meteorological Office. *Proceedings of the Second ERS-1 Symposium, ESA SP-361, Volume I*, 195-200.
- BELL, S. and M. HOLT, 1993: Use of ERS-1 wind and wave products in operational meteorology. *Proceedings of the First ERS-1 Symposium. ESA SP-359, Volume II*, 705-710.
- BENTAMY, A., LENAOUR, M., GRIMA, N. et al., 1993: Method to derive average wind fields from ERS-1 scatterometer measurements. *Proceedings of the Second ERS-1 Symposium, ESA SP-361, Volume II*, 1023-1032.
- BENTAMY, A., GRIMA, N. and Y. Quilfen, 1997: Wind climatology from ERS scatterometer. *Proceedings of the Third ERS Symposium, ESA SP-414, Volume III*, 1187-1193.

- BOEHNKE, K. and V. WISMANN, 1993: Radar signatures of equatorial upwelling regions measured by the ERS-1 scatterometer. Proceedings of the Second ERS-1 Symposium, ESA SP-361, Volume I, 507-512.
- BOEHNKE, K. and V. WISMANN, 1997: Thawing of soils and monitoring of vegetation density in Siberia. Land surface observations using the ERS wind scatterometers, Institute for Applied Remote Sensing (IFARS), Wedel, Germany, 11-14.
- BOEHNKE, K. and V. WISMANN, 1997: Detecting soil thawing in Siberia with ERS scatterometer and SAR. Proceedings of the Third ERS Symposium, ESA SP-414, Volume I, 35-40.
- BORZELLI, G., CAPPELLETTI, A., MANZELLA, G., MARULLO, S. and R. SANTOLERI, 1993: Use of the ERS-1 scatterometer data in numerical models. Proceedings of the Second ERS-1 Symposium, ESA SP-361, Volume I, 571-576.
- BOUTIN, J. and J. ETCHETO, 1990: SEASAT scatterometer versus scanning multichannel microwave radiometer wind speeds: a comparison on a global scale. *J. Geophys. Res.*, 95, No. C12, 22.275-22.288.
- BREIVIK, L.A. and H. SCHYBERG, 1997: Assimilation of scatterometer wind pairs and altimeter wind speeds in a limited area weather prediction model. Proceedings of the Third ERS Symposium, ESA SP-414, Volume III, 1181-1185.
- BREIVIK, L.A., HAUGSE, B. and M. HOMLEID, 1993: Results from assimilation of ERS-1 scatterometer wind information in an operational limited area weather forecast model. Proceedings of the Second ERS-1 Symposium, ESA SP-361, Volume I, 201-206.
- BROWN, R.A., 1990: The scatterometer: data and applications. In: Vaughan (editor): *Microwave Remote Sensing for Oceanographic and Marine Weather Forecast Models*. NATO ASI Series, Vol. 298, 99-123.
- BUSINGER, J.A., WYNGAARD, J.C., IZUMI, I. And E.F. BRADLEY, 1971: Flux-profile relationships in the atmospheric surface layer. *J. Atmosph. Science*, 28, 181-189.
- CAVANIE, A., DEMURGER, J. and P. LECOMTE, 1986: Evaluation of the different parameters in Long's C-band model. Proceedings of the Workshop on ERS-1 Wind and Wave Calibration, Schliersee, Germany, 2-6 June 1986, ESA SP-262, 47-51.
- CAVANIE, A. and P. LECOMTE, 1987: Vol 1 - Study of a method to de-alias winds from ERS-1 data. Vol 2 - Wind retrieval and de-aliasing subroutines. Final report of ESA contract, ESA publications division, ESTEC, Noordwijk, The Netherlands.
- CAVANIE, A., EZRATY, R. and F. GOHIN, 1997: In: *Land Surface Observations using the ERS Windscatterometers*, Summary of the results of ESTEC Study Contract 11103/94/NL/CN, Institute for Applied Remote Sensing (IFARS), Wedel, Germany, 4-6.
- CHELTON, D.B., FREILICH, M. and J.R. JOHNSON, 1989: Evaluation of unambiguous vector winds from the SEASAT scatterometer. *J. of Atmospheric and Oceanic Technology*, 6, 1024-1039.
- CHEN, D., 1997: The impact of NSCAT winds on predicting 1997 El Niño: a case study with the Lamont model. The NSCAT SWT meeting in Maui – Hawaii, 10-14 November 1997.
- CRESSMAN, G.P., 1959: An operational objective analysis system. *Mon. Wea. Rev.*, 87, 367-374.
- DAVISON, J. and D.E. HARRISON, 1989: A day-to-day comparison study of SEASAT scatterometer winds with winds observed from islands in the tropical Pacific. NOAA Tech. Memorandum, ERL PMEL-91, Pac. Mar. Environ. Lab., Seattle, Washington, 71 pp.
- DAVISON, J. and D.E. HARRISON, 1990: Comparison of SEASAT scatterometer winds with tropical Pacific observations. *J. Geophys. Res.*, 95, No. C3, 3403-3410.
- DONELAN, M.A. and W.J. PIERSON, 1987: Radar scattering and equilibrium ranges in wind-generated waves with application to scatterometry. *J. Geophys. Res.*, 92, 4971-5029.
- DUFFY, D.G. and R. ATLAS, 1986: The impact of SEASAT-A scatterometer data on the numerical prediction of the Queen Elizabeth II storm. *J. Geophys. Res.*, 91, 2241-2248.

- DUFFY, D.G., ATLAS, R., ROSMOND, T., BARKER, E. and R. ROSENBERG, 1984: The impact of SEASAT scatterometer winds on the Navy's operational model. *J. Geophys. Res.*, 89, 7238-7244.
- EBUCHI, N., 1997: Statistical distributions of wind speeds and directions observed by NSCAT. CEOS Wind and Wave Validation Workshop, ESTEC, June 1997, ESA WPP-147, 113-119.
- ELFOUHAILY, T.M., 1997: Modèle couplé vent/vagues et son application à la télédétection par micro-onde de la surface de la mer. These de doctorat, Université Denis Diderot (Paris-7), UFR de Physique, 233 pp.
- ESSEN, H., 1993: Scatterometer-retrieved winds from the Iceland-Faeroe area. Proceedings of the Second ERS-1 Symposium, ESA SP-361, Volume II, 1013-1016.
- EZRATY, R., 1985: Study of an algorithm for the estimation of wind speed at the sea surface. IFREMER report to ESA, Contract 6155/85/NL/BI (in French).
- EZRATY, R., CAVANIE, A. and F. GOHIN, 1997: Monitoring Arctic sea ice using C and Ku band scatterometers. The NSCAT SWT meeting in Maui – Hawaii, 10-14 November 1997.
- FREILICH, M.H., 1993: ERS-1 scatterometer measurements over the Southern Ocean. Proceedings of the Second ERS-1 Symposium, ESA SP-361, Volume II, 1111-1116.
- FREILICH, M.H. and R.S. DUNBAR, 1993: A preliminary C-band scatterometer model function for the ERS-1 AMI instrument. Proceedings of the First ERS-1 Symposium. ESA SP-359, Volume I, 79-83.
- FREILICH, M.H., FLAMENT, P., LETELIER, R.M., ABBOTT, M.R. and D.M. Karl, 1997: Wind forcing during a mesoscale upwelling event in the North Pacific Subtropical Gyre. The NSCAT SWT meeting in Maui – Hawaii, 10-14 November 1997.
- GAFFARD, C. and H. ROQUET, 1995: Impact of the ERS-1 scatterometer wind data on the ECMWF 3D-Var assimilation system. ECMWF, Technical Memorandum, No. 217.
- GANDIN, L.S., 1963: Objective analysis of meteorological fields. *Gidromet. Isdat.*, Leningrad [Translated from Russian by Israel Program for Scientific Translations, Jerusalem, 1965], 242 pp.
- GRANTHAM, W.L., BRACALENTE, E.M., JONES, W.L., and J.W. JOHNSON, 1977: The SEASAT-A satellite scatterometer. *IEEE J. Oceanic Eng.*, OE-2(2), 200-206.
- GUDDAL, J., 1993: Impact of ERS-1 wind/wave/ice data on operational ocean forecasting. Proceedings of the First ERS-1 Symposium. ESA SP-359, Volume II, 695-699.
- HALPERN, D., 1997: Accuracy of ERS-1 scatterometer surface wind velocity data. CEOS Wind and Wave Validation Workshop, ESTEC, June 1997, ESA WPP-147, 111.
- HALPERN, D., FREILICH, M.H. and R.S. DUNBAR, 1993: ERS-1 scatterometer estimates of annual variations of Atlantic ITCZ and Pacific NECC. Proceedings of the Second ERS-1 Symposium, ESA SP-361, Volume II, 1003-1008.
- HOFFMAN, R.N., 1992: A preliminary study of the impact of C-band scatterometer wind data on global scale numerical weather prediction. ECMWF, Technical Report, No. 69.
- HOFFMAN, R.N., 1993: A preliminary study of the impact of the ERS-1 C band scatterometer wind data on the European Centre for Medium-Range Weather Forecasts Global Data Assimilation System. *J. Geophys. Res.*, 98, No. C6, 10.233-10.244.
- HOLT, M.V. and D. OFFILER, 1997: Validation of ERS-2 altimeter and wind scatterometer observations against global Wave and Atmospheric NWP Models. CEOS Wind and Wave Validation Workshop, ESTEC, June 1997, ESA WPP-147, 131-132.
- IFREMER, 1996: Scatterometer mean wind field products – user manual. Laboratoire d'Océanographie Spatiale (IFREMER), BP 70, 29280 Plouzané, France, 57 pp.
- INGLEBY, N.B. and R.A. BROMLEY, 1991: A diagnostic study of the impact of SEASAT scatterometer winds on numerical weather prediction. *Mon. Wea. Rev.*, 119, 84-103.

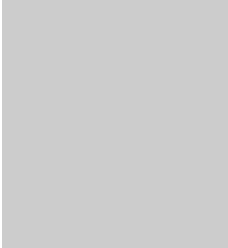
- JANSSEN, P.A.E.M., WALLBRINK, H., CALKOEN, C. et al., 1993: The VIERS scatterometer algorithm. Proceedings of the Second ERS-1 Symposium, ESA SP-361, Volume II, 1033-1038.
- JANSSEN, P.A.E.M., WALLBRINK, H., CALKOEN, C. J., VAN HALSEMA, D., OOST, W.A. and P. SNOEIJ, 1996: The VIERS-1 scatterometer model. Technical Memorandum, No. 231, ECMWF Research Department, 46 pp.
- JONES, W.L., SCHROEDER, L.C., BOGGS, D.H., BRACALENTE, E.M., BROWN, R.A., DOME, G.J., PIERSON, W.J. and F.J. WENTZ, 1982: The SEASAT-A satellite scatterometer: the geophysical evaluation of remotely sensed wind vectors over the ocean. *J. Geophys. Res.*, 87, 3297-3317.
- KERR, Y.H. and R.D. MAGAGI, 1993: Use of ERS-1 wind scatterometer data over land surfaces: arid and semi-arid lands (F1). Proceedings of the Second ERS-1 Symposium, ESA SP-361, Volume I, 383-388.
- KING, P., 1993: An assessment of the use of ERS-1 scatterometer winds in Canadian weather forecasting centres. Proceedings of the Second ERS-1 Symposium, ESA SP-361, Volume I, 207-210.
- KISHTWAL, C.M., RAO, B.M., PAL, P.K. and M.S. NARAYANAN, 1993: ERS-1 surface wind observations over a cyclone system in Bay of Bengal during November 1992. Proceedings of the Second ERS-1 Symposium, ESA SP-361, Volume II, 1127-1132.
- KOMEN, G.J., CAVALERI, L., DONELAN, M., HASSELMANN, K., HASSELMANN, S., and P.A.E.M. JANSSEN, 1994: Dynamics and modelling of ocean waves. Cambridge University Press, Cambridge, 532 pp.
- LACHLAN-COPE, T.A., TURNER, J., THOMAS, J.P. and E.A. RASMUSSEN, 1993: High latitude mesoscale atmospheric circulation features observed with the ERS-1 scatterometer. Proceedings of the Second ERS-1 Symposium, ESA SP-361, Volume II, 809-814.
- LARGE, W.G. and S. POND, 1982: Sensible and latent heat flux measurements over the oceans. *J. Phys. Oceanogr.*, 11, 324-336.
- LAING, A.K. and M.J. REVELL, 1997: ERS scatterometer observations of airflow around mountainous islands. Proceedings of the Third ERS Symposium, ESA SP-414, Volume III, 1579-1584.
- LECOMTE, P. and E.P.W. ATTEMA, 1993: Calibration and validation of the ERS-1 wind scatterometer. Proceedings of the First ERS-1 Symposium. ESA SP-359, Volume I, 19-29.
- LECOMTE, P. and R. CRAPOLICCHIO, 1997: ERS-2 scatterometer calibration and long loop performance since launch comments. CEOS Wind and Wave Validation Workshop, ESTEC, June 1997, ESA WPP-147, 133-144.
- LEGLER, D.M. and J.J. O'BRIAN, 1993: Comparison of ERS-1 scatterometer and Florida State University tropical winds. Proceedings of the Second ERS-1 Symposium, ESA SP-361, Volume II, 1123-1126.
- LE MEUR, D. and L. ISAKSEN, 1997: Wind calibration of the ERS scatterometer data for assimilation purposes at ECMWF. CEOS Wind and Wave Validation Workshop, ESTEC, June 1997, ESA WPP-147, 123-130.
- LE MEUR, D., ISAKSEN, L., HANSEN, B., SAUNDERS, R. and P. JANSSEN, 1998: Global validation of ERS wind and wave products. Final report to the European Space Agency, ESA contract No. 8488/95/NL/CN, ECMWF, Shinfield Park, Reading, Berkshire, RG2 9AX, England.
- LIU, T. and W. TANG, 1997: Application of ERS scatterometer winds to typhoon, monsoon, rain and El Niño studies. Proceedings of the Third ERS Symposium, ESA SP-414, Volume III, 1585-1589.
- LONG, A., 1985: Towards a C-band radar sea echo model for the ERS-1 scatterometer. Proceedings of the third international symposium on spectral signatures, Les Arc, France, December 1985, ESA publication, ESA SP-247, 29-34.

- LONG, A.E., 1991: Summary of CMOD2, Wismann, Cmod2_W & Cmod2_1 models. ESA, Document Number ESTEC/WMA/AEL/9101, Revision 1.
- LONG, M.W., 1988: Radar reflectivity over land and sea. Lexington Books.
- LORENC, A.C., 1993: The use of ERS-1 products in operational meteorology. *Adv. Space. Res.*, 13, 19-27.
- MARSHALL, G.J. and J. TURNER, 1997: ERS scatterometer observations of katabatic winds over a Polynya. *Proceedings of the Third ERS Symposium, ESA SP-414, Volume III*, 1591-1596.
- MCMURDIE, L.A., LEVY, G. and K.B. KATSAROS, 1987: On the relationship between scatterometer-derived convergences and atmospheric moisture. *Mon. Wea. Rev.*, 115, 1281-1294.
- MEJIA, C., BADRAN, F., CREPON, M., THIRIA, S., TRAN, N. and H. ROQUET, 1997: Neural network estimation of the GMFs of the ERS-1/2 and NSCAT scatterometers: application to the wind vector retrieval. *CEOS Wind and Wave Validation Workshop, ESTEC, June 1997, ESA WPP-147*, 161-168.
- MEJIA, C., THIRIA, S., TRAN, N., CREPON, M., ROQUET, H., RICHAUME, P. and F. BADRAN, 1997: Comparison of the neural network GMFs of the ERS-1 and NSCAT scatterometers. *Proceedings of the Third ERS Symposium, ESA SP-414, Volume III*, 1175-1179.
- MONIN and OBUKHOV, 1971: Turbulence in an atmosphere with a non-uniform temperature. *Boundary Layer Meteorology*.
- MOORE, R.J. and A.K. FUNG, 1979: Radar determination of winds at sea. *Proc. IEEE*, 67, 1504-1521.
- MOUGIN, E. and P.-L. FRISON, 1997: Monitoring seasonal vegetation dynamics in the Sahel with ERS wind scatterometer data. *Proceedings of the Third ERS Symposium, ESA SP-414, Volume I*, 163-168.
- MOUGIN, E., LOPES, A., PROISY, C., WARICH, A., FRISON, P.L, LO SEEN, D. and P. LECOMTE, 1993: Analysis of ERS-1 scatterometer data over land surfaces. Preliminary results. *Proceedings of the Second ERS-1 Symposium, ESA SP-361, Volume I*, 393-398.
- NAKAZAWA, T., 1997: 1997 El Niño from ADEOS/NSCAT data. The NSCAT SWT meeting in Maui – Hawaii, 10-14 November 1997.
- OFFILER, D., 1984: A comparison of SEASAT scatterometer-derived winds with JASIN surface winds. *Int. J. Remote Sens.*, 5, 365-378.
- OFFILER, D., 1987: ERS-1 wind retrieval algorithms. UK Met Office, MET O 19, Branch Memorandum, No.86.
- OFFILER, D., 1990: Wind fields and surface fluxes. In: Vaughan (editor): *Microwave Remote Sensing for Oceanographic and Marine Weather-Forecast Models*. NATO ASI Series, Vol. 298, 355-374.
- OFFILER, D., 1993: The calibration of ERS-1 scatterometer winds. *The Meteorological Magazine*, 122, 129-134.
- OFFILER, D., 1994: The calibration of ERS-1 satellite scatterometer winds. *J. of Atmospheric and Oceanic Technology*, 11, 1002-1017.
- ORIOLO-PIBERNAT, E., 1990: The ERS-1 satellite: oceanography from space. In: *Microwave remote sensing for oceanographic and marine weather-forecast models*, edited by R.A. Vaughan, NATO ASI Series, C, Vol. 298, 339-353.
- PARK, J.-D., 1997: NSCAT sea ice flag. The NSCAT SWT meeting in Maui – Hawaii, 10-14 November 1997.
- PRANDTL, L., 1952: *Essentials of Fluid Dynamics*. Blackie and Son Ltd, London.
- PRESS, T.F., BONNER, E.J., CHANG, E., CLEMENTS, G.M., COHEN, D.A., DUBE, C.M., JANG, P.S., MICHELSEN, D.P., NELSON, M.A., PATTON, R.J. and M.L. WEBB, 1996:

- Simulation of SAR ocean imagery – an introduction to DTI's interests and capabilities. Backscatter, Volume 7, Number 1, 17-18.
- QUILFEN, Y., KATSAROS, K., CHAPRON, B. and H. ZHAO, 1993: Surface wind and precipitation patterns in tropical cyclones observed with the ERS-1 scatterometer and with the SSM/I. Proceedings of the Second ERS-1 Symposium, ESA SP-361, Volume II, 1117-1122.
- QUILFEN, Y., CHAPRON, B., ELFOUHAILY, T., KATSAROS, K. and J. TOURNADRE, 1998: Observations of tropical cyclones by high resolution scatterometry. *J. Geophys. Res.*, 103, No. C4, 7767-7786.
- QUILFEN, Y., CHAPRON, B., ELFOUHAILY, T. and K. KATSAROS, 1997: High resolution scatterometry in preparation for the ASCAT instrument. Proceedings of the Third ERS Symposium, ESA SP-414, Volume III, 1233-1237.
- RICHAUME, P., BADRAN, F., CREPON, M., MEJIA, C., ROQUET, H. and S. THIRIA, 1998: Neural network wind retrieval from ERS-1 scatterometer data. Submitted to *J. Geophys. Research*.
- ROQUET, H. and J. POITEVIN, 1993: Tropical cyclone monitoring using ERS-1 scatterometer data. Proceedings of the Second ERS-1 Symposium, ESA SP-361, Volume II, 1133-1138.
- SCHROEDER, L.C., BOGGS, D.H., DOME, G., HALBERSTAM, I.M., JONES, W.L., PIERSON, W.J. and F.J. WENTZ, 1982: The relationship between wind vector and normalised radar cross section used to derive SEASAT-A satellite scatterometer winds. *J. Geophys. Res.*, 87, 3318-3336.
- SCHULTZ, H., 1990: A circular median filter approach for resolving directional ambiguities in the wind fields retrieved from spaceborne scatterometer data. *J. Geophys. Res.*, 95, No. C4, 5291-5303.
- SCHYBERG, H. and L.-A. BREIVIK, 1997: A method for two-dimensional variational analysis of ocean surface wind based on altimeter and scatterometer data. Proceedings of the Third ERS Symposium, ESA SP-414, Volume III, 1219-1224.
- SCHYBERG, H. and L.-A. BREIVIK, 1997: Optimal scatterometer ambiguity removal using a successive correction method. Proceedings of the Third ERS Symposium, ESA SP-414, Volume III, 1229-1232.
- SIEFRIDT, L., LEGLER, D.M., BARNIER, B. and J.J. O'BRIAN, 1993: Mapping ERS-1 wind fields over North West Atlantic using a variable objective analysis. Proceedings of the Second ERS-1 Symposium, ESA SP-361, Volume II, 1017-1022.
- SMITH, S.D., ANDERSON, R.J., OOST, W.A., KRAAN, C., MAAT, N., DE COSMO, J., KATSAROS, K.B., DAVIDSON, K.L., BUMKE, K., HASSE, L. and H.H. CHADWICK, 1992: Sea surface wind stress and drag coefficients. The HEXOS results. *Bound. Layer Meteor.*, 60, 109-142.
- STEWART, R.H., 1985: *Methods of satellite oceanography*. University of California Press, 360 pp.
- STEWART, R.H., 1988: SEASAT: results of the mission. *Bull. Amer. Meteor. Soc.*, 69, 1441-1447.
- STOFFELEN, A., 1994: Surface wind observations from the ERS scatterometers. ECMWF newsletter, Number 66, 3-16.
- STOFFELEN, A., 1996: Error modelling of scatterometer, in-situ, and ECMWF model winds; a calibration refinement. KNMI, Technical Report, TR-193.
- STOFFELEN, A., 1997: Improvement and quality assurance of the scatterometer wind product in the backscatter domain. CEOS Wind and Wave Validation Workshop, ESTEC, June 1997, ESA WPP-147, 159-160.
- STOFFELEN, A., 1998: *Scatterometry*. Ph.D. thesis, KNMI, De Bilt, The Netherlands.

- STOFFELEN, A. and P. VAN BEUKERING, 1997: Implementation of improved ERS scatterometer data processing and its impact on HIRLAM short range weather forecasts. HIRLAM Technical Report No. 31, KNMI.
- STOFFELEN, A. and D.L.T. ANDERSON, 1992: ERS-1 scatterometer calibration and validation activities at ECMWF: A. The quality and characteristics of the radar backscatter measurements. Proceedings of the Central Symposium of the 'International Space Year' Conference, Munich, Germany, 30 March - 4 April 1992, ESA Publication, ESA SP-341, 1019-1024.
- STOFFELEN, A. and D. ANDERSON, 1993a: ERS-1 scatterometer data characteristics and wind retrieval skill. Proceedings of the First ERS-1 Symposium. ESA SP-359, Volume I, 41-47.
- STOFFELEN, A. and D. ANDERSON, 1993b: Wind retrieval and ERS-1 scatterometer radar backscatter measurements. *Adv. Space Res.*, Vol.13, No.5, (5)53-(5)60.
- STOFFELEN, A. and D. ANDERSON, 1993c: Characterisation of ERS-1 scatterometer measurements and wind retrieval. Proceedings of the Second ERS-1 Symposium, ESA SP-361, Volume II, 997-1002.
- STOFFELEN, A. and D. ANDERSON, 1995: The ECMWF contribution to the characterisation, interpretation, calibration and validation of ERS-1 scatterometer backscatter measurements and winds, and their use in Numerical Weather Prediction Models. ECMWF, ESA Contract Report.
- STOFFELEN, A. and D. ANDERSON, 1997a: Ambiguity removal and assimilation of scatterometer data. *Q. J. R. Meteorol. Soc.*, 123, 491-518.
- STOFFELEN, A. and D. ANDERSON, 1997b: Scatterometer data interpretation: measurement space and inversion. *J. Atm. and Ocean Techn.*, 14(6), 1298-1313.
- STOFFELEN, A. and D. ANDERSON, 1997c: Scatterometer data interpretation: estimation and validation of the transfer function CMOD4. *J. Geoph. Res. (C)*, 102(C3), 5767-5780.
- STOFFELEN, A., ANDERSON, D. and C. GAFFARD, 1993: From measurement to model: ERS-1 scatterometer data assimilation. Proceedings of IGARSS'93, (#806), 23-28 August 1993, Tokyo, Japan.
- STOFFELEN, A., ANDERSON, D.L.T. and P.M. WOICESHYN, 1992: ERS-1 scatterometer calibration and validation activities at ECMWF: B. From radar backscatter characteristics to wind vector solutions. Proceedings of the Central Symposium of the 'International Space Year' Conference, Munich, Germany, 30 March - 4 April 1992, ESA SP-341, 1025-1029.
- STOFFELEN, A., GAFFARD, C. and D. ANDERSON, 1993: ERS-1 scatterometer data assimilation. Proceedings of the Second ERS-1 Symposium, ESA SP-361, Volume I, 191-194.
- TOMASSINI, M., LE MEUR, D. and R. SAUNDERS, 1997: Non-surface wind observations of hurricanes and their impact on ECMWF model analyses and forecasts. EUMETSAT/ECMWF Fellowship Programme, Research Report No.5, ECMWF, Shinfield Park, Reading, Berkshire, RG2 9AX, England.
- TURNER, J. and J.P. THOMAS, 1993: A first assessment of the value of ERS-1 scatterometer winds for meteorological studies in the polar regions. Proceedings of the First ERS-1 Symposium. ESA SP-359, Volume II, 701-704.
- TURNER, J. and G. MARSHALL, 1997: The use of ERS scatterometer data to investigate the surface circulation of Antarctic mesocyclones. Proceedings of the Third ERS Symposium, ESA SP-414, Volume III, 1587-1602.
- UNDEN, P., 1989: Tropical data assimilation and analyses of divergence. *Mon. Wea. Rev.*, 117, 2495-2517.

- UNDEN, P., KELLY, G., LE MEUR, D. and L. ISAKSEN, 1997: Observing system experiments with the 3D-Var assimilation system. Technical Memorandum, No. 244, ECMWF Research Department, 32 pp.
- WACKERMANN, C.C., RUFENACH, C.L., SHUCHMAN, R.A., JOHANNESSEN, J.A. and K.L. DAVIDSON, 1996: Wind vector retrieval using ERS-1 Synthetic Aperture Radar Imagery. *IEEE Transactions on Geoscience and Remote Sensing*, Vol.34, No.6, 1343-1352.
- WENTZ, F.J., 1991: A simplified wind vector algorithm for satellite scatterometers. *J. Atmos. and Ocean. Tech.*, **8**, 697-704.
- WIESMANN, A. and C. MÄTZLER, 1993: Monitoring the temporal behaviour of land surfaces with ERS-1 wind scatterometer data. *Proceedings of the Second ERS-1 Symposium*, ESA SP-361, Volume I, 399-404.
- WISMANN, V., 1993: A C-band wind scatterometer model derived from the data obtained during the ERS-1 calibration / validation campaign. *Proceedings of the First ERS-1 Symposium*. ESA SP-359, Volume I, 55-59.
- WISMANN, V., BOEHNKE, K. and C. SCHMULLIUS, 1993: Radar signatures of land surfaces measured by the ERS-1 scatterometer. *Proceedings of the Second ERS-1 Symposium*, ESA SP-361, Volume I, 405-410.
- WISMANN, V. and K. BOEHNKE, 1997: Snow on Greenland. Land surface observations using the ERS wind scatterometers. Institute for Applied Remote Sensing (IFARS), Wedel, Germany, 7-10.
- WOICESHYN, P.M., WURTELE, M.G., BOGGS, D.H., MCGOLDRICK, L.F. and S. PETEHERYCH, 1986: The necessity for a new parameterisation of an empirical model for wind-ocean scatterometry. *J. Geophys. Res.*, **91**, 2273-2288.
- WOODHOUSE, I. and D. HOEKMAN, 1997: Land surface parameter retrieval. In: *Land Surface Observations using the ERS Windscatterometers*, Summary of the results of ESTEC Study Contract 11103/94/NL/CN, Institute for Applied Remote Sensing (IFARS), Wedel, Germany, 15-18.
- YU, T.-W. and R.D. MCPHERSON, 1984: Global data assimilation experiments with scatterometer winds from SEASAT-A. *Mon. Wea. Rev.*, **112**, 368-376.
- ZECCHETTO, S. and P. PAVESE, 1993: The activity of the ERS-1 Venice group on scatterometry. *Proceedings of the First ERS-1 Symposium*. ESA SP-359, Volume I, 71-73.
- ZECCHETTO, S. and M. BORTOLETTO, 1993: Examples of mesoscale meteorology in the Mediterranean Sea using ERS-1 scatterometer data. *Proceedings of the Second ERS-1 Symposium*, ESA SP-361, Volume II, 815-818.



Acronyms and abbreviations

3D/4D-Var	3/4-Dimensional Variational analysis
ADEOS	ADvanced Earth Observing Satellite (NASDA)
AMI	Active Microwave Instrumentation on ERS-1/2
ASCAT	Advanced SCATterometer on Metop
CMF	Circular Median Filter
CMOD	Geophysical transfer function for the ERS (C-band) scatterometer
CMV	Cloud Motion Vector
CNES	Centre National d'Etudes Spatiales (Space Agency of France, Toulouse)
DMSP	Defense Meteorological Satellite Program of the US Department of Defense
DNMI	Det Norske Meteorologiske Institutt (Norwegian Meteorological Institute, Oslo)
ECMWF	European Centre for Medium-Range Weather Forecasts (Reading, UK)
ENSO	El Niño – Southern Oscillation
ERS	European Remote-sensing Satellite (ESA)
ESA	European Space Agency
EUMETSAT	European Organisation for the Exploitation of Meteorological Satellites
FGAT	First Guess at Appropriate Time
FPP	Frequency Power Profile
GEOSAT	GEOdetic/GEOphysical SATellite launched in March 1985 on behalf of the US Navy with a 13.5 GHz radar altimeter on board
GEOS-C	Geodynamics Experimental Ocean Satellite launched in April 1975 on behalf of NASA. GEOS-C was the first radar altimeter mission; end of mission in 1978.
GMT	Greenwich Mean Time
GSFC	Goddard Space Flight Center (Greenbelt, MD, USA)
GTS	Global Telecommunication System (of WMO)
IFREMER	Institut Français de Recherche pour l'exploitation de la mer (French Oceanic Institute, Brest)
IFR-2	Geophysical transfer function for the ERS scatterometer (developed by IFREMER)
IR	InfraRed
JASIN	Joint Air-Sea INteraction experiment
JPL	Jet Propulsion Laboratory (Pasadena, California, USA)

KNMI	Koninklijk Nederlands Meteorologisch Instituut (Meteorological Institute of the Netherlands, De Bilt)
Metop	Meteorological operational polar satellite (EUMETSAT)
MLE	Maximum Likelihood Estimator
MSL	Mean Sea Level
NASA	National Aeronautics and Space Administration (USA)
NASDA	NAtional Space Development Agency (Japan)
NMC	National Meteorological Center (Washington, USA, now National Center for Environmental Prediction)
NSCAT	NASA SCATterometer on ADEOS-1
NWP	Numerical Weather Prediction
OI	Optimum Interpolation
OSE	Observing System Experiment
PRESCAT	Inversion and ambiguity removal scheme developed and applied at ECMWF
PRI	Pulse Repetition Interval
QuickSCAT	NASA mission scheduled for November 1998 with the SeaWinds scatterometer aboard
RENE-91	Campaign to assist in the geophysical calibration of the wind and wave products derived from the ERS-1 satellite
RMS	Root Mean Square
SAR	Synthetic Aperture Radar
SASS	Seasat-A Scatterometer System
SAS-2	Geophysical transfer function for NSCAT
SC	Successive Correction
SEASAT	SEA SATellite launched on 27 June 1978 on behalf of NASA/JPL dedicated to ice and ocean monitoring
SeaWinds	Scatterometer system to be flown on QuickSCAT and ADEOS-2
SLICE	Horizontal filter applied to the retrieved scatterometer winds in order to achieve a better directional consistency
SNR	Signal-to-Noise Ratio
SSM/I	Special Sensor Microwave/Image on DMSP
SSS	Scatterometer Simulator System
SST	Sea Surface Temperature
TC	Tropical Cyclone
TOPEX/ POSEIDON	TOPography EXperiment satellite launched on 10 August 1992 on behalf of NASA and CNES dedicated to the monitoring of ocean circulation. TOPEX/POSEIDON is the heart of the WOCE program.
UKMO	United Kingdom Meteorological Office (Bracknell)
UTC	Universal Time Coordinated
VAR	VARiational

VIERS	Verification and Interpretation ERS-1 (analytical model for the relation between sigma naught triplets and the wind)
VIS	VISible
WAM	WAve Model
WMO	World Meteorological Organization (Geneva, Switzerland)
WOCE	World Ocean Circulation Experiment of the World Climate Research Program
WSC	Wind SCatterometer